



UNIVERSITÀ DEGLI STUDI DI MILANO
FACOLTÀ DI SCIENZE DEL FARMACO
Department of Pharmacological and Biomolecular Sciences

PhD in Pharmacological Biomolecular Sciences, Experimental
and Clinical
XXXVI cycle
BIO/14

**THE IMPACT OF CLEC4A4 DEFICIENCY ON
CARDIOMETABOLIC DISEASES**

Supervisor: Prof. Giuseppe Danilo Norata

PhD coordinator: Prof. Giuseppe Danilo Norata

PhD Thesis of:
Rossella Bellini
R12944

A.A. 2022/2023

TABLE OF CONTENTS

ITALIAN ABSTRACT.....	5
ENGLISH ABSTRACT.....	7
INTRODUCTION	9
1. Cardiometabolic diseases	10
1.1 A focus on obesity	10
1.1.1 The insulin pathway and type 2 diabetes	11
1.1.2 Liver-adipose tissue-skeletal muscle axis during obesity	12
1.2 A focus on atherosclerosis	13
1.2.1 Cholesterol accumulation and Lipid Transport System.....	14
1.2.2 The atherosclerotic plaque development	14
1.2.3 Hints of pharmacological treatments for atherosclerosis	16
2. The immune system in cardiometabolic diseases	17
2.1. The immune cells and obesity crosstalk.....	17
2.1.1. Adipose Tissue and immune cells	18
2.1.2. Liver and immune cells	19
2.1.3. Pancreas and immune cells	20
2.1.4. Hints of pharmacological treatments for obesity-related immune response	21
2.2. The immune cells and atherosclerosis crosstalk	22
2.2.1. Innate and adaptive immune responses in atherosclerosis.....	23
2.2.2. Immune organs related to atherosclerosis: the bone marrow-thymus-lymph nodes axis.....	24
2.2.3. Hints of pharmacological treatments for atherosclerosis: focus on the immune response.....	26
3. C-type lectin receptors	27
3.1. C-type lectin receptor expression and function	28
3.2. C-type lectin Receptors in cardiometabolic diseases	29
3.3. DCIR/Clec4a expression in humans and mice	29
3.3.1. What we know about DCIR2/ <i>Clec4a4</i>	30
AIM OF THE THESIS	32
MATERIALS AND METHODS	35
1. Mouse models	36
1.1. Atherosclerosis experiments	36
1.1.1. Evaluation of <i>Clec4a4</i> deficiency on atherosclerosis background	37
1.1.2. Phenotypic evaluation of new double KO (DKO) lines	37
1.1.3. Confirmation of the KO model	38
1.1.4. Mice sacrifice and tissue collection.....	38

1.2. Obesity experiments	38
1.2.1. Mice sacrifice.....	39
1.2.2. Tissue collection and storing.....	39
1.3 Atherosclerosis and obesity experimental setup	39
1.4. Sample size calculation	40
2. Genotyping	40
2.1. DNA extraction	40
2.2. The PCR protocol.....	41
3. Glucose tolerance and insulin tolerance test.....	42
4. Plasma analysis	43
4.1. Plasma isolation	43
4.2. Insulin plasma quantification (ELISA).....	44
4.3. Plasma cholesterol and triglyceride measurements	44
4.4. Fast protein liquid chromatography (FPLC).....	44
5. Histological analysis	45
5.1. Tissue fixation and paraffin embedding.....	45
5.2. Haematoxylin and eosin (H&E) staining.....	45
a. Quantification of atheroma on aortic sinus	45
b. Quantification of lipid droplets on liver	46
c. Quantification of adipocytes on adipose tissues.....	46
5.3. Masson's trichrome staining.....	46
a. Quantification of fibrosis on aortic plaque.....	46
5.4. Immunofluorescence	47
6. RNA extraction and quantitative real-time PCR	47
6.1. RNA extraction and quantification.....	47
6.2. RNA Reverse Transcription and qPCR.....	48
7. Flow cytometry.....	48
7.1. Blood and Tissue Processing.....	49
a. Blood	49
b. Bone marrow	49
c. Thymus and cardiac lymph nodes	49
d. Spleen.....	50
f. VAT.....	50
7.2. Antibody staining for flow cytometry	51
8. Statistical analysis.....	51
RESULTS	52
1. Clec4a4 deficiency in atherosclerosis: focus on ApoE ^{-/-} and Ldlr ^{-/-} background	53
1.1. Evaluation of Clec4a4 deficiency on Ldlr ^{-/-} or ApoE ^{-/-} under standard diet	53
1.1.1. Body and organ weight of ApoE ^{-/-} and Ldlr ^{-/-} male and female mice	53
1.1.2. Aortic plaque and circulating lipid level analysis.....	53

1.1.3.	The immunophenotype of lymphoid organs:	54
1.1.4.	The Immunophenotype of the circulating immune populations.....	55
1.2.	Evaluation of <i>Clec4a4</i> deficiency on WTD-fed male mice on <i>ApoE^{-/-}</i> background	56
1.2.1.	Evaluation of the total body and organ weight.....	56
1.2.2.	Aortic plaque and circulating lipid level analysis.....	56
1.2.3.	Evaluation of the hepatic phenotype	56
1.2.4.	The immunophenotype of circulating immune populations	57
1.2.5.	The immunophenotype of lymphoid organs: a focus on bone marrow, thymus and cardiac LNs	57
1.3.	Evaluation of <i>Clec4a4</i> deficiency on WTD-fed male mice on <i>Ldlr^{-/-}</i> background	58
1.3.1.	Body and organ weight of WTD-fed mice on <i>Ldlr^{-/-}</i> background.....	58
1.3.2.	Atherosclerotic plaque phenotype and circulating lipid level analysis	58
1.3.3.	Evaluation of the hepatic phenotype	59
1.3.4.	The immunophenotype of circulating immune populations	59
1.3.5.	The immunophenotype of lymphoid organs: a focus on bone marrow, thymus and cLNs	59
1.4.	Evaluation of <i>Clec4a4</i> deficiency on WTD- fed female mice on <i>ApoE^{-/-}</i> and <i>Ldlr^{-/-}</i> backgrounds	60
2.	The role of <i>Clec4a4</i> in HFD-induced obesity	60
2.1.	Body and organ weight of HFD-fed male mice	60
2.2.	Evaluation of the hepatic immune-metabolic phenotype	61
2.3.	Analysis of the glucose metabolism of HFD-fed male mice	61
2.4.	Evaluation of the visceral and subcutaneous adipose tissue phenotype	62
2.5.	The immunophenotype of the bone marrow	63
2.6.	The immunophenotype of secondary lymphoid: focus on Pp, mLNs and spleen.....	64
	DISCUSSION AND CONCLUSIONS	65
	FIGURES.....	72
	REFERENCES	108
	APPENDIX.....	117
	APPENDIX I – Composition of Western-Type Diet (WTD) and High-Fat Diet (HFD):	118
	APPENDIX II – Mice models	120
	APPENDIX III – Experimental setup.....	122
	APPENDIX IV - List of antibodies for immunofluorescence of aortic sections .	124
	APPENDIX V - qPCR primer sequences	125
	APPENDIX VI - Antibodies used in flow cytometry.	126
	APPENDIX VII - Gating strategy of flow cytometry immunophenotype.....	129

APPENDIX VIII – Total body weight and organ weight of male and female mice
on atherosclerosis backgrounds: ChowD- and WTD feeding 134
ACTIVITY REPORT 137

ITALIAN ABSTRACT

Introduzione e scopo

Dendritic cell immunoreceptor 2 (DCIR2 o *Clec4a4*) è un recettore prevalentemente espresso dalle cellule dendritiche di tipo 2 e modula la risposta immunitaria dei linfociti T. È ormai risaputo che nelle patologie metaboliche croniche la risposta immunitaria svolge un ruolo importante, non solo nell'eziopatogenesi, ma anche nel mantenimento della condizione patologica. Per questo motivo, abbiamo deciso di studiare il ruolo di *Clec4a4* in due patologie endemiche caratterizzate da alterazioni di carattere metabolico come l'aterosclerosi e l'obesità.

Metodi

Per lo studio dell'aterosclerosi, modelli murini *Clec4a4*^{-/-} e WT sono stati generati su background aterogeno *Ldlr*^{-/-} o *ApoE*^{-/-} e successivamente sottoposti a dieta ipercolesterolemica per indurre la formazione della placca aterosclerotica. Il fenotipo di questi modelli è stato valutato attraverso analisi istologiche, citofluorimetriche e il dosaggio lipidico.

L'effetto del recettore *Clec4a4* sullo sviluppo dell'obesità è stato valutato sui modelli *Clec4a4*^{-/-} e WT sottoposti ad una dieta ad alto contenuto di grassi per 20 settimane. Sono stati esaminati parametri quali il peso e l'assunzione di cibo, il metabolismo glucidico e, successivamente, è stato valutato il profilo lipidico circolante, parallelamente a un'indagine immuno-fenotipica e istologica.

Risultati

I modelli sperimentali di aterosclerosi deficitari del recettore *Clec4a4* hanno mostrato una significativa diminuzione della formazione della placca aterosclerotica (-26% e -49%, rispettivamente su background *ApoE*^{-/-} e *Ldlr*^{-/-}; $p < 0.05$) e una diminuzione dei neutrofili circolanti (-59% e -47%, rispettivamente su background *ApoE*^{-/-} e *Ldlr*^{-/-}; $p < 0.05$). Seppur queste evidenze vadano di pari passo nei due modelli di aterosclerosi, il modello doppio KO su background *Ldlr*^{-/-} ha

mostrato anche una diminuzione dei lipidi circolanti (-59% di colesterolo e -33% di trigliceridi plasmatici; $p < 0.01$, $p < 0.05$ rispettivamente).

Il modello *Clec4a4*^{-/-} sottoposto per 20 settimane a HFD non ha mostrato segni di alterazione nello sviluppo dell'obesità, così come della composizione immunitaria degli organi linfoidi primari e secondari, nel parenchima epatico e adiposo. Unica eccezione è rappresentata dal fegato, nel quale è stata osservata una diminuzione della componente dendritica (-35%, $p < 0.05$) con effetto su una sottopopolazione specifica di linfociti T, i Th2, ma non sui markers infiammatori analizzati nel tessuto epatico. In parallelo, gli esperimenti *in vivo* hanno mostrato una maggior resistenza al glucosio del modello *Clec4a4*^{-/-} rispetto ai controlli WT.

Conclusione

I nostri dati hanno evidenziato un ruolo ridondante di *Clec4a4* nello sviluppo dell'obesità, mentre nel contesto aterosclerotico una forte influenza di questo recettore nello sviluppo della placca aterosclerotica con un maggior effetto a carico dei neutrofili circolanti. Sarà ulteriore oggetto di studio l'analisi del meccanismo alla base di questa alterazione.

ENGLISH ABSTRACT

Introduction and aim

Dendritic cell immunoreceptor 2 (DCIR2 or *Clec4a4*) is a C-type lectin receptor mainly expressed by type 2 dendritic cells involved in T lymphocyte training. Since the strong involvement of the immune system in chronic cardiometabolic diseases, we decided to deep investigate the contribution of *Clec4a4* in the development of atherosclerosis and obesity.

Material and methods

Clec4a4^{-/-} mice were crossed with *Ldlr*^{-/-} or *ApoE*^{-/-} mice to generate double or single KO on atherogenic backgrounds. Male and female littermates were fed for 12 weeks with a Western-Type Diet (WTD) to exacerbate atherosclerosis and histological and flow cytometry analysis were performed. Obesity and metabolic syndrome were induced by feeding *Clec4a4*^{-/-} and WT male mice with a High-Fat Diet (HFD) for 20 weeks and *in vivo* glucose and insulin tolerance test and *ex vivo* histological and flow cytometry analysis were performed.

Results

Clec4a4 showed a proatherogenic role (-26% and -49% aortic plaque in DKO mice compared to *ApoE*^{-/-} and *Ldlr*^{-/-} respectively; $p < 0.05$) with a major effect on circulating neutrophils on male mice (-59% and -47% on *ApoE*^{-/-} and *Ldlr*^{-/-} background respectively; $p < 0.05$). Moreover, *Clec4a4*^{-/-} male mice on *Ldlr*^{-/-} background revealed an impact on plasma lipid distribution (-59% of cholesterol and -33% of triglycerides; $p < 0.01$, $p < 0.05$ respectively), not observed on *ApoE*^{-/-} background.

In parallel, the data from the obese model showed a comparable immunophenotype between *Clec4a4*^{-/-} and WT mice after 20 weeks of diet, parallel to a similar hepatic and adipose parenchyma. The exception was represented by the distribution of immune cells within the liver which revealed a significant decrease of dendritic cells (-35%, $p < 0.05$) mainly driven by

conventional type 2 DCs impacting on Th2 polarization. Furthermore, *Clec4a4*^{-/-} mice displayed alterations in the systemic metabolism with glucose intolerance without impacting downstream insulin pathways.

Conclusions

Our data showed a redundant role of *Clec4a4* in the development of obesity, while a meaningless impact on hepatic dendritic cell distribution and glucose resistance. Our atherosclerosis experimental models showed a proatherogenic role for *Clec4a4*, with a major impact on circulating neutrophil amount. Future studies will be aimed at understanding the molecular mechanisms existing between this receptor and atherosclerosis.

INTRODUCTION

1. Cardiometabolic diseases

Cardiometabolic diseases are silent disorders that develop within years and, if left untreated, progress to worse and visible conditions. Among them, obesity and atherosclerosis have reached epidemic proportions worldwide, affecting people of all ages and being primarily detected when symptoms emerge (1). Notably, after avoiding premature death, people now face the repercussions of atherosclerosis, such as myocardial infarction, ischemic cardiomyopathy, strokes, and peripheral arterial disorders, which account for the majority of deaths globally (2) (Fig.1).

Particularly, while atherosclerosis anticipates acute coronary syndromes, obesity predicts type 2 diabetes mellitus (T2DM) when insufficiency of β cells occurs (3). For this reason, researchers are attempting to uncover a comprehensive collection of predictors capable of identifying at-risk individuals and delaying or preventing the onset of these diseases using pharmacological therapies in conjunction with weight loss and physical activity (3). Indeed, excess weight, obesity, insulin resistance, hyperglycaemia, dyslipoproteinemia, and hypertension are currently known risk factors of cardiometabolic diseases (1).

1.1 A focus on obesity

Obesity is a multifactorial condition primarily caused by an abnormal energy balance, which is then stored as triglycerides in adipocytes increasing fat mass, with the side consequences of decreased blood flow and oxygen availability within tissues. The obese condition is clinically determined by the body mass index (BMI), which reflects the ratio of a person's height to weight and divides the obese growth into stages. Obese people have a BMI of more than 30 kg/m² and have an immune response that, as part of the metabolic syndrome, increases the risk of diseases such as type 2 diabetes, hypertension, cardiovascular disease, asthma, and cancer (4).

Obesity is related to a variety of factors that could impact people of all ages. The initial point might be described as a changed nutrition, overeating, or poor

nutrition with high-calorie foods. Other risk factors, such as stress, age, lack of physical activity, and changed hormones, can exacerbate this complex condition, and contribute to fat buildup and obesity (Fig.2). It is concerning that the number of obese people has tripled in the previous 40 years, and that, while it initially afflicted only underdeveloped countries, it is now widespread and affects people of all ages. The repercussions of this pathology affect various organs, including the heart, liver, and kidneys, and it can lead to serious disorders such as high blood pressure, cancer, and diabetes (5). Particularly, the transition from obesity to T2DM is characterized by a particular situation of insulin resistance (6).

1.1.1 The insulin pathway and type 2 diabetes

Type 2 diabetes (T2D) is a multifactorial disease caused by a combination of inherited and environmental factors. This condition is linked to hyperglycaemia and is characterized by altered insulin secretion and/or action and β cell dysfunction, resulting in inadequate insulin production for glycaemic balance (6,7).

Insulin is a hormone that primarily regulates carbohydrate, protein, and fat metabolism by controlling glucose absorption from the circulation (6). This helps us understand why insulin production and secretion are so tightly controlled. Within the pancreas, under fasting conditions, α cells produce glucagon which keeps glucose levels in the blood within a normal range. Following feeding, the glucose binds to the GLUT receptors on cells, activating an intracellular pathway that results in the secretion of insulin-enriched granules and the synthesis of insulin. Particularly, circulating glucose is specifically taken up by GLUT2 insulin-independent receptors on the cell surface, initiating glycolysis and ATP generation. Increased intracellular ATP causes K^+ channels to close, depolarizing the cellular membrane. This causes Ca^{2+} voltage-dependent ion channels to open, allowing Ca^{2+} uptake from the extracellular area. The increase of intracellular Ca^{2+} leads to insulin granules release (Fig.3). Insulin is produced as pre-proinsulin, then

cleaved, releasing a small peptide in the circulation, the C peptide and, finally, the insulin is in its mature form ready to be stored or released (8).

The chronic increase and accumulation of fat alters glucose circulating levels that cannot be contrasted by insulin production, resulting in a condition in which the cells of the organism become insulin intolerant, such as not responding to insulin levels. In response, β pancreatic cells increase insulin synthesis to compensate for the increase in circulating glucose levels to the point of cell exhaustion and dysfunction. In this case, glycaemic levels rise, as a result of uncontrolled circulating glucose levels parallel to insulin resistance (IR), and medication should follow (5). Next, compensatory hyperinsulinemia emerges, consisting of chronically elevated insulin levels, that rise further after a glycaemic load (9). As a consequence, patients with T2DM and IR have altered lipid metabolism, deposition, and concentration in the blood and target organs (6).

1.1.2 Liver-adipose tissue-skeletal muscle axis during obesity

Obesity develops in parallel to a change in the composition or quantity of nutrients available, resulting in modifications in the cellular signature, which affects the distribution and function of the cells themselves, leading to the expansion of adipose tissue (AT), particularly white adipose tissue (4). However, since the AT is not the only organ interested by these alterations, one should mention its tightly collaboration with the liver and the skeletal muscle. Indeed, since the visceral adipose tissue (VAT) is drained by the portal vein, hypertrophic adipocytes expose the liver to high concentrations of fatty acids (FAs) and glycerol, resulting in an impaired liver metabolism with reduced hepatic insulin clearance – contributing to hyper-insulinemia – parallel to the increased production of triglyceride-rich lipoproteins and hepatic glucose (10). According to this, an increased influx of free FAs into the liver promotes the transcription of limiting enzymes of triglyceride synthesis, contributing to hypertriglyceridemia development (10). Excess of hepatic fat production (i.e., *de novo* lipogenesis) in the high-risk metabolic phenotype may represent an early common pathway of

non-alcoholic fatty liver disease (NAFLD), atherogenic dyslipidaemia, pancreatic β cell dysfunction, insulin resistance, and concomitant atherosclerotic cardiovascular disease (ASCVD) risk (9). This explains why fatty liver disease severity is strongly related to typical metabolic syndrome components, such as central obesity, insulin resistance, elevated insulin levels, increased triglycerides, high blood sugar levels, or altered glucagon secretion (11).

This situation gets worse when obese people have impaired skeletal muscle lipid clearance, which, along with higher FA release from adipose tissue, results in hyperlipidemia and a greater dependence on the liver for FA clearance (6). Furthermore, the relationship between the AT and the liver is strengthened by the AT production of adipokines, such as adiponectin, TNF- α , resistin, and IL-6, all of which contribute to the disease (6). They have diverse roles, with adiponectin increasing insulin sensitivity and resistin having insulin-antagonistic properties (6).

1.2 A focus on atherosclerosis

Atherosclerosis is a silent lipid-driven disease that develops over time and is characterized by the accumulation of low-density lipoproteins (LDLs), residual lipoprotein particles, and immune cells in focal areas of medium and large arteries making atherosclerosis visible once the structure ruptures and the thrombus forms (12). Predilection sites for lipid entry and retention in the subendothelial area are seen at artery branch points with disrupted, non-laminar flow (13). It is worth noting that, while lipids surely contribute to atherosclerosis, this is accompanied by an inflammatory response that orchestrates the disease's course and outcome (13) and is positively correlated with other risk factors besides LDL-C levels, such as age, smoking, hypertension, and inflammatory biomarkers (14).

1.2.1 Cholesterol accumulation and Lipid Transport System

Cholesterol is necessary for the structure of the cell and serves as a substrate for other steroids, including bile acids, vitamin D, sex, and adrenocortical hormones. The intestine and the liver play critical roles in the cholesterol homeostasis. While the first absorbs dietary-intake cholesterol and FAs, then packaged in chylomicrons, the latter combining cholesterol and triglycerides with apolipoproteins to form very low-density lipoproteins (VLDLs), subsequently released into the plasma. Thus, chylomicrons and VLDLs are both triglyceride-rich lipoproteins with the difference that the former are produced in enterocytes in response to dietary intake, whereas VLDLs are packaged within the liver (15). Furthermore, studies highlighted a link between elevated plasma triglyceride levels and atherosclerotic cardiovascular risk (15).

Once triglyceride content reduces, VLDLs convert into LDL particles composed of a core of cholesterol esters and triglycerides surrounded by phospholipid, cholesterol, and the Apolipoprotein B (ApoB) -100 (16). Once internalized, lipoproteins are digested by specialized lysosomal hydrolases into free cholesterol and free fatty acids (FFAs). These are energy sources that can be used immediately or stored in intracellular lipid droplets (15). However, high plasma LDL-C levels have been identified as a risk factor for cardiovascular events, making it the primary target to dampen cardiovascular risk. On the contrary, high density lipoprotein (HDL) cholesterol has been connected to athero- and cardioprotective properties (15,17), including enhancing cholesterol efflux from foam cells and reversing cholesterol transport in general, as well as protecting LDL from oxidative damage (15) (Fig.4).

1.2.2. The atherosclerotic plaque development

As anticipated, atherosclerosis is the result of lipid accumulation, inflammatory response, cell death, and fibrosis inside the arterial wall, where LDL and HDL levels play a major role. Lipoproteins are macroparticles able to transport lipids throughout the body and, particularly, LDL is in charge of

delivering cholesterol to peripheral tissues. Furthermore, it accumulates within the arterial wall beneath impaired endothelium, alongside VLDL and chylomicron remnant particles, thus starting the process defined as atherosclerosis (Fig.5).

The first stage of atherosclerotic lesion development is characterized by endothelial dysfunction, which is characterized by reduced endothelial barrier integrity and causes the release of proinflammatory cytokines, chemokines, and reactive oxygen species (ROS). Additionally, it promotes pro-inflammatory leukocyte recruitment, adhesion, and subsequent transmigration into the subendothelial region.

Subsequently, as LDL accumulates within the intima of the arteries, endothelial cells activate, recruiting blood leukocytes. Among them, mononuclear phagocytes proliferate and phagocytose lipids becoming foam cells, while the adaptive immune response interacts with the innate one, resulting in a proinflammatory cytokine production. During the early phases, LDL particles are retained and oxidized in the subendothelial vascular wall, becoming part of the damage-associated molecular patterns (DAMPs) class. This results in an unsuccessful resolution of lesional inflammation, mainly driven by a decrease of specialized pre-resolving mediators (SPMs) and the proinflammatory lipids such as leukotrienes paralleled by the shift from the anti-inflammatory M2-like to proinflammatory M1-like macrophages.

In advanced phases, arterial smooth muscle cells migrate to the intima layer, where they proliferate and differentiate into macrophage-like cells. The atheroma is thus composed of lipids surrounded by a fibrous cap that determines the stability of the atherosclerotic lesion, while a layer of endothelial cells persists on the atheroma's surface, allowing the interaction with the bloodstream. The acute event takes place when the thickness of the fibrous cap - determined by the production of collagen and prevented by the presence of

collagenases from inflammatory cells – results in thrombosis or blood clot formation.

1.2.3. Hints of pharmacological treatments for atherosclerosis

Statins are the first-line drug because of their high efficacy and safety in lowering LDL cholesterol; however, a combined drug therapy is advised in those patients with severely elevated cholesterol levels and a poor response to statin alone. Between lipid-lowering medications, the addition of Ezetimibe or a Proprotein Convertase Subtilisin/Kexin type 9 (PCSK9) inhibitor to statin therapy has been found to improve cardiovascular outcomes by acting on cholesterol absorption, hepatic LDL-c absorption, and cholesterol production, respectively. Recently, Inclisiran, a short interfering RNA, has been approved as the most sophisticated non-antibody approach against PCSK9 (15).

As represented in Fig. 6, different targets have been identified throughout time, such as bile acid sequestrants, which inhibit bile acid reabsorption, or Bempedoic acid, which interferes with the cholesterol synthesis process. It is even attempting to reduce apolipoproteins, such as ApoB100, a target of the ASO Mipomersen or impacting chylomicron and VLDL packaging by blocking microsomal triglyceride transfer protein (MTP) with Lomitapide (15).

Even though lifestyle changes can reduce plasma triglycerides (TG), as well as statins in addition to Fibrates, Niacin and Omega-3 fatty acids, other triglyceride-lowering candidates have been investigated, such as Volanesorsen, which reduces ApoC-III present on the cell surface of triglyceride-rich lipoproteins and facilitates Lipoprotein lipase (LPL) -mediated TG hydrolysis. Moreover, Evinacumab targeting Angiopoietin-like 3 (ANGPTL3), and Pradigastat which can lower fasting and postprandial triglycerides as well as chylomicron levels, are promising treatment in the lower TG category (15).

Considering the HDL rising approaches, therapeutic strategies for raising HDL levels include Niacin - inhibiting ATP synthase β -chain (ATPase-B1) - Cholesteryl ester transfer protein (CETP) inhibitors and recombinant HDL strategies (15).

2. The immune system in cardiometabolic diseases

The immune system represents the defence of our organisms and is composed, among others, of immune cells. The immune response acts on multiple levels, as a first line of defence through innate immunity, as well as secondary defence of formerly encountered pathogens through the adaptive immune system. These two systems have different origins. The first is the most ancient and well-preserved among species, capable of recognizing a wide range of pathogens, converting them into minute particles known as antigens, and then presenting them to the adaptive immune system. This second one is more advanced, present only in the most evolved species and capable of preserving a “memory” of the antigen interaction to act faster in future encounters (18).

The lymphatic system is a group of organs, vessels, and tissues that protects from infection and keep a healthy balance of fluids throughout the body. Recently, it has been demonstrated that dietary changes and adipose tissue accumulation have an impact on the lymphatic system. This is in line with obese patients showing impaired clearance of macromolecules and developing lymphedema, as well as atherosclerosis experimental models revealing progressive lymphatic dysfunction and resulting in tissue swelling, lymphatic vessel leakage, and impaired immune cell trafficking (18).

2.1. The immune cells and obesity crosstalk

While it is widely accepted that obesity is connected with insulin resistance and diabetes, the role of the immune system in this disease remains a hotly disputed topic. Previously, obesity was linked to immune dysfunctions (19), with an overall increase in leukocyte numbers. Evidence pointed to a relationship

between adipose tissue (AT) and the immune system, namely AT-resident macrophages and their phenotype during obesity development. These cells increase low-grade chronic inflammation by producing pro-inflammatory mediators such as TNF- α , IL-6, and IL-1 β , which contribute to insulin resistance and T2DM development (20).

However, as previously observed, obesity is the result of different organs dysfunction, namely adipose tissue, liver and endocrine pancreas, in which the altered immune response plays a pivotal role.

2.1.1. Adipose Tissue and immune cells

Given the high concentration of leukocytes in the AT, this has been classified as a secondary immune organ in which resident immune cells control immune responses, making the AT one of the most important immunometabolic modulators in the body (4). The connection between AT and immune cells is so tight that the composition of immune populations changes during obesity, leading to increased adiposity (21). For this reason, researchers have focused their attention on the role of innate and adaptive immune responses in the development of obesity, with a particular emphasis on the activation of innate immunity cells and the subsequent control of adaptive response - governed by T lymphocytes (6).

Dysfunctional AT is distinguished by a rise in macrophage and lymphocyte infiltration, as well as an increase in the abundance of senescent cells. They release fatty acids as well as proinflammatory and chemotactic compounds that promote fat accumulation and chronic inflammation (5,9) and IR (22,23). Moreover, AT-infiltrating myeloid cells produce CD26 (also known as dipeptidyl-peptidase IV – DPP4), an aminopeptidase that inhibits the action of incretin peptides (glucagon-like peptide-1 and glucose-dependent insulinotropic polypeptide), hence reducing insulin secretion. In obese humans and mice, this promotes a pro-inflammatory environment, leading to insulin resistance (24).

Adipose tissue also produces adiponectin, an adipokine implicated in insulin sensitization, atherosclerotic plaque prevention, and metabolism regulation,

which decreases in obese models (24). Lower adiponectin levels in obese people are associated with a pro-inflammatory profile in the bone marrow, which is defined by the reduced proliferation of hematopoietic stem and progenitor cells (HSPCs) and increased TNF generation by bone marrow-derived macrophages in mice (25).

Moreover, leptin, another adipokine produced by AT, has been found to increase during obesity and regulate immune function by acting directly on monocytes and natural killer (NK) cells (19,26).

a. Dendritic cell in the adipose tissue

Intriguingly, both obese mice and diabetics have increased toll like receptor 4 (TLR4) expression in adipocytes, hepatocytes, muscles, and hypothalamus, with a negative impact on insulin sensitivity (6). TLR4 plays a fundamental role in pathogen recognition and activation of innate immunity, particularly antigen-presenting cells (APCs), namely DCs and macrophages (27).

While under physiological conditions DCs have a tolerogenic signature – characterized by Wnt/-catenin pathway in cDC1 and PPAR in cDC2 – it has been revealed over the years that a persistent over-nutrition, as well as a deletion of these pathways, is correlated with increased visceral AT-resident DC maturation and T cell recruitment. This results in an increased pre-adipocyte differentiation towards a pro-inflammatory state which accelerates obesity-induced chronic inflammation and insulin resistance (28,29). Of note, it has been observed that animals without DCs had fewer AT and hepatic macrophages, making them resistant to weight gain and metabolic abnormalities (30) while reducing insulin resistance (31,32).

2.1.2. Liver and immune cells

Obesity-related visceral fat accumulation predominantly affects the liver, a vital organ responsible for both cholesterol synthesis and fat storage. This excessive lipid buildup in the liver causes non-alcoholic fatty liver disease (NAFLD). This disease is correlated with type 2 diabetes mellitus, dyslipidaemia,

cardiovascular disease, and obesity and is defined by the presence of excess liver fat, inflammation, and cell destruction, and can evolve in non-alcoholic steatohepatitis (NASH). An initial phase, induced by an imbalance between TG acquisition and depletion, develops in a second phase, defined by increased hepatocyte stress and inflammation via pro-inflammatory cytokine production, leading to chronic inflammation and increased expression of chemokine receptors, resulting in increased leukocyte hepatic infiltration (33) (Fig.7).

Among other immune cells, hepatic DCs are physiologically present in an immature state, allowing for the maintenance of liver tolerance via IL-10-dependent decreased T cell proliferation accompanied by T helper (Th)₂ and/or Treg polarization. Aside from DCs, there are other hepatic antigen-presenting cells (APCs) involved in antigen presentation, including resident hepatocytes and non-parenchymal cells such as Liver sinusoidal endothelial cell (LSECs), Kupffer cells, and hepatic stellate cells (HSCs), which promote adaptive immune tolerance in the liver (34).

However, the role of DCs during obesity is more difficult to grasp, because on one hand they may exert their pro-inflammatory activity as APCs, and on the other a decreased antigen presentation due to altered DC function was observed in obesity, which makes the DC phenotype and function during obesity poorly understood (33).

2.1.3. Pancreas and immune cells

Various factors influence β cell function, ranging from changed metabolic pathways during development to oxidative stress (35), not to mention the impact of the immune system (7). HFD-fed mice develop islet inflammation (36) which is worsened by the elevated levels of FFAs, TG, and cholesterol, all of which lead to insulin resistance and the production of reactive oxygen species (ROS) (36), recruiting infiltration of immune cells closely to β cells (37). Pancreatic islet inflammation following obesity comes with increased production

of inflammatory cytokines and chemokines such as IL-1 β , TNF- α , and CCL2, contributing to cell malfunction and progression to type 2 diabetes (38,39). This occurs most frequently in the early stages of diabetes development where low-grade inflammation intensified by macrophage activity and adipocyte-produced inflammatory intermediates injure pancreatic β cells, resulting in insufficient insulin synthesis, as shown in the form of hyperglycaemia (39).

Antigen-presenting cells are found in pancreatic islets and, although their function in the pancreas is barely known, it has been observed an increase of TLR4 expression in both obese mice and diabetics, negatively influencing insulin sensitivity (40).

Indeed, pro-inflammatory cytokines produced by pancreas-resident innate and adaptive immune cells affect insulin secretion both directly and indirectly, contributing to β cell dysfunction and T2D-related complications (39) (Fig.8).

2.1.4. Hints of pharmacological treatments for obesity-related immune response

Since the inflammatory response following lipid accumulation in metabolic tissue leads to IR and cell malfunction, anti-inflammatory techniques have been proposed as a therapeutic option for T2D prevention (7). Indeed, "one size does not fit all" refers to the fact that treating obesity is extremely difficult. The initial goal is to lose weight and it should be accomplished by a combination of methods, including lifestyle changes, behavioural and pharmacological therapy, and/or bariatric surgery (41).

Metformin is one of the most used medicines for the treatment of T2D (7), improving insulin sensitivity and lowering blood glucose levels while also acting as an anti-inflammatory drug, suppressing NF- κ B (42), raising Tregs, and decreasing Th17 cells (43). Moreover, DPP4 inhibitors and glucagon-like peptide 1 (GLP-1) receptor agonists work increasing insulin production and have also anti-inflammatory properties, decreasing TNF- α , IL-6, and IL-1 β production in white AT

as well as inflammatory macrophages (44,45). Furthermore, to prevent β cells dysfunction, the IL-1 signalling pathway has been inhibited by IL-1 receptor antagonist (IL-1Ra), resulting in enhanced insulin secretion and improved glycemia in T2D patients (46).

2.2. ***The immune cells and atherosclerosis crosstalk***

Although arterial wall macrophage proliferation has been associated with increased plaque development in advanced atherosclerotic lesions, the starting point of this disease is the activation of the endothelium which triggers leukocyte recruitment within the vascular intima followed by *in situ* monocyte differentiation into macrophages. Internalizing and collecting lipoproteins, macrophages maintain inflammation and promote plaque development. The accumulation of lipids and immune cells grows over time, turning macrophages into foam cells loaded with lipid droplets. Furthermore, in advanced plaques, macrophages, smooth muscle cells, and foam cells undergo apoptosis and necrosis, resulting in the formation of the necrotic core within the atheroma. This exacerbates the inflammatory cell build-up and inhibits the clearance of dead cells (efferocytosis), increasing plaque size and vulnerability (15). While the stability of the plaque depends on the thickness of the fibrous cap, soluble erosive agents such as matrix proteases and immune cell cytokines can weaken this structure, resulting in plaque rupture and occlusion of the downstream artery (47,48).

M2 macrophages, on the other hand, play an anti-inflammatory and atheroprotective role by inhibiting cell recruitment and tissue remodelling, resulting in reduced foam cell production and increased plaque stability (48). Furthermore, data emphasized the significance of the macrophage subset ratio, which is altered within atheroma in favour of M1 pro-inflammatory ones, accelerating plaque development, necrotic core formation, and plaque vulnerability. The pro-inflammatory and anti-inflammatory composition of

intraplaque macrophages can be used to predict plaque progression/instability or regression (49).

2.2.1. Innate and adaptive immune responses in atherosclerosis

Monocytes, particularly pro-inflammatory Ly6C^{high} monocytes, are attracted within the atherosclerotic plaque and, by releasing pro-inflammatory molecules such as TNF- α , aid in the progression of atherosclerosis. This was true even for macrophages, which produce reactive oxygen species (ROS) and inflammatory cytokines and chemokines such as TNF- α , IL-1, IL-6, IL-8, and TGF- β , promoting B and T lymphocyte recruitment within the plaque. In line with this, it has been demonstrated that by blocking chemoattractant molecules such as CCL2, CXCR1, CCR5, and M-CSF in ApoE^{-/-} mice, atherogenesis can be reduced (48). Moreover, mice fed a cholesterol-enriched diet displayed inflammatory rewiring of monocytes and bone marrow progenitors, as well as increased immune response and circulating neutrophils, whereas neutrophil reduction resulted in small lesions and macrophage accumulation (13).

In addition to the LDL receptor (LDLr), which is responsible for LDL uptake and whose expression is regulated by cytoplasmic free cholesterol levels, scavenger receptors such as A (SR-A), CD36, and lectin-like ox-LDL receptor- 1 (LOX- 1) are responsible for modified LDL uptake. Indeed, LDL particles undergo various alterations inside the blood flow and vascular wall - including oxidation, enzymatic processing, desialylation, and aggregation - that affect their size, density, and chemical characteristics, resulting in the formation of oxidized LDL (oxLDL) (50). Because their uptake is unregulated and they accumulate in phagocytic cells, oxLDL are strong inducers of foam cells (15). Thus, in early atherosclerotic lesions, DCs and macrophages both contribute to plaque foam cell pools by using scavenger receptors to uptake modified lipoproteins, then becoming lipid-laden cells (49).

OxLDL can operate as DAMPs, activate TLRs, and enhance the plaque's inflammatory state, resulting in decreased cholesterol efflux, decreased efferocytosis, and increased cell death driven by both macrophages and dendritic cells. This involves not only the innate immunity but even the adaptive one. Indeed, after being processed by innate immune cells, oxLDL-related antigens are presented to adaptive immune cells - such as T lymphocytes - in secondary lymphoid organs or even within the atheroma itself, resulting in the production of a variety of cytokines and inflammation mediators that worsen the plaque progression (48).

2.2.2. Immune organs related to atherosclerosis: the bone marrow-thymus-lymph nodes axis

Since the hyperinflammatory nature of monocyte-derived macrophages within the atherosclerotic plaque, the significance of activated innate immune cells in the development of atherosclerotic plaques has been deeply investigated. The presence of innate and adaptive immune cells within the aortic plaque greatly influences the course of atherosclerosis. Classical monocytes are drawn from the circulation by the interplay of CCR2 and CCL2, eventually reaching the plaque where they develop into macrophages or monocyte-derived DCs. They highlighted the inflammatory reprogramming of hematopoietic stem cells (HSCs) within the bone marrow during the development of atherogenesis in patients with CAD, which was characterized by a spread towards the myeloid lineage, particularly neutrophils, and monocytes (51). This was previously observed in atherosclerosis animal models, which showed altered myelopoiesis associated with accumulation of cholesterol in progenitors and accelerated atherosclerosis (52). Through the lymphatic flow, immune cells reach the mediastinal (or cardiac) lymph nodes, where antigen presentation take place (53). Moreover, lymphatic veins serve an important function in maintaining fluid balance in the body by collecting lymph from peripheral tissues via lymphatic capillaries. As a result, lymph is high in lipoproteins like HDL, immune cells, electrolytes, minerals, and

antibodies. A functional and quantitative study validated the lymphatic system's critical role in removing cholesterol from arterial walls, stressing the critical significance of the lymphatic network in the process of macrophage reverse cholesterol transport (mRCT) (54).

In parallel, it has been proved that changes in the thymus function may play a role in atherogenesis through altering inflammatory responses (55). The thymus is a specialized and critical centre for the production and maturation of T lymphocytes *in vivo*. It activates and facilitates commitment to certain T cell lineages, promotes differentiation, and supports the survival of cells in the thymus within this milieu. Even though the thymus is an organ associated with aging, and that there are quantitative losses in cortical and medullary thymocytes in the aged thymus, research suggests that positive and negative selection mechanisms remain qualitatively intact.

The thymus is both the site of T cell repertoire generation and the site of T cell positive and negative selection, resulting in a diverse repertoire of functional MHC-restricted naive TCR repertoire. The mechanism of thymus function in the progression of atherosclerosis remains unknown. As a result of the imbalance between T cell subsets, changes in the thymus can lead to atherogenesis via an altered immune response of T lymphocytes. Indeed, Th cell development and Treg differentiation can result in a changed environment characterized by pro- (TNF- α , IL-1,8,12, and IFN- γ) or anti-inflammatory (TNF- β , IL-4, and IL-10) cytokines. Thus, the thymus can directly or indirectly influence the aforementioned factors or cells, which may influence the atherosclerotic process (55).

A. Focus on DCs in atherosclerosis

DCs are active players in the link between the innate and adaptive immune systems: they patrol tissues up to the meeting with the antigen, e.g. those formed from altered lipoproteins, which are then presented to T cells. Precursors of dendritic cells (pre-DCs) form in the bone marrow and are subsequently

released into the bloodstream, reach target tissues and develop into XCR1⁺ cDC1 or Sirp1α⁺ cDC2. While the former is focused on the cross-presentation to cytotoxic CD8⁺ T cells, the latter presents exogenous antigens to CD4⁺ T cells, regulating a T helper response towards Th1, Th2, Th17, or Treg lymphocytes (29,48).

Although it is well known that after the recognition of environmental signals, DCs migrate to secondary lymphoid organs and modulate the T cell response, in the shape of T helper cell polarization and tolerance induction (29), in recent years it has been demonstrated that antigen presentation can occur in non-lymphoid tissues as well, implying a central role for DCs in tissue-induced inflammation. Therefore, immature DCs can acquire antigens and present them immediately where they reside, which leads vascular DCs in the adventitia to ingest atherosclerosis-related antigens and then accumulate within the aortic plaque after the maturation (47). Canonically, once activated they express MHC II as well as costimulatory molecules CD80, CD86, and CD83 which allow the antigen presentation to T lymphocytes (29,48), but different subsets with unique roles are present within the atheroma, so that the overall contribution of DCs to atherosclerosis is still a matter of debate (56) (Fig.9).

2.2.3. Hints of pharmacological treatments for atherosclerosis: focus on the immune response

Since the positive correlation observed between atherosclerosis and LDL-C levels, current atherosclerosis treatments, such as statins or inhibitors of the serine protease PCSK9, try to regulate LDL cholesterol levels in the blood (57). However, a dampening of the immune response is under study, as in the Canakinumab Anti-inflammatory Thrombosis Outcome Study (CANTOS), which investigates the effects of immunomodulation by IL-1 suppression. This resulted in a successful reduction in major adverse cardiovascular events (MACEs) and offered the first important evidence for the feasibility of treating the

inflammatory component of atherothrombosis. MACEs were also lowered in the Colchicine Cardiovascular Outcomes Trial (COLCOT). However, in both studies, systemic immune suppression caused a higher incidence of infections, leading to an increase in major adverse events and even death. This highlights the importance of developing immune-targeted therapies that are safe, long-lasting, and effective in modulating atherosclerosis. As a result, a thorough understanding of the cellular and molecular processes that drive atherosclerosis is required before selectively targeting specific immune network components that promote atherogenesis (57). Now, immunomodulatory therapeutics in cardiovascular disease are being explored, such as mobilizing Treg cells to reestablish immune tolerance (58) or targeting ApoB (59).

Experimental studies in animal models of atherosclerosis have revealed reprogramming of hematopoietic stem and progenitor cells (HSPCs) in the bone marrow as a cause of the changes in circulating innate immune cells under conditions that predispose to CVD, including hyperlipidemia (60), and stress (61). This opens the door to a new way of thinking about immune cells, with the goal of modulating not only mature immune cells, but also progenitors.

3. C-type lectin receptors

While TLRs help in recognize antigens based on their structure, C-type lectin receptors (CLRs) are unique pattern recognition receptors (PRRs) that recognize antigens based on their sugar moieties, which is facilitated by the presence of a carbohydrate recognition domain (CRD) on their extracellular region (62). Thus, they can distinguish a variety of sugar residues, which results in the activation of the intracellular pathways. They usually present an immunoreceptor tyrosine-based activation or inhibitory motif (ITAM or ITIM), leading to the activation or inhibition of downstream pathways, respectively. (Fig.10) It is worth noting that even activating an ITIM motif, can result in immune cell activation (63). Particularly, the ITIM binds to Src Homology 2 (SH2)

domain-containing protein tyrosine phosphatase (SHP) 1 or 2, which are phosphates that can dephosphorylate signalling molecules (64,65).

3.1. C-type lectin receptor expression and function

When DCs encounter pathogens in an activated environment characterized by activation signals from TLRs and CLRs, the former based on antigenic structure and the latter on carbohydrate components, they mature and migrate to secondary lymphoid organs, where T lymphocyte training occurs. Thus, once engaged, they can generate a specific adaptive immunity to respond to various stimuli (66), as dendritic cell-associated lectin-1 (DCAL) expression is linked to IL-12 production and hence Th1 activation, whereas DCIR2⁺ DCs increase Th2 response through OX40L upregulation (67). Overall, CLRs aid in the internalization of MHC I and II-loaded antigens and modify TLR activation, influencing antigen presentation to T cells, albeit it is unknown whether it can be recycled to the membrane (68). Chemokines, adhesion, and co-stimulatory molecules orchestrate these steps (69), as previously stated.

The different response of DCs depend by the distinct TLR and CLR repertoires, with immature monocyte-derived DCs expressing the mannose receptor (CD206), DEC-205 (CD205), DC-SIGN (CD209), BCDA-2, Dectin-1, DCIR, DCAL-1, C-LEC, and DC-ASGPR/MGL-1 (70). Thus, beyond their role in modulating immune response, all these CLRs are used to identify immune cell subsets (e.g., Clec12A is expressed by cDC1 and plasmacytoid DCs (pDCs), and Dectin is expressed by myeloid cells (70)). Moreover, they can be employed as an indicator of cellular status or by targeting certain CLRs can help in establishing tolerance, such as DEC-205, showing tolerance induction and immune suppression (66).

The pattern of CLR and TLR expression *in vivo* is an uncharted field, but it needs to be developed since the knowledge about the expression of certain sets of antigen recognition receptors is critical for understanding how various DC subsets handle antigens and promote or inhibit immunity. In the context of T

cells, it is worth noting that Th1, Th2, and Th17 cells have been shown to have distinct glycosylation patterns, implying highly controlled interactions with lectin receptors (71).

3.2. C-type lectin Receptors in cardiometabolic diseases

The presence of various receptors that affect immune cell function, such as Clec9A, a receptor expressed by conventional type 1 DC (cDC1) primarily involved in phagocytosis of dead cells, has been shown to have an atherogenic role modulating macrophages and T cell content within lesions (47).

Recently, it was discovered that Clec4a2 is expressed in vascular resident macrophages that have atheroprotective properties, and that Clec4a2 deficiency results in the loss of resident vascular macrophages as well as their homeostatic properties, leading to altered cholesterol metabolism and increased toll-like receptor triggering (72). Moreover, Clec4e is expressed in human and animal atherosclerotic plaque and is triggered by necrotic lesion extract where, it inhibits cholesterol efflux and promotes a proinflammatory response in *Ldlr*^{-/-} mice (73). As well, Mannose receptor impairment affects bone marrow and circulating immune cell subsets following HFD eating, related with lower systemic inflammation and resistance to obesity development (74).

Moreover, it has been showed that DCIR2⁺ DCs activate tolerant responses in autoreactive CD4⁺ T cells in NOD mice, reducing type 1 diabetes and other autoimmune disorders confirming that targeting the correct DC subset can be beneficial (75).

3.3. DCIR/Clec4a expression in humans and mice

DCIR is a 237aa transmembrane glycoprotein with a single carbohydrate recognition domain (CRD) and an intracellular ITIM motif that is preferentially expressed in hematopoietic organs, particularly granulocytes and APCs (DCs, monocytes, macrophages, and B cells) in humans and mice, where it works as a target receptor (76). While humans only have one DCIR isoform, mice have four,

which are distinguished by their localization. While DCIR1 is expressed by macrophages, DCIR2 is a marker for a subset of DCs, and DCIR3 and DCIR4, which are essentially unknown, do not present the ITIM domain (77–79). It is still matter of debate the expression of DCIR2, since in contrast to what Bates and colleagues found following human DC maturation, Kanazawa et al. revealed that DCIR expression increased in DC *in vitro* culture during maturation (76,77).

DCIR is responsible for receptor-mediated endocytosis, and its expression is regulated by the stage of activation of the cell (76). The lower expression of DCIR following maturation could be explained by the mature DC diminished antigen uptake function (68). As MICL, DCIR does not generate immune responses on its own but rather modifies signalling pathways activated by other PRRs (80), as suppressing TRL-induced cytokine production – such as IL-1, IL-6, TNF, IL-12, and IFN (81)- while having no effect on the expression of CD80 and CD86 co-stimulatory markers (82,83). DCIR co-localizes with clathrin, implying that the antigen is internalized by clathrin-mediated endocytosis, while the ITIM phosphorylation results in the recruitment of SH2 domain-containing phosphates (SHP1 or 2), which leads to the downregulation of IL-12, TNF, or IFN- α by DC subsets (65,84) (Fig.11).

DCIR has a role in the aetiology of arthritis, and mutations in this gene in humans are linked to an increased vulnerability to rheumatoid arthritis (85). Furthermore, mice deficient in DCIR1 demonstrated an overabundance of DCs and develop more aging-associated or experimentally induced antibodies- and T cell-mediated autoimmune disorders which coincided with the spontaneous development of autoimmune collagen-induced arthritis (86).

3.3.1. What we know about DCIR2/*Clec4a4*

Focusing on DCIR2, which has been shown to identify D-mannose (Man), L-fucose (Fuc), N-Acetylglucosamine (GlcNAc), and N-Acetylgalactosamine (GalNAc) moieties on glycans (63,87), it reduces autoimmunity by modulating T

cell response via cDC2 (63). cDC2 are Irf4 reliant, express DCIR2, SIRP α (CD172a), and Cd11b, and present antigens to CD4⁺ T cells on MHC II, in contrast to cDC1, which are Irf8-dependent, express XCR1, DEC205, or CD103, and preferentially present antigens to CD8⁺ T cytotoxic cells on MHC I. It should be noted that both DC subsets can activate CD4⁺ and CD8⁺ T lymphocytes *in vitro* (88). Because of the presence of an ITIM, DCIR2 has the potential to deliver an inhibitory signal that has been shown to affect cDC2 activation and CD4⁺ T cell activity under inflammatory conditions, making *Clec4a4*^{-/-} cells more prone to activation and implying that the DCIR2 signal inhibits the TLR downstream pathway, thereby withdrawing cDC2 activation (63).

AIM OF THE THESIS

Beyond the well-known metabolic component that characterizes cardiometabolic disorders, the hypothesis that immune-inflammatory response can participate in the cardiometabolic disease development has gained ground in recent years. Macrophages were among the first immune cells discovered to be involved in atherogenesis and obesity, notably as atheroma related-foam cells or as adipose tissue-resident macrophages, respectively. However, the spotlight is now on additional immune performers from both the innate and the adaptive immune systems.

Dendritic cells are innate immune cells whose activity influences adaptive immunity, particularly that of T lymphocytes, and are thus recognized as a link between innate and adaptive immune responses, as well as a target for immune modulation in the development of cardiometabolic diseases. Dendritic cells identify antigens via Toll-like receptors (TLRs) and C-type lectin receptors (CLRs), based on their structure or sugar moieties, respectively. Modulating CLRs has been shown to change DC activity, which in turn influences T cell responsiveness. Peculiar for its intracellular inhibitory motif, *Clec4a4*/DCIR2 is a CLR expressed by a specific subset of DC, type 2 conventional DC, capable of modulating immune response, specifically impacting CD4⁺ Th immune cells. Since DCs represent the bridge between the innate and adaptive immune system, we decided to explore how the lack of *Clec4a4* could impact the development of atherosclerosis and obesity, cardiometabolic diseases resulting from the accumulation of lipids within the arterial wall in the first and metabolic tissue in the latter, parallel to a strong immune component activation and alteration. Thus, discovering new targets that interfere with the excessive cardiometabolic-related immune cell response could pave the way for a potential therapeutic approach to improve atherosclerosis and obesity.

This study was performed by exploring the atherosclerotic plaque characteristics and the immune components of primary and secondary lymphoid organs in the atheroprone male and female mice on *Ldlr*^{-/-} or *ApoE*^{-/-} backgrounds.

In parallel, given the raising impact of antigen presenting cells (APCs) in the adipose tissue and the liver of dysmetabolic subjects, we explored the impact of *Clec4a4* and dendritic cells in the development of obesity and metabolic syndrome as a promoter of an unbalanced immune response.

MATERIALS AND METHODS

1. Mouse models

WT, *Ldlr*^{-/-} and *ApoE*^{-/-} mice were purchased from the Jackson Laboratory (USA) (<https://www.jax.org/strain/002207>, <https://www.jax.org/strain/002052>); *Clec4a4*^{-/-} mice were generated by prof. Katsuraki Sato (Division of Immunology, Department of Infectious Disease, Faculty of Medicine, University of Miyazaki, 5200 Kihara, Kiyotake, Miyazaki 889-1692, Japan) and provided from Prof. Olivier Neyrolles and Dott. Yoann Rombouts (Institut de Pharmacologie et de Biologie Structurale, Toulouse).

1.1. Atherosclerosis experiments

ApoE^{-/-} and *Ldlr*^{-/-} mice are viable and fertile. They are used for the study of atherosclerotic as they lack a protein, respectively apolipoprotein E (ApoE) and the receptor of low-density lipoproteins (LDLr), necessary for the correct catabolism of plasma lipoproteins. While *Ldlr*^{-/-} animals are viable and fertile and show no signs of suffering, *ApoE*^{-/-} animals show mild signs of distress. This is due to a mild hyperlipidemia and the activation of the immune response which result in the onset of atherosclerotic plaques in the arterial vessels at Chow diet; this phenotype is exacerbated by the consumption of a cholesterol-enriched diet. Conversely, a cholesterol-enriched diet results in the formation of atherosclerotic plaques in *Ldlr*^{-/-} animals, causing in these conditions a moderate disturbance.

Thus, for atherosclerosis experiments *Ldlr*^{-/-} or *ApoE*^{-/-} mice were crossed with *Clec4a4*^{-/-} mice to obtain *Ldlr*^{-/-} or *ApoE*^{-/-} or double knock-out (DKO) mice on atherosclerosis background. Couplings were performed with one male mouse with two female mice fed with an enriched diet (Ssniff VRF1- Breeding composed of 14% KJ fat, 23% KJ proteins, 63% KJ carbohydrates) and provided with stuffs for the building of the nest.

After 21 days of life, littermates were housed 3-4 per cage as previously reported (89), and 8-week-old male and female mice were then fed a standard or high-cholesterol diet for 12 weeks (Appendix I). Daily, mice were monitored, and their weight was tracked weekly.

1.1.1. Evaluation of *Clec4a4* deficiency on atherosclerosis background

The evaluation of the new lines generated did not reveal any signs of suffering; in detail, the birth/mortality rate, the growth curve, and the frequency of the three genotypes for each line were analysed. The parameters examined did not differ from those of C57BL/6J control mice, and of commercial reference mice *Ldlr*^{-/-} and *ApoE*^{-/-} (information available at the website www.jax.org) (Appendix II).

According to the breeding scheme of project 788/2019, *Ldlr*^{-/-} *Clec4a4*^{+/-} or *ApoE*^{-/-} *Clec4a4*^{+/-} females were crossed respectively with *Ldlr*^{-/-} *Clec4a4*^{+/-} or *ApoE*^{-/-} *Clec4a4*^{+/-} males in trio to evaluate parameters as the birth rate, the growth curve, and the weaning weight of *Ldlr/Clec4a4* or *ApoE/Clec4a4* line animals compared to C57BL/6J mice (information taken from Jackson's website, <https://www.jax.org/>), *Ldlr*^{-/-} and *ApoE*^{-/-} (Appendix II).

Furthermore, it was possible to evaluate the percentage of different genotypes, on *Ldlr*^{-/-} and *ApoE*^{-/-} background after weaning.

1.1.2. Phenotypic evaluation of new double KO (DKO) lines

The births and characteristics of 7 males and 7 females per genotype (WT, He, KO) were evaluated at different time points:

1. At birth the number of births and in the first days of life the size and possible presence of morphological deformations.
2. At weaning, growth curve and behaviour (motor skills and social interactions).
3. During adulthood, signs of illness (up to 6 months of life).

This evaluation allowed us to check - during the first phases of life - the impact of *Clec4a4* deletion and to exclude significant signs of suffering in mice (Appendix II).

1.1.3. Confirmation of the KO model

Gene expression analyses were performed on the spleen of WT and KO mice to confirm that the ablation of *Clec4a4* successfully occurred and to check whether this deficiency could affect *Clec4a2* expression. Indeed, *Clec4a2* is one of the isoforms of *Clec4a* genes present in mice which, since its similarity, could exert a comparable role to *Clec4a4*, although it is not marker specific for cDC2 as the latter (79,90). Thus, gene expression analysis confirmed that *Clec4a4* was significantly reduced in KO mice compared to WT ones and that this did not significantly affect the expression of *Clec4a2* (Appendix II).

1.1.4. Mice sacrifice and tissue collection

Once the procedure was completed, mice were fasted overnight and then sacrificed by isoflurane (2%) inhalation. First, blood was collected by intracardiac puncture and organs were then perfused with PBS 1x. After this, the aorta, heart, mediastinal/cardiac lymph nodes (cLNs), and spleen were collected and weighed. All animal procedures were performed conform to the guidelines from directive 2010/63/EU of the European Parliament on the protection of animals used for scientific purposes and approved by the Ethical Committee (Progetto di Ricerca 2012/02, Autorizzazione Ministeriale 788/2019-PR).

1.2. Obesity experiments

For obesity experiments, WT were crossed with *Clec4a4*^{-/-} mice to obtain WT and *Clec4a4* KO littermates; couplings were performed with one male mouse with two female mice fed with an enriched-diet (Ssniff VRF1- Breeding composed of 14% KJ fat, 23% KJ proteins, 63% KJ carbohydrates) and providing stuffs for the building of the nest.

After 21 days of life, animals were caged 3-4 in a temperature- and light/dark cycle-controlled environment (20±2°C, 50±5% relative humidity, and 12h light/dark) with free access to food and water. 8-week-old male littermates WT and *Clec4a4*^{-/-} were randomized at high-fat diet (HFD 45% Kcal from fat,

Cat#D12451, Research diets Inc., New Brunswick, NJ, USA) (Appendix I) for 20 weeks. During this period, mice were housed 2-3 per cage paying attention to their mobility inside the cage. Daily, mice were monitored, and their weight was tracked weekly, as well as their food intake.

1.2.1. Mice sacrifice

Once the procedure was completed, mice were fasted overnight and then sacrificed by isoflurane (2%) inhalation. First, blood was collected by intracardiac puncture and organs were then perfused with PBS 1x. After this, liver, mesenteric lymph nodes (mLNs), Peyer's patches, spleen, thymus, pancreas, visceral (VAT), subcutaneous (SCAT), and brown (BAT) adipose tissues as well as femur and tibia were collected. All animal procedures performed conform to the guidelines from directive 2010/63/EU of the European Parliament on the protection of animals used for scientific purposes and were approved by the Ethical Committee (Autorizzazione Ministeriale 65/2020-PR).

1.2.2. Tissue collection and storing

Once harvested, tissues were washed in MACS (PBS 1x, 2% EDTA, 10% FBS) solution. A part of VAT, SCAT, and liver was put in 4% paraformaldehyde (Sigma-Aldrich, Cat#F8775) in PBS 1x overnight at 4°C for histological analysis. A piece of VAT, liver, spleen, as well as mLNs and Peyer's patches, was processed to obtain a cell suspension for flow cytometry analysis and the remaining part was stored at -80°.

1.3 Atherosclerosis and obesity experimental setup

The effect of *Clec4a4* deficiency on atherosclerosis was studied in male and female mice with *Ldlr*^{-/-} or *ApoE*^{-/-} backgrounds. Once the mice with the required genotype were obtained, they were divided into two groups, one male and one female, both of which consisted of WT and KO for *Clec4a4*, placed on a Chow diet for 12 weeks; and the other, placed at WTD for the same time. For obesity experiments, WT and *Clec4a4*^{-/-} male mice were fed a HFD for 20 weeks,

during which glucose and insulin tolerance tests were performed. Please check Appendix III for a more detailed view of the experimental setup.

1.4. Sample size calculation

The calculation of the sample size was carried out with the aid of the G*Power3.1 software by setting a confidence limit of 95% and a power of 80%, based on the results of previous experiments conducted in our laboratory or reported in the literature (91–93).

For the atherosclerosis models, the number of animals was calculated (equally divided between the groups), keeping fixed:

- the probability of first type error (α , false positives) at 5%;
- a power equal to 0.8;
- effect size equal to 0.56

For the obesity model, the number of animals was calculated (equally divided between the groups), keeping fixed:

- the probability of first type error (α , false positives) at 5%;
- a power equal to 0.8;
- effect size equal to 0.58

This allowed us to reduce the number of animals to the minimum necessary to observe the statistical significance of the observed phenotype.

2. Genotyping

2.1. DNA extraction

An ear-puncher will be used for animal identification. This technique allows to obtain a small biopsy of tissue that can be used to genotype animals without suffering, as suggested by FELASA guidelines for the refinement of methods for genotyping genetically modified rodents (94).

The biopsies were then stored at -20° or as soon lysed within a 1.5 tube with 0.5mL of lysis buffer (0.5% SDS (Sigma-Aldrich), 0.2 M NaCl (Sigma-Aldrich), 50 mM Tris HCl pH=8 (AppliChem), 4 mM EDTA (Sigma-Aldrich)) and 25 μ L of

Proteinase K (10 mg/ml, PanReac AppliChem, Cat#A3830) for each sample. Samples were then vortexed and incubated O/N at 56°C. After the incubation, lysed samples were vortexed and centrifuged at 16000g for 3 minutes and the supernatant was poured into another 1.5 mL Eppendorf tube. Subsequently, 500 µL of Phenol/Chloroform/Isoamyl alcohol 25:24:1 (Fisher molecular biology, Cat#FS-1200) was added and gently mixed before the 16000g 5-minute centrifuge. The upper layer was then transferred into a new 1.5mL Eppendorf tube where 800µL of 95% Ethanol was added and mixed. After the 16000g centrifuge for 5 minutes, the supernatant was discarded and the Eppendorf tubes with the DNA pellet were left to dry at room temperature O/N. Once dried, the pellet was resuspended with 50µL of autoclaved deionized water, vortexed, incubated for 5 minutes at 56°C, and then stored at 4°C.

2.2. The PCR protocol

PCR amplification solution was composed of 10 µL of Buffer 5x (BiotechRabbit, Cat#K00475-1800), 6 µL of 25 mM MgCl₂ (BiotechRabbit, Cat#K00002-1500), 1 µL of dNTPs 2.5 mM, 1 µL of 10mM forward primer (5'-CATACTACAGAGCCTTAGAGAGAG-3'), 1 µL 10mM of wild type reverse primer (5'-GTGCCACCTGGCCTACAACCTTTTC-3'), 1 µL of 10mM mutant reverse primer (5'-ATATAGACGTTGTGGCTGTTGTAGTTGTA-3'), 0.5 µL of Taq DNA Polymerase (BiotechRabbit, Cat#BR0100102) and 27.5 µL of nuclease-free water. After vortexing the mix, 48 µL of it was put in 0.5 mL autoclaved Eppendorf tubes where 2 µL of extracted DNA of selected samples were added. After resuspension, tubes were placed in the thermal cycler (Mastercycler Nexus Gradient Eppendorf). Specific thermal cycles were necessary for *Ldlr*, *ApoE*, and *Clec4a4* genes as follows:

Ldlr

- 2 minutes at 94°C
- 40 repeats of these three steps in order
 1. 30 seconds at 95°C

2. 30 seconds at 58°C

3. 40 seconds at 72°C

- 2 minutes at 72°C.

ApoE

- 3 minutes at 94°C

- 35 repeats of these three steps in order

1. 20 seconds at 94°C

2. 40 seconds at 68°C

3. 2 minutes at 72°C

- 5 minutes at 72°C.

Clec4a4

- 2 minutes at 94°C

- 30 repeats of these three steps in order

1. 10 seconds at 98°C

2. 30 seconds at 60°C

3. 2 minutes at 68°C

- 10 minutes at 72°C

Once PCR finished, tubes were removed from the thermos cycler and loaded into Agarose gels to evaluate the product of the amplification.

The Agarose 1.8% (Fisher Molecular Biology, Cat#AS-101) dissolved in TAE Buffer 1X (TAE buffer 50X prepared from a stock solution of 500mL of 121 g of Tris, 28 ml of Acetic Acid, 50 ml of 0.5 M EDTA and distilled water) was used for *Clec4a4* PCR and 1.5% for *Ldlr* and *ApoE* genes respectively, with the addition of 1.5 µL of GelStar™ Nucleic Acid Gel Stain (Lonza, Rockland, ME, USA, Cat#50535) necessary to visualize DNA bands during UV exposure.

3. Glucose tolerance and insulin tolerance test

The glucose tolerance test (GTT) consisted of intraperitoneal injection of 1mg/g glucose in saline solution (10% w/v in physiological solution (NaCl 0.9%))

after O/N fasting, while Insulin tolerance test (ITT) consisted of intraperitoneal injection of 0.75UI/Kg insulin (0.75 mU per gram of body weight, Humulin R U-100, 100 U/mL) in a physiological solution (NaCl 0.9%) with 3% of bovine serum albumin (BSA Sigma-Aldrich, Cat#A7030) after 4h fasting (95). At the end of both tests, mice had ad libitum access to food.

Both injections were performed with a needle between 25 and 27G under local anaesthesia by application of 2.5% lidocaine and 2.5% prilocaine for 10-15 minutes to reduce pain at the site of administration. The injection site was in the lower right quadrant of the abdomen to avoid damage to the urinary bladder, caecum, and other abdominal organs and the volume injected was a maximum of 0.5 mL. Subsequently, a drop of blood was collected for glycaemic measurement following the collection of a blood drop using a glucose meter (ONE-TOUCH Ultra, Lifescan, Milpitas, CA, USA) by caudal puncture after application of local anaesthetic for 10-15 minutes at timepoints of 0 (before injection), 20, 40, 60 and 120 minutes from the injection. At the end of the blood collection, haemostasis by pressure on the tail was performed to avoid hematomas, and food was provided. GTT and ITT were performed at weeks 9 and 19, and weeks 10 and 20, respectively (95). Before GTT and ITT, the mice were moved to the room where the procedure was performed for a few hours to allow them to adapt, and in the weeks leading up to the procedure, the person performing the procedure spent time with the mice to get them to adapt to his presence.

During GTT, at 0 and 60-time points, 40 μ L of blood were collected in Eppendorf tubes with 0.5% EDTA by caudal puncture, from which plasma was isolated and stored at -20°.

4. Plasma analysis

4.1. Plasma isolation

After overnight fasting and during GTT, blood was collected from animals, and plasma was then separated by centrifugation (6000g for 10 minutes at 4°C).

4.2. *Insulin plasma quantification (ELISA)*

The concentration of insulin was measured by using an Ultrasensitive Mouse insulin ELISA assay (Mercodia, Cat#10-1249-01) following instructions, with a plasma dilution of 1:5. Briefly, after preparing 1x enzyme conjugate solution and wash buffer 1x solution, 25 μ L of each calibrator, controls, and samples in duplicate were loaded into each well. 100 μ L of enzyme conjugate 1x solution were then added and incubated on a plate shaker at 700rpm per 2h at RT. Then, 96-well plate was washed 6 times with abundant wash buffer 1x solution discarding the wash solution between every washing step and tapping firmly on absorbent paper to remove excess liquid.

200 μ L of Substrate TMB were then added to each well and incubated for 15 minutes at RT. The incubation was then stopped with the addition of 50 μ L of Stop solution and 5 seconds of shaking. The optical density lecture was performed at 450nm (Bio-Rad iMark microplate reader) and results were calculated on MyAssays Online (<https://www.myassays.com>)

4.3. *Plasma cholesterol and triglyceride measurements*

Plasma cholesterol and triglycerides concentrations were quantified by colorimetric enzymatic techniques using the Cholesterol CP KIT (ABX Pentra, HORIBA Medical, Cat#A11A01634) or the Triglyceride CP KIT (ABX Pentra, HORIBA Medical, Cat#A11A01640) at optical density lecture of 490 nm (Bio-Rad iMark microplate reader).

4.4. *Fast protein liquid chromatography (FPLC)*

Size fractionation of lipoproteins was performed by fast-performance liquid chromatography (FPLC) using a Superose 6 column (GE Healthcare, Chicago, IL, USA) on an NGCTM chromatography system FPLC (BioRad Laboratories Inc., Hercules, CA, USA). Samples were eluted with a solution of 0.15M NaCl pH 7.2, 0.01% EDTA, 0.02% Sodium azide. Serum of mice from the same experimental group was pooled and a total of 250 μ L was loaded into the device.

The constant flow rate was 0.25 mL/min and 500 µL of each fraction was collected to quantify cholesterol and triglycerides concentrations as above.

5. Histological analysis

5.1. *Tissue fixation and paraffin embedding*

After O/N in 4% paraformaldehyde in PBS 1x, tissues were subsequently dehydrated following 2h 0.18M of phosphate buffer, and then 30 minutes at ethanol 50%, 75%, 95% and 2h at ethanol 100% at room temperature. Next, after 1h of xylene, tissues were transferred in liquid paraffin and left for 2h at 58°C. They were then transferred to a mould full of paraffin at RT, to allow them to solidify. Tissue sections of 5 µm thickness were then obtained using the microtome (Leica Biosystems) on glasses and let them dry O/N.

5.2. *Haematoxylin and eosin (H&E) staining*

The paraffin from tissue sections was removed by immersing twice in xylene for 6 minutes, followed subsequently steps of 3 minutes each in ethanol 100%, 95%, 75%, and 50%, and two steps of 5 minutes each in deionized water. After, the slices were immersed in haematoxylin (Sigma-Aldrich, Cat# H3136) for 2 minutes and washed with running water for 15 minutes. Slices were then immersed in 0.3% eosin in water for 2 minutes and then quickly dehydrated by subsequent steps of ethanol 75%, 95%, 100%, and twice in xylene for 6 minutes. Coverslips were put on slides after synthetic mounting medium addition (Bio-Optica Cat#05-BMHM100), and they were left to dry O/N.

a. Quantification of atheroma on aortic sinus

Plaque at the aortic sinus has been drawn using the *freehand selection* tool on ImageJ (Fiji) and calculated both as area and percentage of the total aortic sinus area.

b. Quantification of lipid droplets on liver

Lipid droplets on hepatic parenchyma were quantified using the *analyze particles* tool on ImageJ (Fiji) adjusting the threshold to correctly consider only the lipid droplets. Then, particles were subdivided and considered their dimension in different categories.

c. Quantification of adipocytes on adipose tissues

The adipocyte area was quantified using the *Adiposoft* tool on ImageJ (Fiji) and the data was expressed as the average between the adipocyte area.

5.3. **Masson's trichrome staining**

Similarly, slices for Masson trichrome staining were first deparaffined as previously described for H&E staining and stained with Masson's trichrome with aniline blue kit (Cat#04-010802, Bio-Optica) following the manufacturer's instructions. Briefly, from distilled water, sections were put horizontally, and 12 drops of reagent mixed with reagent B (*Weigert's iron haematoxylin*) were put and incubated for 10 minutes. Then, reagent C (*Picric acid alcoholic solution*) was added, followed by 4 minutes of incubation and a quick wash with distilled water, as well as reagent D (*Ponceau acid fuchsin according to Mallory*). After the washing, 10 drops of reagent E (*Phosphomolybdic acid solution*) were put in, followed by 10 minutes of activation and, without washing, 10 drops of reagent F (*Masson aniline blue*) were put in and left for 5 minutes. After washes in distilled water and dehydration as previously described, coverslips were put on slides after synthetic mounting medium addition, and they were left to dry O/N.

a. Quantification of fibrosis on aortic plaque

The quantification of fibrosis within the atheroma was performed using the *Masson's trichrome* option on ImageJ (Fiji), then considered the colour related to the fibrotic part. Here, after drawing the atheroma, the adjustment of the threshold was necessary to correctly consider the fibrosis of the aortic plaque.

This data was represented as the percentage of the fibrotic area on the total amount of the atherosclerotic plaque.

5.4. Immunofluorescence

Slides were deparaffined as previously described and then put in 0.1M pH 6 sodium citrate dihydrate and warmed for 1 min in the microwave at 750W, followed by ionized water addition. After the wash with PBS 1x, slides were dried, and incubated with 3% BSA (SigmaAldrich, Cat# A7030) in Tris HCl 0.1M pH 7.5, 20% FBS (FBS South America origin EU Approved, Euroclone Cat# ECS0180L) for 30 minutes at RT to prevent non-specific bindings. After the incubation, slides were washed quickly with PBS 1x and incubated with the primary antibody in BSA 1% in PBS 1x O/N at 4°C.

The next morning, the antibody was removed with PBS 1x washes three times, and a secondary antibody diluted in BSA 1% in PBS 1x was added and incubated for 1h at RT. After three washes with PBS 1x, slides were incubated for 8 minutes with Hoechst (SigmaAldrich, Cat# 63493) (1:4000 in BSA 1% in PBS 1x) followed by 2 washes with PBS 1x and a drop on each slide of Fluoroshield™ histology mounting medium (SigmaAldrich Cat# F6182).

A list of antibodies used, and their concentration is present in the Appendix IV.

Samples were visualized and acquired at the Zeiss confocal microscopy by LSM software (Zeiss ZEN) and images were taken at 5x magnification.

6. RNA extraction and quantitative real-time PCR

6.1. RNA extraction and quantification

20 mg of spleen or 10 mg of liver or 20 mg of pancreas were lysed and homogenized with Tissue Ruptor II (Qiagen) and total RNA was extracted using Monarch® Total RNA Miniprep Kit (Cat#T2010S, New England BioLabs) following manufacturer's instructions. Moreover, the thoracic and abdominal aorta was lysed and homogenized with Tissue Ruptor II (Qiagen) and total RNA was extracted using RNeasy Fibrous Tissue Mini Kit (Cat#74704, Qiagen) following the

manufacturer's instructions. RNA quality and quantity were assessed by absorption measurements at NanoDrop™ 1000 Spectrophotometer (ThermoFisher Scientific).

6.2. RNA Reverse Transcription and qPCR

RNA was retro-transcribed to cDNA with 4 µL of iScript™ Reverse Transcription Supermix (Cat#1708841, Bio-Rad) mixed with 1000 ng of RNA and RNAase-free water up to the final volume of 20 µL to obtain a final concentration of cDNA of 50 ng/µL.

The total amount of 15 µL amplification solution was constituted by 1.5 µL of both forward and reverse primers, 7.5 µL of PCR with Luna® Universal qPCR Master Mix (Cat#M3003E, NEB), 2.5 µL of RNAase-free water and 2 µL of cDNA (contained 10 ng of cDNA). The amplification was performed on the CFX Connect Real-Time PCR Detection System instrument (Cat#1855201, Bio-Rad).

The thermal cycling profile was a two-step amplification (95 °C for 5 min, followed by 45 cycles of 95 °C for 10 s and 55 °C for 30 s). The sequences of the qPCR Primers are listed in the Appendix V.

The expression of investigated genes was determined as $2^{-\Delta\Delta Ct}$ and then as a fold of difference of *Clec4a4* KO or DKO to the control group adjusted to the expression of the housekeeping *Rpl-13a*.

7. Flow cytometry

Flow cytometry is a technique used to identify the immune cell signature of tissues, in this case mainly impacted by metabolic changes during the development of cardiometabolic diseases such as atherosclerosis and diabetes. Indeed, a set of antibodies – listed in Appendix VI - bind chosen peculiar markers on immune cells surface thus allowing the identification and separation of the most popular immune populations. These include, among myeloid cells, monocytes, neutrophils, macrophages, and dendritic cells and, among lymphoid populations, T and B lymphocytes, as well as NK cells. It was possible to use this

technique both on blood and in different tissues, from the most lymphoid ones as bone marrow, thymus, spleen, and lymph nodes, to metabolic ones as the liver or the adipose tissue. The gating strategies used for blood and tissues are reported in Appendix VII.

7.1. Blood and Tissue Processing

Briefly, after harvesting the tissue, part of them were processed for flow cytometry analysis as follows:

a. Blood

50 μ L of blood were stained with 50 μ L of antibody combination for 30 minutes at RT, at the end of which fix/lyse solution was added (eBioscience™ 1-step Fix/Lyse Solution (10X), Cat# 00-5333-54) and incubated for 30 minutes at RT after which 2 ml of MACS were added and 2 washes were performed before being resuspended in 250 μ L and get ready for the acquisition.

b. Bone marrow

The femur and tibia were cleaned and after the cut of the epiphysis, bone marrow was drained with MACS buffer from the diaphysis, and red blood cells were lysed with 5 minutes RBC lysis (eBioscience™ 1X RBC Lysis Buffer, Cat#00-4333-57) incubation in ice. Samples were then washed once with MACS buffer, and cells were counted. 3×10^6 cells from bone marrow suspension were then put in a 96 V-bottom well ready to be stained.

c. Thymus and cardiac lymph nodes

A part of the thymus or cardiac lymph nodes were weighted and smashed into a 70 μ m cell strainer (Corning®, Cat#431751) till a single cell suspension was obtained. This was then pelleted, resuspended in 200 μ L of MACS buffer and put in a 96 V-bottom well ready to be stained.

d. Spleen

A part of the spleen was cut, weighted, and smashed into a 70 μm cell strainer to obtain a single-cell suspension. After RBC lysis incubation for 5 minutes in ice, cells were pelleted, resuspended in 200 μL of MACS buffer and put in a 96 V-bottom well ready to be stained.

e. Liver

A lobe of the liver was cut, weighted, and smashed into a 100 μm cell strainer with PBS 1x added with 2% FBS and 2mM EDTA. After 1 minute of a 50g centrifuge with brake off, the supernatant was recovered and centrifuged for 8 minutes at 700g high-brake followed by the resuspension of the pellet in 10 mL of 37.5% Percoll (Sigma-Aldrich, Cat# 17-5445-01), 3.75% di PBS 10x, 58.75% di RPMI 1640 (Euroclone S.p.A., Milan, Italy, Cat#ECB9006L) and centrifuged at 850g brake off for 30 minutes at RT, keeping then the pellet and incubating it in RBC lysis buffer for 5 minutes in ice. The resulting pellet was then resuspended in 200 μL of MACS buffer and put in a 96 V-bottom well ready to be stained.

f. VAT

Visceral adipose tissue single-cell suspension was obtained after collagenase digestion as previously described (96). Briefly, a part of the VAT was cut in 200 mg/mL (Collagenase NB4 standard grade, Nordmark, Cat#11427503) and 5 mM CaCl_2 and incubated at 37°C for 40 min under agitation, at the end of which MACS buffer was added and samples were eluted through a 100 μm first, and 70 μm later, cell strainer. After the 5 minutes of 652g centrifuge, the pellet was resuspended in RCB lysis buffer and incubated for 5 minutes in ice. After being spun, samples were resuspended in 200 μL of MACS buffer and put in a 96 V-bottom well ready to be stained.

7.2. Antibody staining for flow cytometry

After 96 V-bottom wells with the single cell suspension of different tissues were centrifuged at 800g for 5 minutes the surfactant was discharged. Thus, the pellet was resuspended in 50 μ L of antibody combination (see the Appendix VI-VII for the antibody list and gating strategy related to each tissue) and incubated for 30 minutes at 4°C, after which cells were washed with MACS buffer, centrifuged as before, resuspended in 250 μ L and transferred in 5 mL tubes, being thus ready at flow cytometer acquisition. Samples were then acquired through BD LSRFortessa™ Cell Analyzer flow cytometry analysis was performed using Agilent NovoExpress flow cytometry software.

8. Statistical analysis

Microsoft Excel and Graph Pad Prism were used to perform all the analyses and generate the graphs. Results are expressed as mean \pm SEM and the statistical unpaired analysis was performed on Graph Pad Prism, using an unpaired parametric two-sides T-test with a 95% confidence interval when the samples are normally distributed, otherwise, Mann-Whitney nonparametric unpaired T-test was applied. For multiple comparisons, Two-way ANOVA with Sidak's multiple comparisons was used. A p -value of $p < 0.05$ was considered significant.

To test normal/Gaussian distribution, a Graph Pad tool was used considering Anderson-Darling test, D'Agostino-Pearson omnibus normality test, Shapiro-Wilk normality test and Kolmogorov-Smirnov normality tests. Outlier samples were removed following Graph Pad Prism Grubbs' method with a 95% confidence interval.

RESULTS

1. *Clec4a4* deficiency in atherosclerosis: focus on *ApoE*^{-/-} and *Ldlr*^{-/-} background

To investigate the role of *Clec4a4* during atherogenesis, we first generated a DKO mouse model based on two atherosclerosis experimental models with *ApoE*^{-/-} or *Ldlr*^{-/-} background. These differ in terms of the origin of atherosclerosis; the former leads in changed lipoprotein distribution in favour of VLDLs, even influencing inflammation, whilst the latter is biased toward LDLs.

1.1. Evaluation of *Clec4a4* deficiency on *Ldlr*^{-/-} or *ApoE*^{-/-} under standard diet

First, we evaluated the lack of *Clec4a4* on a modest formation of non-complex plaques, resulting from feeding with a standard diet (ChowD), as a mirror of atherosclerosis at early stages.

1.1.1. Body and organ weight of *ApoE*^{-/-} and *Ldlr*^{-/-} male and female mice

Both male and female mice, on *ApoE*^{-/-} and *Ldlr*^{-/-} background, were fed for 12 weeks with a ChowD, at the end of which body and organs were weighted; this analysis revealed an increased ratio of inguinal lymph nodes (iLNs) and spleen on total body weight for male *Ldlr* DKO mice compared to the control counterpart, without affecting male and female mice on *ApoE*^{-/-} background (Appendix VIII).

1.1.2. Aortic plaque and circulating lipid level analysis

Although at ChowD, being atherosclerosis experimental models, we expected increased plasma lipid levels and a hint of atherosclerotic plaque formation.

Our data showed that, on both atherosclerosis backgrounds, the deficiency of *Clec4a4* did not reveal alterations in plasma lipid levels compared to single KO mice (Fig.12A-D). Intriguingly, *Clec4a4*^{-/-} on *ApoE*^{-/-} background showed comparable aortic plaque area in both male and female to *ApoE*^{-/-} mice (Fig.12E-F),

while *Clec4a4*^{-/-} on *Ldlr*^{-/-} background showed an increased atherosclerotic lesion, compared to mice *Ldlr*^{-/-} both male and female (Fig.12G-I).

Of note, mice on *ApoE*^{-/-} background showed higher plasma cholesterol levels compared to mice on *Ldlr*^{-/-} background, with a greater aortic plaque area compared to the one on *Ldlr*^{-/-} background. The very low magnitude of atherosclerotic lesion formed on *Clec4a4*^{-/-} *Ldlr*^{-/-} male mice suggested that the alterations observed between DKO and *Ldlr*^{-/-} mice were not biologically relevant and the lack of *Clec4a4* seemed to have a redundant role in the development of atherosclerosis at the first stages.

1.1.3. The immunophenotype of lymphoid organs:

Since *Clec4a4* is a receptor expressed by immune cells, the aim of the characterization of our atherosclerosis experimental models on ChowD focused then on the immunophenotyping of primary and secondary lymphoid organs.

a. The immunophenotype of the thymus

The thymus is a primary lymphoid organ where the training of T lymphocytes takes place, governed by thymocytes and antigen-presenting cells, such as dendritic cells (97).

Thus, we performed an immunophenotype of the thymus particularly focusing on antigen-presenting cells and T lymphocytes, with related subsets. Intriguingly, male *Clec4a4* *ApoE* DKO mice showed an augmented number of dendritic cells, with an increasing trend of both cDC1 and cDC2, parallel to a significant prevalence of CD8⁺ T cells (Fig.13A). These observations were not replicated in female DKO mice on *ApoE*^{-/-} background that did not show alterations compared to the control counterpart (Fig.13B). In parallel, on *Ldlr*^{-/-} background, DKO male and female mice showed a decreasing trend of thymus resident leukocytes, significant in females, for which the reduction was driven by double positive CD4⁺ CD8⁺ T cells (Fig.13C-D). Yet, if these alterations had a biological significance were excluded by deepening the T cell subsets distribution, that did not reveal changes in the proportion of T central memory (TCM), T effector (TE), T effector

memory (TEM), and Naïve T cells within the thymus, in DKO mice both on *ApoE*^{-/-} and *Ldlr*^{-/-} background (Fig.13E).

b. The immunophenotype of cardiac lymph nodes

After being trained, T cells are in an inactivated stage up to when the antigen-presenting cell presents the antigen to them: the crosstalk between these two populations takes place in specific organs, named lymph nodes. Thus, we proceeded with the immunophenotype of mediastinal/cardiac lymph nodes (cLNs), the ones draining the heart, which however did not highlight differences in DKO T cells and T cell subsets neither on *ApoE*^{-/-} nor in *Ldlr*^{-/-} background (Fig.14).

c. The immunophenotype of the spleen

Although *Clec4a4* is highly expressed by splenic DCs (98), the immunophenotyping performed on the spleen of both males and females on *ApoE*^{-/-} or *Ldlr*^{-/-} background did not reveal changes in the immune cell distribution (Fig.15).

1.1.4. The Immunophenotype of the circulating immune populations

We lastly analysed the distribution of circulating immune cells in our atherosclerosis experimental models at ChowD. Our analysis revealed a similar pattern of myeloid cells between DKO and the control counterpart (Fig.16). However, male DKO mice on *ApoE*^{-/-} background showed increased levels of CD3⁺ T cells driven by both CD4⁺ T cells and CD8⁺ T cells (Fig.17A), while the deficiency of *Clec4a4* on female (Fig.17B) and on the *Ldlr*^{-/-} background (Fig.17C-D) did not alter adaptive immune cell distribution.

These findings indicated that *Clec4a4* plays a redundant role throughout the early stages of atherogenesis, with little effect on plasma lipid levels or atherosclerotic plaque. Furthermore, we found relatively minor alterations in immune cell distribution within the thymus and in the blood, primarily affecting T

cells, a phenotype that was not widely distributed but was restricted to the atherogenesis background or based on gender.

1.2. Evaluation of *Clec4a4* deficiency on WTD-fed male mice on *ApoE*^{-/-} background

To exacerbate the atherosclerotic plaque formation, we proceeded with the administration of a cholesterol-enriched diet for 12 weeks. Since the involvement of ApoE in inflammatory processes, we started to characterize mice on the *ApoE*^{-/-} background.

1.2.1. Evaluation of the total body and organ weight

After the sacrifice of male *ApoE*^{-/-} and *Clec4a4*^{-/-} *ApoE*^{-/-} mice, body and organs (thymus, spleen, iLNS, Liver, and visceral adipose tissue (VAT)) were weighted without evidencing any significant change (Appendix VIII).

1.2.2. Aortic plaque and circulating lipid level analysis

Then, we proceeded with the examination of the atherosclerotic pattern, from the characterization of the aortic plaque to the evaluation of plasma lipid levels – cholesterol and triglycerides. Indeed, male DKO mice revealed a decreased percentage of aortic occlusion, which extended along the aortic plaque progression within the first 300 µm from the aortic sinus (Fig.18A-B). More specific analysis, regarding the necrotic and fibrotic content besides SMCs and macrophage infiltration did not reveal significant differences (Fig.18C-E) in DKO mice compared to *ApoE*^{-/-} male mice. This was in line with the comparable plasma lipid levels observed in the two mouse models (Fig.18F).

1.2.3. Evaluation of the hepatic phenotype

Paralleled to the aortic plaque characterization, we checked for the lipid deposition within the liver - the metabolic organ mainly involved in lipoprotein

metabolism and catabolism – through histological analysis. The lipid quantification did not reveal major changes in the total lipid content with the same trend of lipid droplet dimensions on male DKO mice compared to the *ApoE*^{-/-} counterpart (Fig.19A-C). These results, together with the unchanged plasma lipid levels – both cholesterol and triglycerides - lead to the hypothesis that the improvement of plaque progression could be mediated by an altered immune response.

1.2.4. The immunophenotype of circulating immune populations

Since lipids did not seem the driving cause of the aortic plaque decrease in male DKO mice, we proceeded with an extensive flow cytometry analysis of circulating and lymphoid organ-resident immune populations. Thus, our analysis on circulating innate and adaptive immune populations revealed a significant decrease of circulating myeloid cells, mainly driven by the neutrophil reduction, in DKO male mice compared to the control counterpart (Fig.20A-B). These results suggest that the decrease in myeloid cells primarily influenced by neutrophils could be the effector of the reduction of the aortic plaque.

1.2.5. The immunophenotype of lymphoid organs: a focus on bone marrow, thymus and cardiac LNs

We then proceeded with the immunophenotype of primary and secondary lymphoid organs, such as bone marrow, thymus, and cardiac lymph nodes (cLNs), to understand whether alterations during the immune cell differentiation occurred. Our analysis revealed no changes in bone marrow resident progenitors (Fig.21A) and, consequently, similar levels of CD45⁺ leukocytes, dendritic cells – with related subsets cDC1 and cDC2 - CD4⁺CD8⁺ T cells and the subsets of CD4⁺ or CD8⁺ single positive cells were observed in the thymus (Fig.21B-C). Physiologically, once APCs encounter the antigen, they move toward the nearest lymph node where the encounter with T cells takes place. In line with the previous results, total CD45⁺ leukocytes and CD3⁺ T cells, paralleled to the CD4⁺

or CD8⁺ in cLNs subsets of DKO mice showed a comparable signature compared to *ApoE*^{-/-} mice (Fig.21D).

1.3. Evaluation of *Clec4a4* deficiency on WTD-fed male mice on *Ldlr*^{-/-} background

Previous results showed that *Clec4a4* deficiency impacts atherosclerosis plaque on *ApoE*^{-/-} background mainly impacting the circulating myeloid compartment. We then generated *Clec4a4*^{-/-} mice on *Ldlr*^{-/-} background, to deepen the role of *Clec4a4* on a more lipid-driven atherogenesis.

1.3.1. Body and organ weight of WTD-fed mice on *Ldlr*^{-/-} background

Total body weight was monitored during the 12 weeks of WTD up to the sacrifice when also primary and secondary lymphoid organs – thymus, iLNs, and Spleen – as well as Liver and VAT of male mice on the *Ldlr*^{-/-} background were weighted. Neither the body weight nor the ratio of the organs to total body weight highlighted differences between *Clec4a4*^{-/-} *Ldlr*^{-/-} and *Ldlr*^{-/-} mice (Appendix VIII).

1.3.2. Atherosclerotic plaque phenotype and circulating lipid level analysis

Histological analysis of the atherosclerotic plaque at the aortic sinus and the first part of the ascending aorta revealed a significant decrease of the aortic occlusion parallel to a strong reduction of the aortic plaque area in DKO male mice compared to the control counterpart (Fig.22A-B). The following analysis aimed at defining the features of this atheroma and highlighted a reduced necrotic core of male *Clec4a4*^{-/-} *Ldlr*^{-/-} atherosclerotic plaque compared to *Ldlr*^{-/-} ones, without affecting neither the stability – represented by the content of fibrosis – nor the content of SMCs and macrophages. (Fig.22C-D).

The decreased level of atherosclerosis was likewise parallel to a significant decrease in cholesterol and triglyceride levels, impacting even the lipoprotein distribution within the blood (Fig.22E-F).

1.3.3. Evaluation of the hepatic phenotype

Given the reduction in circulating lipoproteins, we investigated the organ responsible for lipoprotein metabolism and catabolism, focusing on histological and gene expression analysis. Thus, DKO male mice revealed a significantly less fat liver characterized by a different dimension of lipid droplets favouring the smaller ones ($<30\mu\text{m}^2$) compared to the control counterpart (Fig.23A-C). Moreover, the gene expression analysis revealed how in male DKO mice the liver significantly expressed less *CD36* compared to *Ldlr*^{-/-} mice (Fig.23D), and this decrease was in line with the minor hepatic steatosis observed in DKO mice.

1.3.4. The immunophenotype of circulating immune populations

We then proceeded with a wide immunophenotyping of circulating immune cells, which revealed no major changes in the total amount of *CD45*⁺ leukocytes, but a significant decrease of neutrophils and monocytes, particularly *Ly6C*^{hi} proinflammatory monocytes in DKO compared to *Ldlr*^{-/-} mice (Fig.24A-C). The *Clec4a4* deletion did not impact other myeloid immune populations, such as DCs (Fig.24D) as well as B and NK cells and the major subsets of *CD3*⁺ T cells – *CD4*⁺ and *CD8*⁺ T cells (Fig.24E).

1.3.5. The immunophenotype of lymphoid organs: a focus on bone marrow, thymus and cLNs

In parallel to the comparable amount of circulating dendritic and lymphoid cells, flow cytometry analysis on cardiac lymph nodes (cLNs), as well as on the thymus did not highlight changes in the amount of myeloid lymphoid cells analysed (Fig.25A-B). However, the bone marrow of male DKO mice showed an increased amount of granulocyte-macrophage progenitors (GMPs), the precursors of both neutrophils and monocytes compared to *Ldlr*^{-/-} counterpart (Fig.25C,D), which could explain the decrease in the mature form of these immune populations in the circulation.

1.4. Evaluation of *Clec4a4* deficiency on WTD-fed female mice on *ApoE*^{-/-} and *Ldlr*^{-/-} backgrounds

WTD-fed female mice, on the other hand, did not show the same changes as male mice due to *Clec4a4* deficiency. Indeed, they revealed comparable atherosclerotic plaque area and plaque advancement - within the first 300 μm from the aortic sinus - compared to single KO on *ApoE*^{-/-} or *Ldlr*^{-/-} backgrounds (Fig.26A-B and Fig.26F-G). The same was true for atheroma characteristics, such as necrosis, fibrosis, SMC and macrophage content, which were comparable throughout the models studied (Fig.26C-E and Fig.26H-J). In line with these observations, *Clec4a4* deficiency on female mice did not affect circulating plasma lipid levels (Fig.27A-B) or hepatic lipid distribution in both *ApoE*^{-/-} (Fig.27C-E) or *Ldlr*^{-/-} (Fig.27F-H) backgrounds. As well, on both experimental atherosclerosis models, circulating immune cells were similar in DKO and single KO female mice (Fig.28).

2. The role of *Clec4a4* in HFD-induced obesity

So far, we proved that *Clec4a4* deficiency has an impact on atherosclerosis by changing the circulating myeloid cell composition and, in the case of mice on the *Ldlr*^{-/-} background, even the plasma lipid levels and the hepatic steatosis was affected. For these reasons, we wondered whether the deletion of *Clec4a4* could impair obesity-related immune responses and fat deposition, perhaps contributing to the pathogenesis of this disease.

Thus, we fed WT and *Clec4a4*^{-/-} mice with a High-Fat Diet (HFD) for 20 weeks to induce obesity and to investigate the role of *Clec4a4* both in the immunophenotype and in the development of obesity.

2.1. Body and organ weight of HFD-fed male mice

During the 20 weeks of HFD feeding, male mice were weighed weekly, and the food uptake was similarly monitored. Our data showed no differences in the total body weight as well as in the weight gain of *Clec4a4*^{-/-} mice compared to

the control counterpart (fig.29A-B); observations in line with the cumulative food intake (fig.29C). After 20 weeks of HFD feeding, lymphoid (thymus, spleen, pLNs) and metabolic (liver, pancreas, adipose tissues) organs were collected and weighted, although no major changes were revealed between KO and WT mice (fig.29D-K). This suggested that *Clec4a4* deficiency did not play a role in total weight gain.

2.2. Evaluation of the hepatic immune-metabolic phenotype

We then proceeded with an extensive immunophenotyping of the liver of *Clec4a4*^{-/-} and WT mice, which did not reveal major changes in the total amount of CD45⁺ leukocytes as well as in the main myeloid populations such as monocytes and macrophages (fig.30A-C). However, dendritic cells of KO mice underwent a significant reduction, mainly driven by cDC2 decrease without affecting cDC1 or moDCs (fig.30D-E). Intriguingly, while the total amount of lymphoid cells was intact compared to the control counterparts (Fig.30F-H), deeper gene expression analysis of immune cell markers revealed a significant decrease of CD11c, a marker of DCs, confirming what we previously observed with flow cytometry, as well as a significant reduction of *Gata3*, marker and transcriptional factor of Th2, immune cells commonly known to be trained by cDC2 (99) (Fig.30I).

Despite the changes in the immunophenotype, liver histological analysis did not uncover alterations in the hepatic parenchyma, which showed a comparable percentage of steatosis between the two animal models (Fig.30J-L) parallel to similar circulating lipid levels (Fig.30M).

Thus, these results suggested that the lack of *Clec4a4* affects specifically the distribution of dendritic cells within the liver, impacting Th2 polarization, without affecting lipid accumulation.

2.3. Analysis of the glucose metabolism of HFD-fed male mice

We then wanted to assess *in vivo* whether the *Clec4a4* deficiency under HFD could play a role beyond the one related to immune modulation, affecting

glucose metabolism. Thus, the Glucose Tolerance Test (GTT) was performed after 9 and 19 weeks of diet (Fig.31A-B respectively), revealing an increased glucose intolerance only induced by long term HFD feeding parallel to a minor increase of insulin plasma levels during the test, in *Clec4a4*^{-/-} compared to the control counterpart (Fig.31C). To exclude alterations in the insulin response, we performed an Insulin Tolerance Test (ITT). Despite a difference in basal glycemia after 4-hours fasting in *Clec4a4* KO mice, no differences were reported in circulating glucose after both short and prolonged exposure to HFD (Fig.31D-E respectively), thus implying a proper insulin activation pathway. While these changes were not accompanied by an altered hepatic parenchyma, as previously appreciated, the increased glucose intolerance suggested an involvement of *Clec4a4* in the glucose metabolism, and thus, in the response in the form of insulin secretion without affecting insulin downstream pathways. However, the gene expression analyses performed on the liver regarding some of the fundamental steps of glycolysis, did not highlight any major changes (Fig.31F).

2.4. Evaluation of the visceral and subcutaneous adipose tissue phenotype

We then wondered whether the altered DC distribution could be reflected in other metabolic organs, such as adipose tissues. Flow cytometry analysis performed on visceral adipose tissue (VAT) did not highlight any changes in the immune signature of KO mice compared to the control counterpart (Fig.32A-C). In line, we analysed adipocyte area both from VAT and subcutaneous adipose tissue (SCAT). These, although have different metabolisms, with the former producing FFAs and absorbing glucose, and the latter primarily absorbing FFAs and TG (100), revealed comparable histological analysis in the two experimental groups (Fig.32D-F).

Moreover, we checked for the expression of peculiar markers tightly associated with adipocytes, such as adiponectin, PPAR γ and CD26. Gene

expression levels of *adiponectin* and *PPAR γ* , both involved in regulating glucose levels and fatty acid breakdown, were comparable between the two experimental models (Fig.32G) and the same was true for CD26 MFI (Fig.32H). However, although this excluded the involvement of *Clec4a4* in adipocyte metabolic remodelling, our data appeared to be in conflict regarding the glucose resistance of the KO mice. Indeed, CD26 (or dipeptidyl peptidase-4) is an amino peptidase that reduces the activity of incretin peptides (glucagon-like peptide 1 and glucose-dependent insulinotropic polypeptide) resulting in reduced insulin secretion and, even, insulin resistance (24). The similar expression of CD26 in visceral DCs of WT and DCIR2 KO led us to hypothesize a compensatory mechanism that masks the contribution of *Clec4a4* to HFD-induced metabolic alterations.

2.5. **The immunophenotype of the bone marrow**

Based on the decrease in hepatic DCs, we hypothesized that *Clec4a4* could be involved in an altered distribution of progenitor or mature cells in primary and secondary lymphoid organs. Then, progenitors and mature cells from bone marrow of WT and *Clec4a4*^{-/-} mice were examined through flow cytometry, revealing no significant changes in early progenitors of myeloid and lymphoid lineages (common myeloid progenitors, CMPs; granulocyte-monocytes progenitors, GMPs; common lymphoid progenitors, CLPs) (Fig.33A-D) and dendritic cell progenitors (common DC progenitors, CDPs; monocyte and DC progenitors, MDPs; preDCs) which showed comparable number of cells between the two experimental models (Fig.33E-G). *Vice versa*, changes were observed in resident mature DCs where, although the total amount of CD45⁺ leukocytes did not change (Fig.33H), dendritic cells revealed an increasing trend mainly driven by cDC2, while cDC1 significantly decreased (Fig.33I). After this observation, we speculated about a role for *Clec4a4* under HFD feeding in DC differentiation or release from the BM, which could have an impact restricted on hepatic DC distribution.

2.6. The immunophenotype of secondary lymphoid: focus on Pp, mLNs and spleen

To exclude altered antigen presentation, we proceeded with an extensive immunophenotype of the main secondary lymphoid organs which could be involved in the overall inflammatory state. Thus, to assess whether the food uptake was associated with an altered immune response, we first focused our attention on Peyer's patches (Pp), the lymphoid organs within the intestines where the modulation of adaptive immune responses against potentially hostile foreign agents as well as non-harmful commensal microorganisms takes place (101). Thus, Pp were extracted and analysed, without revealing differences in the composition of both myeloid (macrophages and dendritic cell subsets) as well as in the lymphoid compartment, considering both the total amount of CD3⁺ T cells and their subsets CD4⁺ and CD8⁺ T cells (Fig.34A-F). The same was true for mLNs, protectors of the tolerance against food proteins and commensal intestinal bacteria (102), of which our data showed a comparable phenotype between *Clec4a4*^{-/-} and WT mice, both in myeloid and lymphoid immune populations (Fig.34G-L), thus suggesting once again that the deficiency of *Clec4a4* did not impact the food-related immune inflammation.

In line with these results, the immunophenotype of the spleen, the organ dedicated to blood filtration of pathogens and abnormal cells (103), did not show major differences in the immune compartment (Fig.34M-U), thus excluding any remarkable modifications of the immune cell distribution within the lymphoid organs.

DISCUSSION AND CONCLUSIONS

Despite the availability of several cardiometabolic drugs, lipid-lowering therapies remain the first line of treatment, while the prevalence of type 2 diabetes is increasing over time as a result of changes in lifestyle behaviours that promote sedentarism. Therefore, cardiometabolic disorders are still the leading causes of death in Western societies, and they are becoming increasingly common in low- and middle-income countries. The majority of cardiometabolic disorders are avoidable by adopting a healthy lifestyle that includes appropriate physical activity, moderate alcohol consumption, and nutritional eating. However, rather than seeing these illnesses solely as metabolic-driven, it has recently been recognized that the immune system plays a significant role (104).

In this scenario, we focused on dendritic cells, which act as a bridge between the innate and adaptive immune systems, as critical participants in the immune response modulation throughout the development of atherosclerosis (56,105) and obesity (24,30). Our purpose was to investigate the involvement of *Dendritic cell immunoreceptor 2* (DCIR2 or *Clec4a4*), a peculiar C-type lectin receptor mainly expressed by type 2 conventional dendritic cells involved in antigen uptake and modulation of adaptive immunity, in atherosclerosis and obesity development. This investigation took advantage from *Clec4a4*^{-/-} mice bred with atherosclerosis prone experimental models (*ApoE*^{-/-} or *Ldlr*^{-/-}). These are the two most utilized animal models for exploring the effects of multiple genes and cell types during atherogenesis. Both models result in hypercholesterolemia, although the distribution of lipoproteins and atherogenic mechanisms varies, such as ApoE participation in inflammatory processes. VLDLs are prevalent in the first model due to ApoE role as a ligand for chylomicron and VLDL absorption, whereas LDLs are prevalent in the latter (106). Mice were then fed with a cholesterol-enriched diet to accelerate atherosclerosis development. In parallel, we investigated the role of *Clec4a4* during metabolic challenges of diet-induced obesity, in WT and *Clec4a4*^{-/-} male mice fed with a high-fat diet (HFD).

Our findings on *Clec4a4*^{-/-} mice on atherosclerotic backgrounds fed a high-cholesterol diet, allowed us to highlight the metabolic involvement of *Clec4a4*, revealing a role for this C-type lectin receptor in atherogenesis during the advanced stages.

Indeed, standard diet-fed mice on *ApoE*^{-/-} or on *Ldlr*^{-/-} backgrounds had no impact on aortic plaque accumulation or circulating lipids, except for a slight difference on DKO male mice on the *Ldlr*^{-/-} background, which showed increased aortic occlusion along with increased inguinal lymph nodes (LNs) and spleen weight but no changes in the immune cell composition. However, while the increased atherosclerosis appeared to be related to a substantial inflammation beginning in the inguinal LNs and in the spleen, it should be noted that the total area of the aortic plaque was lower compared to mice on *ApoE*^{-/-} background. Furthermore, the differences between DKO and *Ldlr*^{-/-} mice are modest in comparison to the differences between the other models, thus having no biological significance. This prompted us to challenge these mice by feeding them with a cholesterol-enriched diet to better understand the contribution of *Clec4a4* in atherogenesis.

In male DKO mice with *ApoE*^{-/-} or *Ldlr*^{-/-} backgrounds, 12 weeks of WTD feeding resulted in a more mature and larger atheroma compared to the standard diet, revealing a decrease in the atherosclerotic plaque area with different patterns based on the KO background. Of note, in the female mouse model, differences between DKO and single KO were not observed.

Considering male mice, while *Clec4a4* *ApoE* DKO mice had less aortic occlusion and plaque progression along the ascending aorta, this was not associated with altered plasma lipid levels but with a significant decrease in circulating neutrophils. In line with these findings, male DKO mice on a *Ldlr*^{-/-} background showed a comparable association between aortic plaque levels and circulating neutrophils, which was supported by the reduction of circulating inflammatory monocytes and a significant decrease of plasma lipid levels.

It should be highlighted that the consistent feature in the two atherosclerosis mouse models is the lower circulating neutrophil count in DKO animals compared to the single KO equivalent. It is not surprising that neutrophil count is associated with the atherosclerosis plaque development (107); nonetheless, the discovery of a link between *Clec4a4* and neutrophils was unexpected. Then, after observing an increase of neutrophil and monocyte progenitors within the bone marrow, we considered the involvement of *Clec4a4*⁺ DCs in the releasing of granulocyte-monocyte progenitors (GMPs) (89). However, this difference was present only between DKO mice on *Ldlr*^{-/-} background versus *Ldlr*^{-/-}, prompting us to propose a second hypothesis about *Clec4a4* expression. Indeed, it is known from the literature that human DCIR is expressed by neutrophils (64,108,109), which led us wonder about *Clec4a4* expression in innate immune cells other than DCs, that could explain the robust phenotype observed in neutrophils. In favour of this hypothesis, it has been recently unveiled the presence of *Clec4a4*⁺ eosinophils within the small intestine, which could lead to new discoveries about *Clec4a4*⁺ immune populations (110).

Intriguing is the observation that *Clec4a4* deficiency affects not just the myeloid compartment but also lipoprotein metabolism/catabolism in *Ldlr*^{-/-} background mice, with reduced systemic levels of cholesterol and triglycerides mainly in LDL and VLDL lipoproteins, resulting in a less fat liver, and a considerable decrease of the aortic plaque area (89). In addition, the liver of DKO mice showed a decrease in *CD36* gene expression, indicating a reduced uptake of lipids within the liver, that can explain the less steatosis observed. This was linked to an increasing trend of *Cyp7a1* gene expression representing the first step in the generation of bile acids, suggesting that cholesterol intake in the liver is preferentially transformed into bile acids and excreted. However, to explain the low circulating plasma levels, we can only speculate on an altered immune response within the intestine, thus impacting the diet cholesterol uptake.

The second part of this project focused on the study of *Clec4a4* in obesity development. This condition is accompanied by a chronic inflammatory component caused by a connection between metabolic organs such as adipose tissue, liver and skeletal muscles, and the immune system. Obese patients have altered leukocyte numbers and cell-mediated immune responses, both of which contribute to obesity development. Over the years, researchers have endeavoured to broaden their understanding of the aetiology of obesity and its immune component, revealing the involvement of many immunity-related receptors on both the innate and adaptive immune systems (4,18,32,33,44,96,111).

Thus, after 20 weeks of high-fat diet feeding, we first checked body weight and food intake of the WT and *Clec4a4*^{-/-} groups and then performed a more in-depth study of the role of *Clec4a4* deficiency on glucose metabolism and immune signature in different organs. Because of the similar phenotypes of the two experimental groups, we were able to confirm that *Clec4a4* plays a redundant function in the development of obesity. However, we detected a different distribution of DCs within the bone marrow - where they increased - and in the liver - where they decreased. This prompted us to propose that *Clec4a4* plays a role in the release of DCs from the bone marrow - as was previously suspected for DKO mice on *Ldlr*^{-/-} background - influencing downstream organs such as the liver. It is worth noting that these observations could be completely unrelated, with different roles of DCs in the bone marrow and the liver. It should be also noted that the wide range of sample distribution affecting the immunophenotype could mask other altered immune cell distributions across the two experimental models. The processing of metabolic organs to obtain the single cell suspension required for flow cytometry analysis could explain this heterogeneity. As a result, we cannot exclude the possibility that as sample size increases, variability lowers, and new effects emerge on the immune distribution. Also, it is well known that other factors, such as the environmental settings and

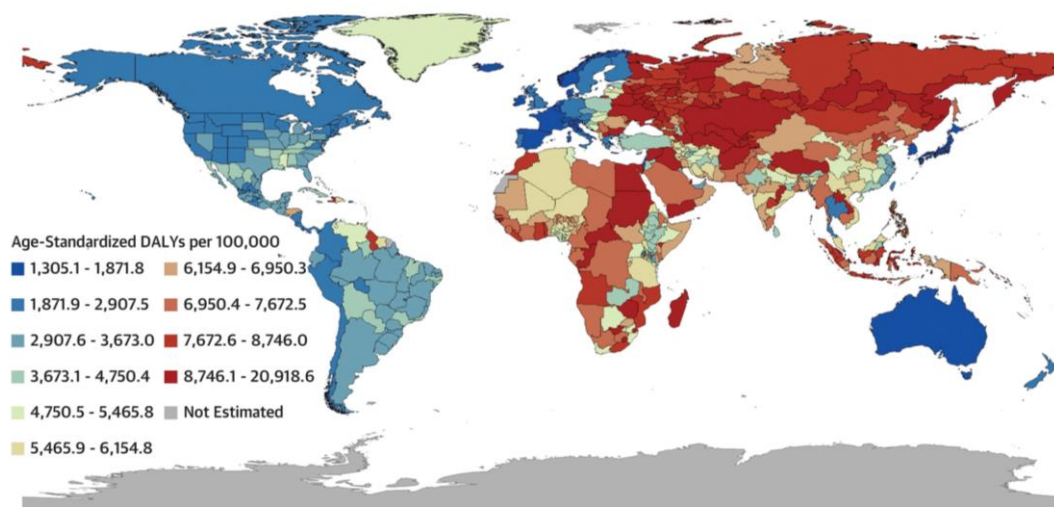
the stress, may affect experimental results (112). However, the combined results of body weight, food consumption, histological analysis and insulin tolerance tests (ITT) – all of which depict the obese phenotype - suggest that *Clec4a4* plays a redundant function in obesity development (113). Thus, aside from a reduction in DCs in the liver of KO animals, the inflammatory status of this organ, as well as the hepatic lipid accumulation, were unaffected, demonstrating once again a compensatory mechanism in response to *Clec4a4* deletion. The GTT revealed that *Clec4a4*^{-/-} mice were less glucose tolerant compared to WT after extended HFD feeding, with a preserved insulin tolerance from the ITT. In this scenario, our hypothesis points to *Clec4a4* playing a collaborative role in glucose recognition/uptake even within the pancreas which could affect β cells sensitivity to plasma glucose levels. This is just theory, but it could be a starting point for furthering *Clec4a4* participation in glucose metabolism.

Taken together, our results support a pro-atherogenic role for *Clec4a4*, albeit the full molecular mechanism, acting on neutrophils as well as lipid metabolism, has to be investigated further. In addition, these data exclude the modulation of T cell response by *Clec4a4*, previously observed in physiological conditions. This could be described by a compensatory mechanism in the modulation of the adaptive immune system from DCs during low-grade chronic inflammation. Of note, one evident limiting factor in this project is the difference in atherosclerotic pattern between male and female mice in *ApoE*^{-/-} and *Ldlr*^{-/-} backgrounds, with the major alterations affecting males whilst *Clec4a4* deficiency had little effect on female mice. This could be explained by the molecular mechanisms underlying differences in lipid metabolism, immuno-inflammatory reactivity, and vascular response in males and females, all of which affect atherosclerosis progression (110).

In conclusion, in an effort to discover new therapeutic targets to treat the inflammation that underpins cardiometabolic diseases, this project demonstrated how *Clec4a4* is an important modulator of immune cell distribution

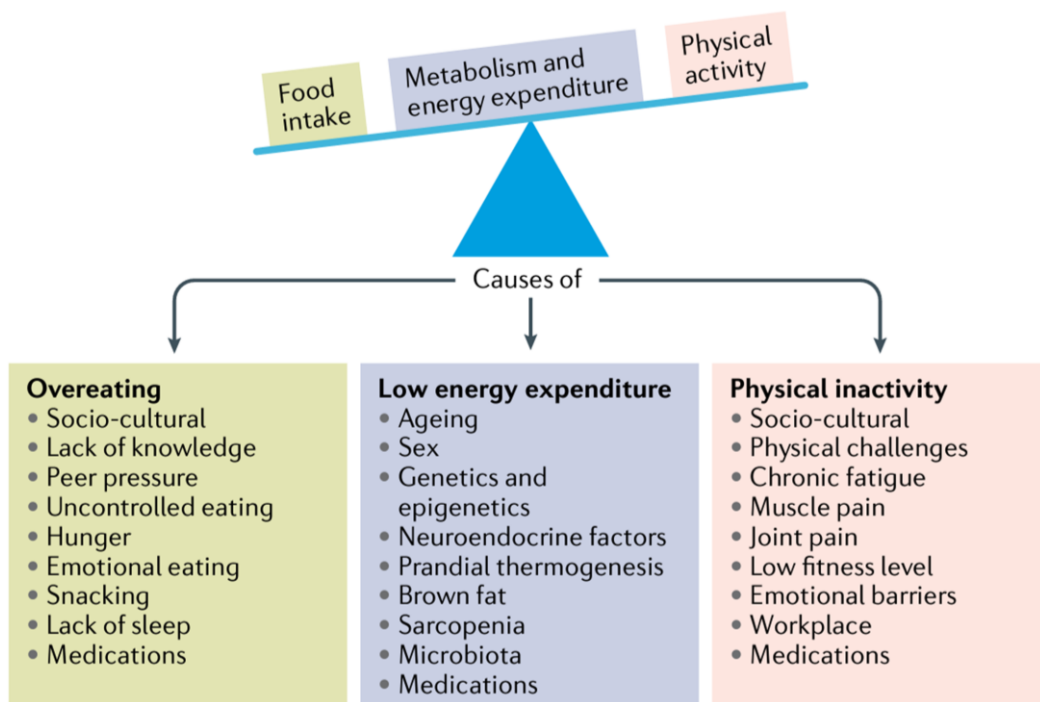
in atherosclerosis experimental models, where its absence leads to lower circulating neutrophils and improved atherosclerosis. Although these findings are encouraging, various limitations have been identified, needing a greater understanding of molecular mechanisms. Furthermore, our results demonstrated how *Clec4a4* deletion is ineffective in reducing obesity-related inflammation, with KO mice showing a preserve diet-induced obesity development with impaired glucose metabolism.

FIGURES



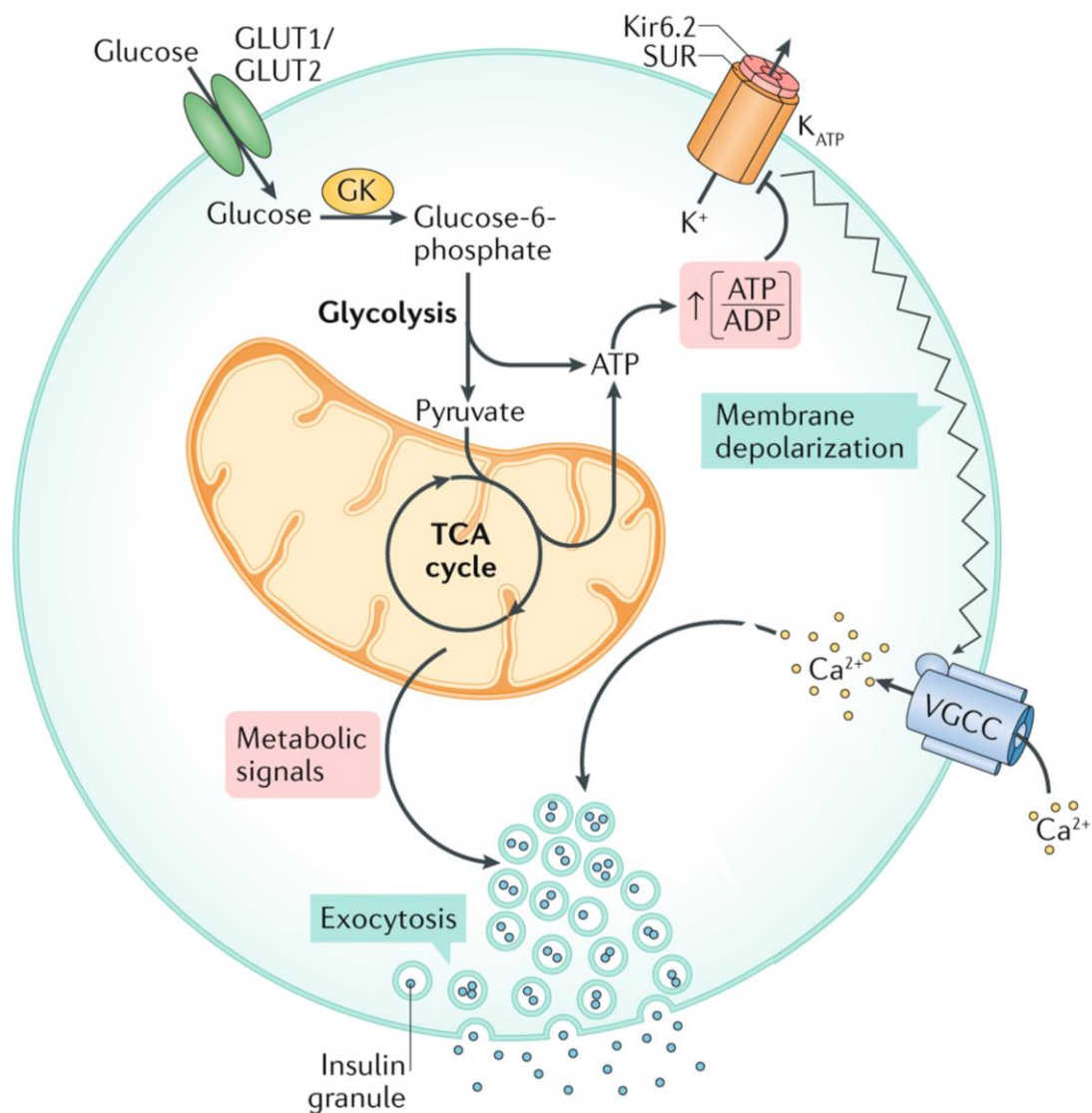
Adapted from (114) Vaduganathan M, et al. The Global Burden of Cardiovascular Diseases and Risk: A Compass for Future Health. *J Am Coll Cardiol* (2022).

Fig.1 Global burden of cardiovascular diseases update to 2021.



Adapted from (115) Blüher M. Obesity: global epidemiology and pathogenesis. *Nat Rev Endocrinol* 2019 155 (2019).

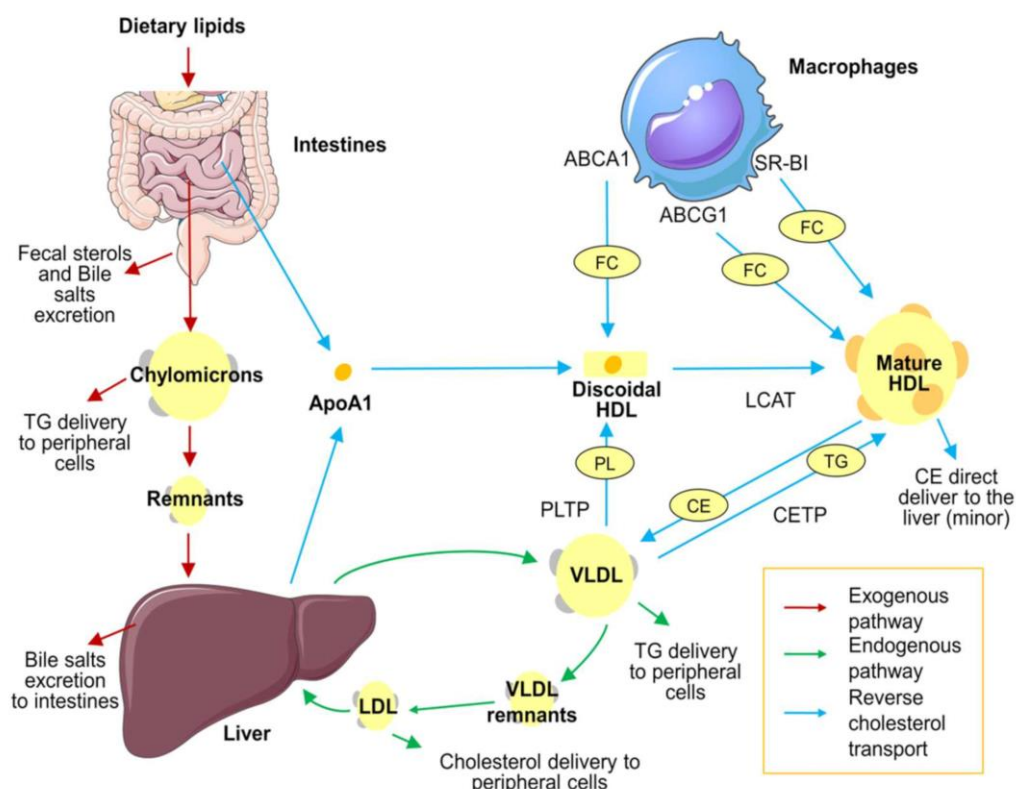
Fig.2 Several causes of obesity. Different factors, such as the overeating, the low energy expenditure and the physical inactivity, can alter the homeostasis of the energy balance thus leading to obesity.



Adapted from (116) Campbell JE, Newgard CB. Mechanisms controlling pancreatic islet cell function in insulin secretion. *Nat Rev Mol Cell Biol* 2021 22:2 (2021).

Fig. 3 The insulin release system. Glucose uptake into β -cells occurs via GLUT1 (human) or GLUT2 (rodent) transporters. Then glucose, after being converted in glucose 6 phosphate by glucokinase (GK), undergoes glycolysis followed by the oxidation via the tricarboxylic acid (TCA) cycle and generation of ATP. The increased ATP levels results in the closure of K_{ATP} channels and following membrane depolarization, which leads to the opening of voltage-gated calcium channels (VGCC). The augmented income of calcium triggers the release of insulin granules.

(cAMP, cyclic AMP; GIP, gastric inhibitory polypeptide; GLP1, glucagon-like peptide 1.)

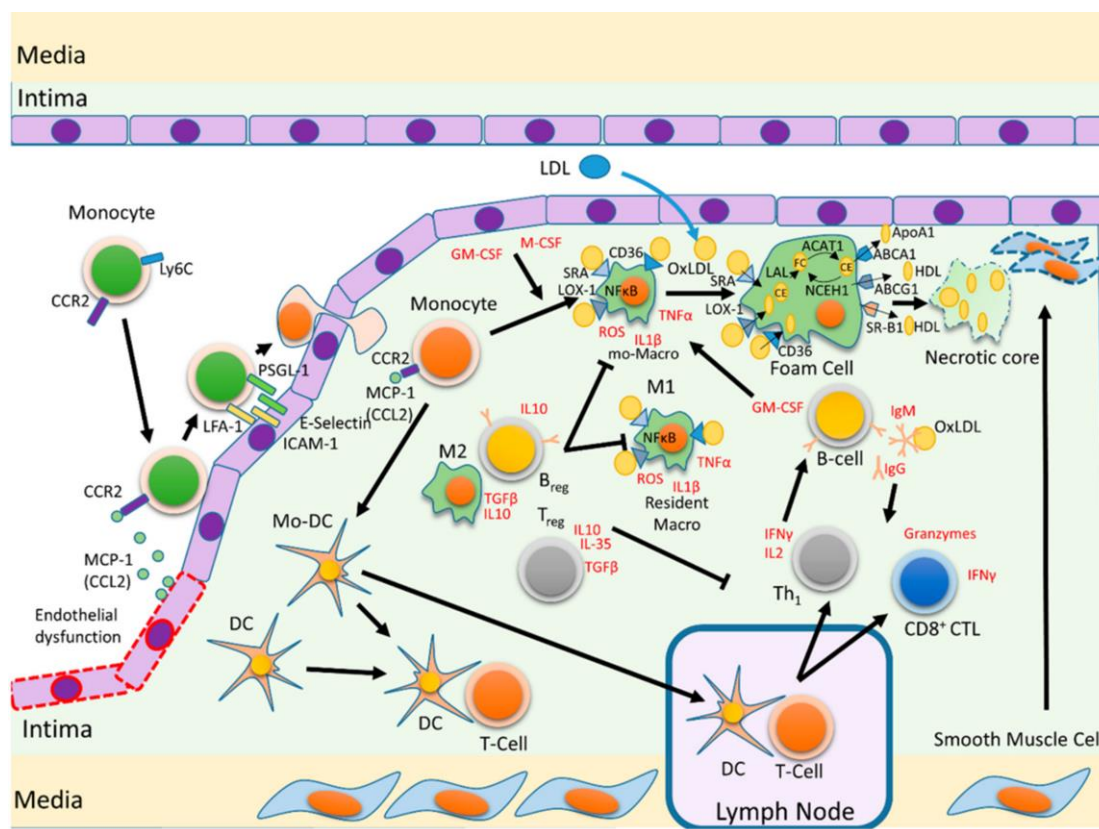


Adapted from (117) Sanllorente A, et al. Modification of high-density lipoprotein functions by diet and other lifestyle changes: A systematic review of randomized controlled trials. *J Clin Med* (2021).

Fig.4 The lipid transport system through the bloodstream. Lipid distribution in the body occurs in three different pathways, the exogenous (red arrows), the endogenous (green arrows) and the reverse one (blue arrows).

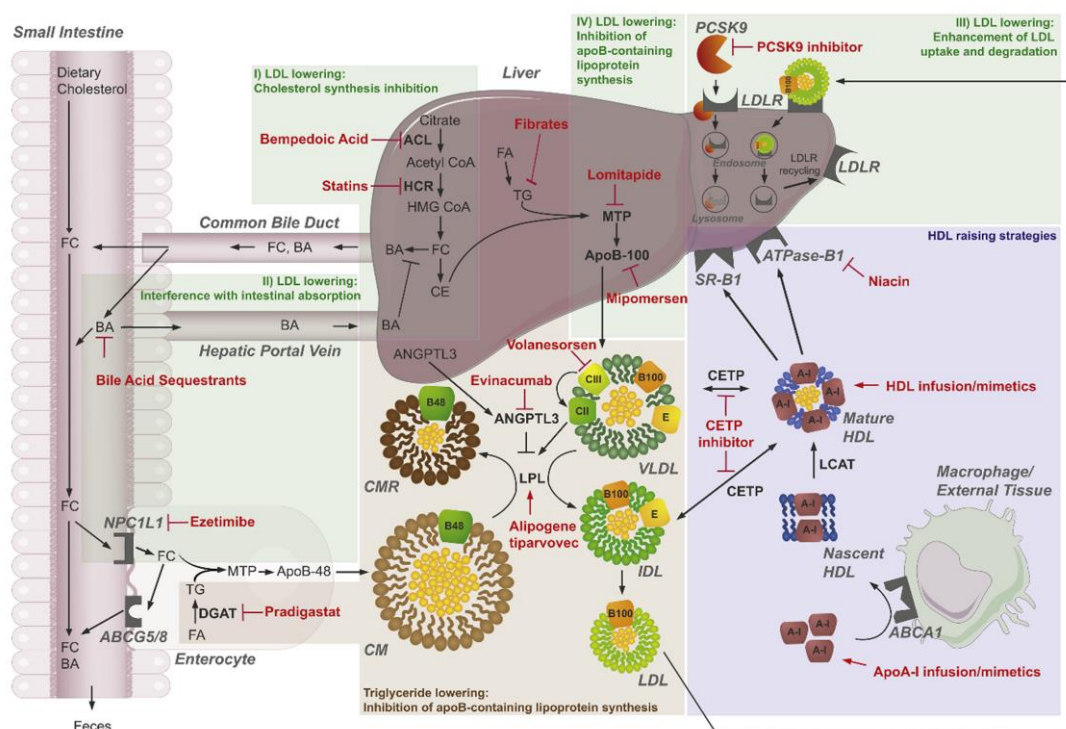
The first shows the absorption of dietary triglycerides, free cholesterol, and cholesteryl esters through the enterocytes, which package them into chylomicrons, then released in the bloodstream. The endogenous pathway regards the liver packaging of TG and cholesterol in VLDL: while these transport lipids to peripheral tissues, VLDL remnants come back to the liver and are converted to LDL. HDLs are responsible for reverse cholesterol transport. ApoA1 is produced by the liver and release as a lipid-free monomer, able to collect free cholesterol of peripheral cells, such macrophages, through the ABCA1 receptor. LCAT enzymes continuously internalize free cholesterol in the HDL core, converting it to cholesteryl esters and producing the mature form of HDL. The accumulated cholesterol can be transported back to the liver.

(ABCA1: ATP-binding cassette transporter A1. ABCG1: ATP-binding cassette transporter G1. ApoA1: Apolipoprotein A1. CE: cholesterol esters. CETP: cholesteryl ester transfer protein. FC: free cholesterol. HDL: high-density lipoprotein. LCAT: lecithin cholesterol acyltransferase. LDL: low-density lipoprotein. PL: phospholipid. PLTP: phospholipid transfer protein. TG: triglycerides. VLDL: very low-density lipoprotein.)



Adapted from (48) Herrero-Fernandez B, et al. Immunobiology of atherosclerosis: A complex net of interactions. *Int J Mol Sci* (2019).

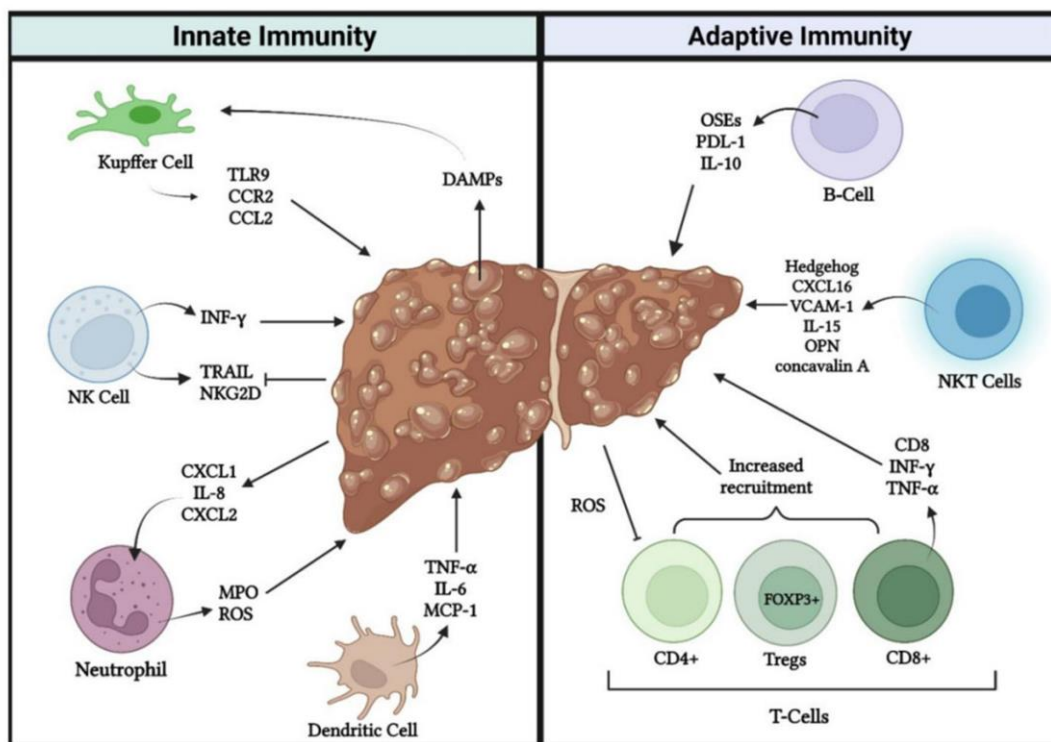
Fig.5 The net of interactions between immune system and lipids during atherogenesis. Once activated, endothelial cells express leukocyte adhesion molecules such as E and P-selectins, the glycoproteins ICAM-1 and VCAM-1, and the chemokine MCP-1, which signals via CCR2, thus recruiting inflammatory monocyte. LDL deposition stimulates the release of M-CSF and GM-CSF which induce the maturation of invading monocytes into macrophages or dendritic cells. These cells, which express scavenger receptors such as CD36, LOX-1, and SR-A, detect and fill with modified LDLs, transforming into foam cells. Cholesterol esters (CE) are transformed into free cholesterol (FC) and free fatty acids by LAL or NCEH1, while ACAT1 and ACAT2 can both convert FC to CE; ABCA1, ABCG1, and SR-B1 can transfer FC outside the foam cell. The release of pro-inflammatory cytokines from antigen presenting cells (APCs) exacerbates this step. In the meantime, they process intraplaque oxLDLs and promote the adaptive immune response in atheromatous plaques and secondary lymphoid organs by presenting oxLDL-derived antigens T lymphocytes. On the other hand, tolerogenic cells such as Bregs, Tregs, M2 macrophages, and tolerogenic DCs are involved in inflammation suppression and atheroma stabilization.



Adapted from (15) Soppert J, et al. Lipoproteins and lipids in cardiovascular disease: from mechanistic insights to therapeutic targeting. *Adv Drug Deliv Rev* (2020).

Fig. 6 Therapeutic targeting to lipoproteins and lipids to limit atherosclerosis. There are different therapeutic strategies to reduce the cardiovascular risk, involving LDL-lowering, triglyceride-lowering, Lp(a)-lowering and HDL-rising approaches. The LDL-lowering agents act on a plethora of mechanism, including I) inhibition of cholesterol synthesis; II) impairment of intestinal absorption of cholesterol and bile acids; III) enhancement of LDL uptake and degradation; and IV) interference with synthesis of ApoB-containing lipoprotein particles.

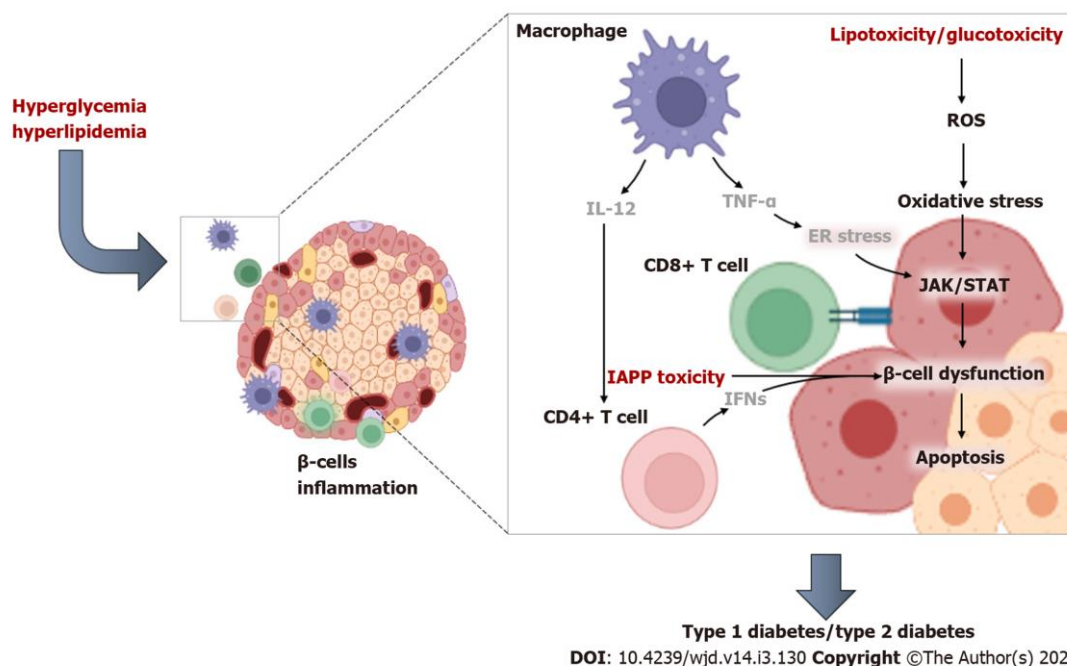
(A-I, ApoA-I; ABCG5/8, ATP-binding cassette transporters G5 and G8; Acetyl CoA, acetyl coenzyme A; ACL, ATP citrate lyase; ATPase-B1, ATP synthase β -chain; ANGPTL3, angiopoietin-like 3; B48, ApoB-48; B100, ApoB-100; BA, bile acid; CII, ApoC-II; CIII, ApoC-III; CE, cholesteryl ester; CETP, cholesterol ester transfer protein; CM, chylomicron; CMR, chylomicron remnant; DGAT, diacylglycerol acyltransferase; E, ApoE; FA, fatty acid; FC, free cholesterol; HCR, HMG CoA reductase; HDL, high-density lipoprotein; HMG CoA, 3-hydroxy-3-methylglutaryl coenzyme A; IDL, intermediate-density lipoprotein; LCAT, lecithin-cholesterol acyltransferase; LDL, low-density lipoprotein; LDLR, LDL receptor; LPL, lipoprotein lipase; MTP, microsomal triglyceride transfer protein; NPC1L1, Niemann-Pick C1 like 1; PCSK9, proprotein convertase subtilisin/kexin type 9; SR-B1, scavenger receptor class B member 1; TG, triglyceride; VLDL, very low-density lipoprotein).



Adapted from (118) Gregory SN, et al. Alteration in immune function in patients with fatty liver disease. *Hepatoma Res* (2022).

Fig. 7 Innate and adaptive immune responses within the liver. In parallel by the triglyceride accumulation within hepatocytes, subsequent inflammatory pathways activate, both from innate immunity, such as dendritic cell, neutrophils, NK cells and Kupffer cells, as well as from adaptive immunity, comprising T and B cells and NKT cells. Together they release pro-inflammatory cytokines which worsen the hepatic metabolic phenotype leading to more severe diseases.

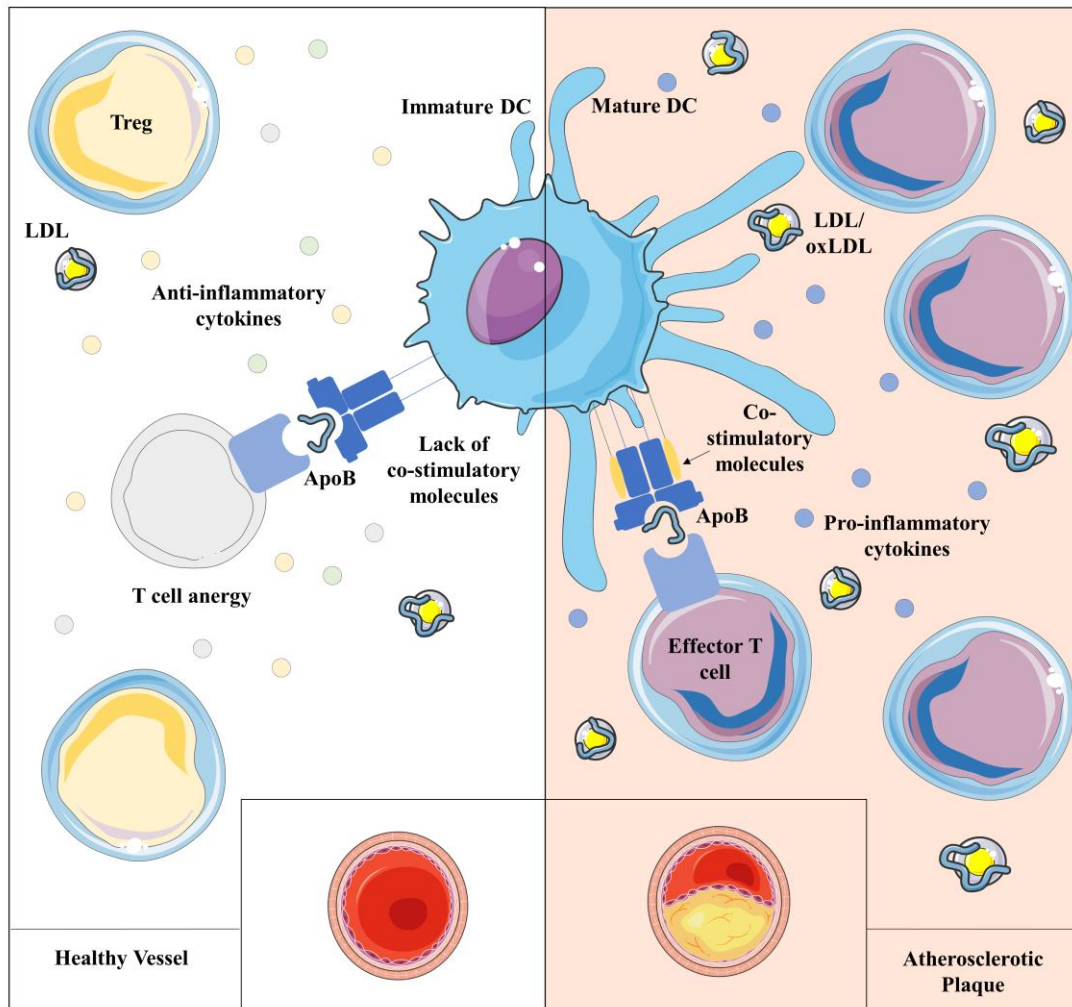
(MPO: myeloperoxidase; TNF: tumor necrosis factor; TLR: toll-like receptor; TRAIL: tumor necrosis factor-related apoptosis-inducing ligand; OSEs: oxidative stress-derived epitopes; OPN: Osteopontin; VCAM: vascular cell adhesion molecule; IL: interleukin; PDL: programmed death ligand).



Adapted from (39) Dłudla P V, et al. Pancreatic β-cell dysfunction in type 2 diabetes: Implications of inflammation and oxidative stress. *World J Diabetes* (2023).

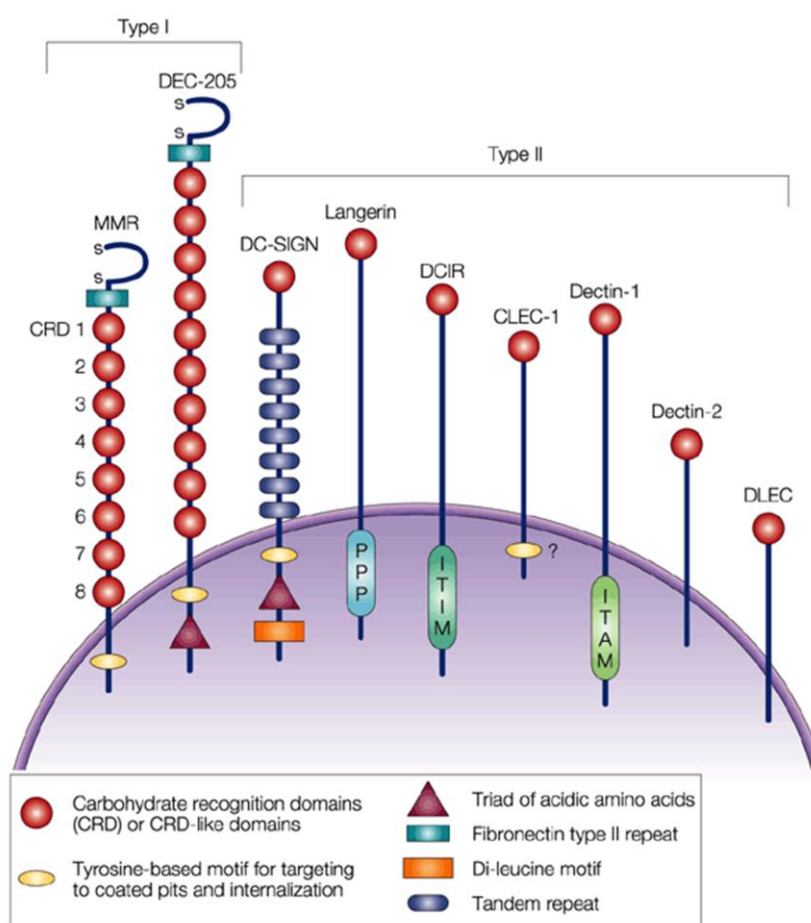
Fig. 8 The involvement of immune response in β-cell dysfunction in conditions of type 2 diabetes. Resident antigen presenting cells, such as macrophages and dendritic cells, recruit and activate CD4⁺ and/or cytotoxic CD8⁺ T cells through the release of cytokines and interleukins within the pancreatic islets. This leads to a worsen inflammatory phenotype, driven by TNF-α and the activation of pro-inflammatory signals thus promoting β-cell failure.

(IL-12: Interleukin-12; TNF-α: Tumor necrosis factor-alpha; IFNs: Interferons; IAPP: Islet amyloid polypeptide; ROS: Reactive oxygen species; ER stress: Endoplasmic reticulum stress; JAK/STAT: Janus kinase/signal transducer and activator of transcription).



Adapted from (56) Bellini R, Bonacina F, Norata GD. Crosstalk between dendritic cells and T lymphocytes during atherosclerosis: Focus on antigen presentation and break of tolerance. *Front Cardiovasc Med* (2022).

Fig. 9 The delicate crosstalk between DCs and T lymphocytes: when its alteration leads to worsen atherosclerosis. Atherosclerosis is caused by a disruption in lipid homeostasis as well as a shift in the balance of innate and adaptive immune responses mediated by DCs and T and B lymphocytes. Inflammation stimulates the maturation of DCs capable of activating T lymphocytes against self-antigens, which contributes to atherosclerosis once immune homeostasis is disrupted.

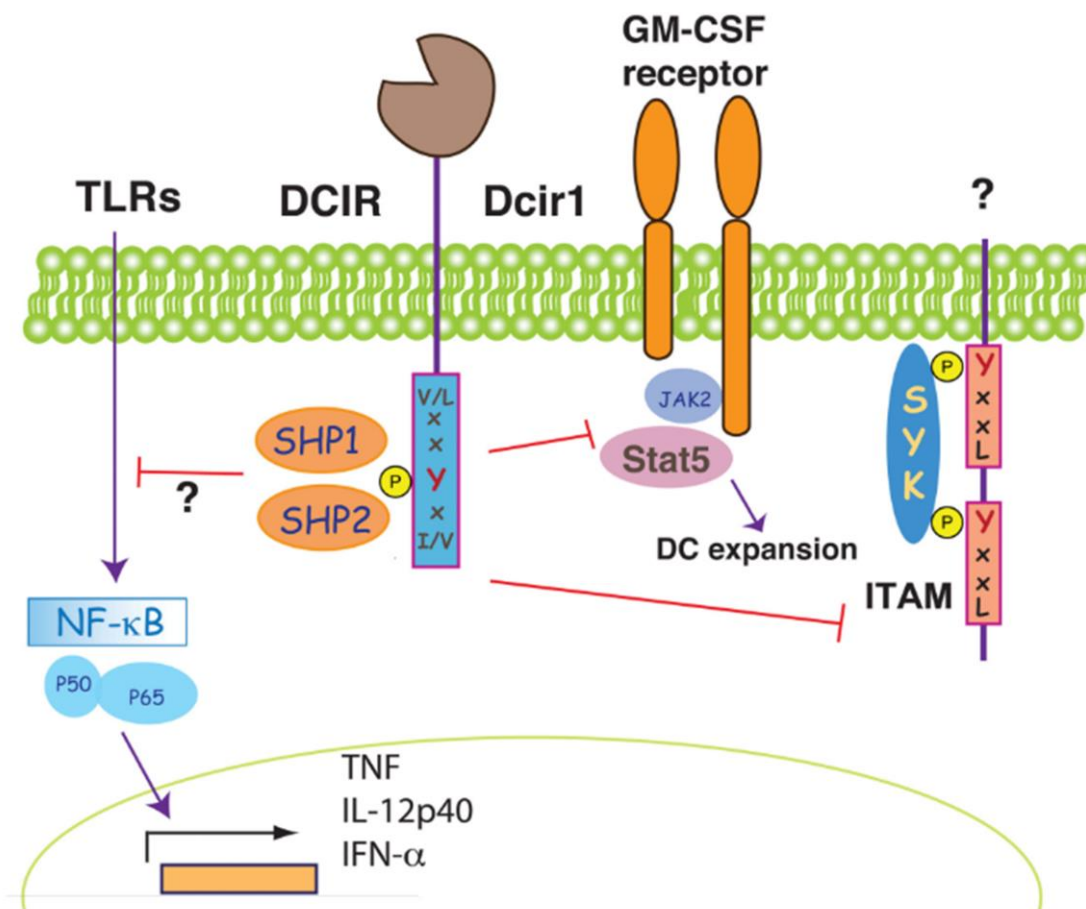


Nature Reviews | Immunology

Adapted from (62) Figdor CG, et al. C-type lectin receptors on dendritic cells and Langerhans cells. *Nat Rev Immunol* (2002).

Fig.10 Several C-type lectin receptors are necessary to manage the immune response. Innate immune cells, particularly dendritic cells, express and need several C-type lectin receptors (CLRs), together with Toll-like receptors, to precisely control antigen uptake and following immune response. Among C-type lectin receptors, it is possible to distinguish between type I - including MMR and DEC-205 - and type 2, including different receptor with the peculiarity to expose only one carbohydrate recognition domain (CRD) at their carboxy-terminal extracellular domain. Intracellularly, CLRs can contain several conserved motifs important for antigen uptake as well as potential signalling motifs (ITIM, ITAM, proline-rich regions (P)).

(CLEC-1, C-type lectin receptor 1; DCIR, dendritic cell immunoreceptor; DC-SIGN, dendritic-cell specific ICAM-3 grabbing non-integrin; DLEC, dendritic cell lectin; ITAM, immunoreceptor tyrosine-based activation motif; ITIM, immunoreceptor tyrosine-based inhibitory motif; MMR, macrophage mannose receptor).



Adapted from (65) Sancho D, Reis e Sousa C. Signaling by Myeloid C-Type Lectin Receptors in Immunity and Homeostasis. *Annu Rev Immunol* (2012)

Fig. 11 Intracellular pathway and interactions of DCIR/Clec4a. Peculiarity of DCIR, is the presence of an intracellular ITIM domain. This, when phosphorylated, binds SHP1 and SHP2 phosphatases able to inhibit TLR-NFκB signalling with effects on pro-inflammatory genes downstream. ITIM interacts even with ITAM signalling of unidentified receptors and act on STAT5 activation of GM-CSF receptor modulating DC expansion.

Parts of the results of this dissertation have been published in:

Bellini R, Moregola A, Nour J, Rombouts Y, Neyrolles O, Uboldi P, Bonacina F, Norata GD. Dendritic cell marker *Clec4a4* deficiency limits atherosclerosis progression. *Atherosclerosis Plus* (2023) 51:8–12. doi: 10.1016/J.ATHPLU.2022.12.001

Bellini R, Moregola A, Nour J, Uboldi P, Fabrizia Bonacina |, Norata GD. Dendritic cell immunoreceptor 2 (DCIR2) deficiency decreases hepatic conventional dendritic cell content but not the progression of diet-induced obesity. *Immunity, Inflamm Dis* (2023) 11:e1024. doi: 10.1002/IID3.1024

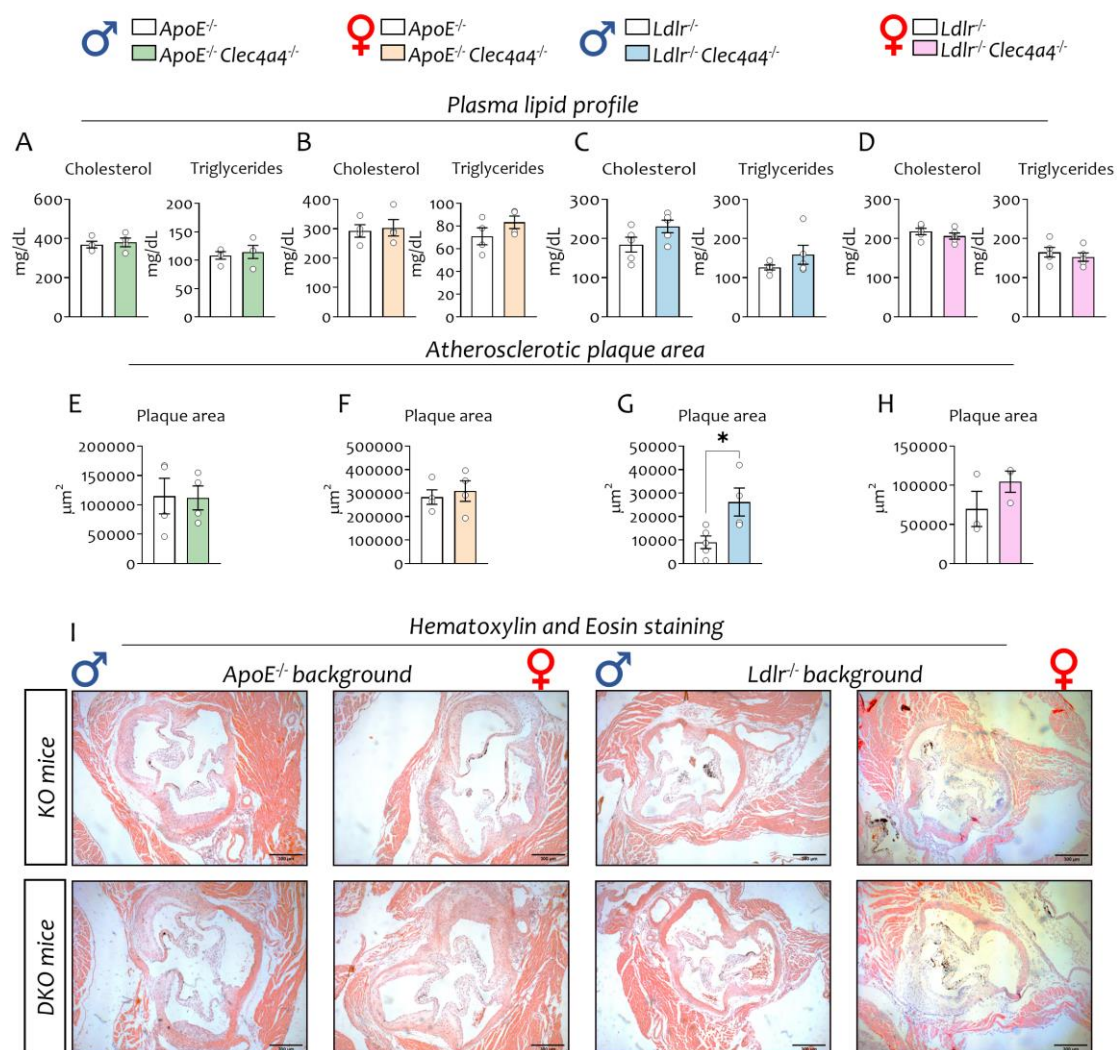


Fig. 12 Plasma lipid profile and atherosclerotic plaque phenotype on ApoE^{-/-} or Ldlr^{-/-} background. A-D) Plasma lipid levels (cholesterol and triglycerides, respectively) of male and female mice on ApoE^{-/-} and Ldlr^{-/-} background expressed as mg/dL. E-H) Atherosclerotic lesion area analysed at the aortic sinus of DKO mice compared to the ApoE^{-/-} and Ldlr^{-/-} counterpart, considering male and female mice separately. I) Representative images of Haematoxylin and Eosin staining acquired at the aortic sinus of ApoE^{-/-} or Ldlr^{-/-} (above) and DKO (below) mice, both for males and females. 4x of magnification and 300 µm of scale bar. Results are expressed as mean±SEM. n=5 per group. Statistical analyses were performed with parametric two-sides unpaired T-test. *p<0.05.

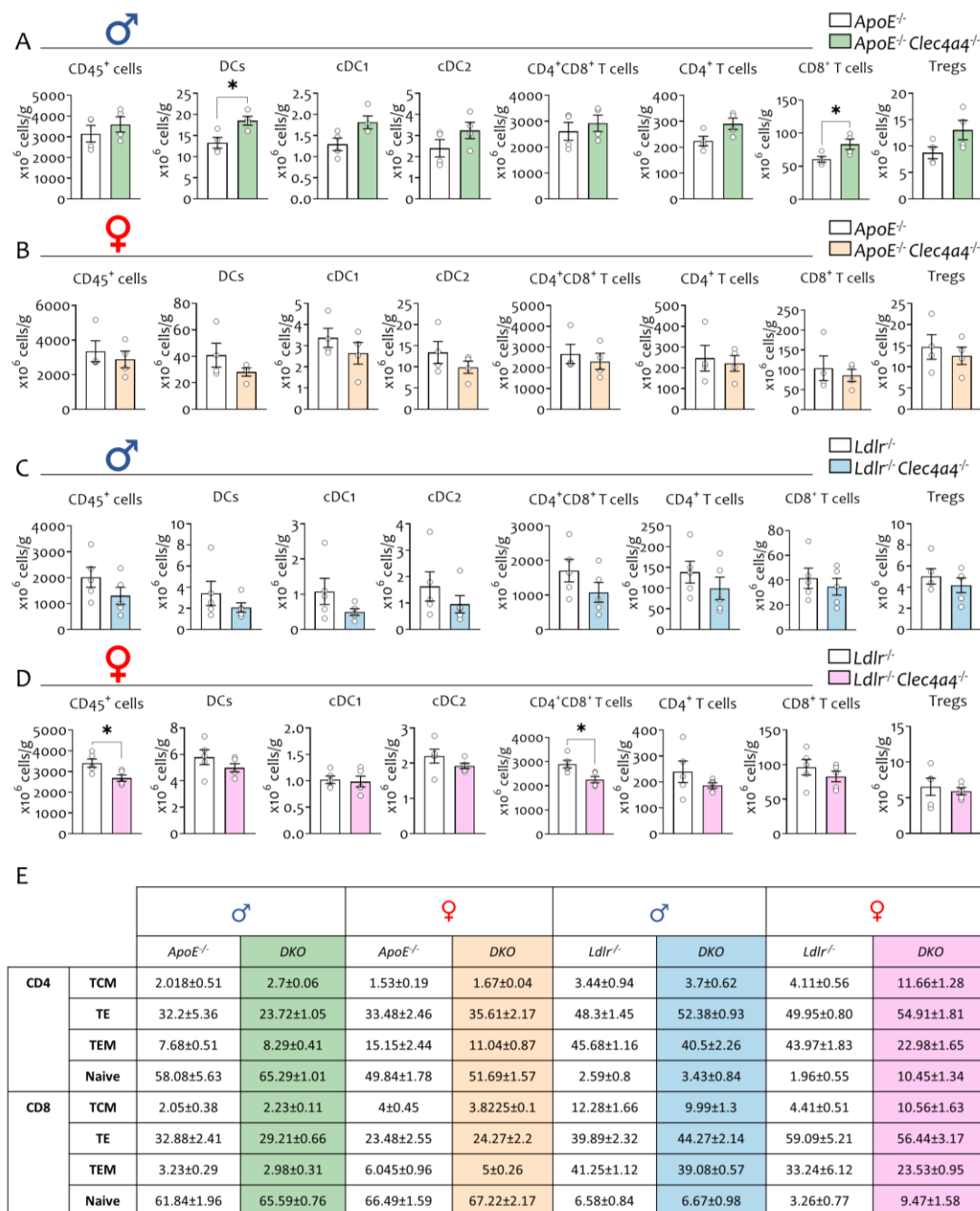


Fig. 13 Flow cytometry immunophenotype of the thymus of mice on ApoE^{-/-} or Ldlr^{-/-} background.

A-D) Flow cytometry analysis of CD45⁺ leukocytes, DCs and related subsets as well as T lymphocytes (CD4⁺CD8⁺ and CD4⁺ or CD8⁺ cells) and Tregs expressed as number of cells per gram of thymus. E) Percentage of CD4⁺ or CD8⁺ T cell subsets (T central memory, TCM; T effector, TE; T effector memory, TEM; and T naive) of male and female mice on ApoE^{-/-} or Ldlr^{-/-} background. Results are expressed as mean±SEM. n=5 per group. Statistical analyses were performed with parametric two-sides unpaired T-test or Mann-Whitney nonparametric unpaired T-test when needed. *p<0.05.

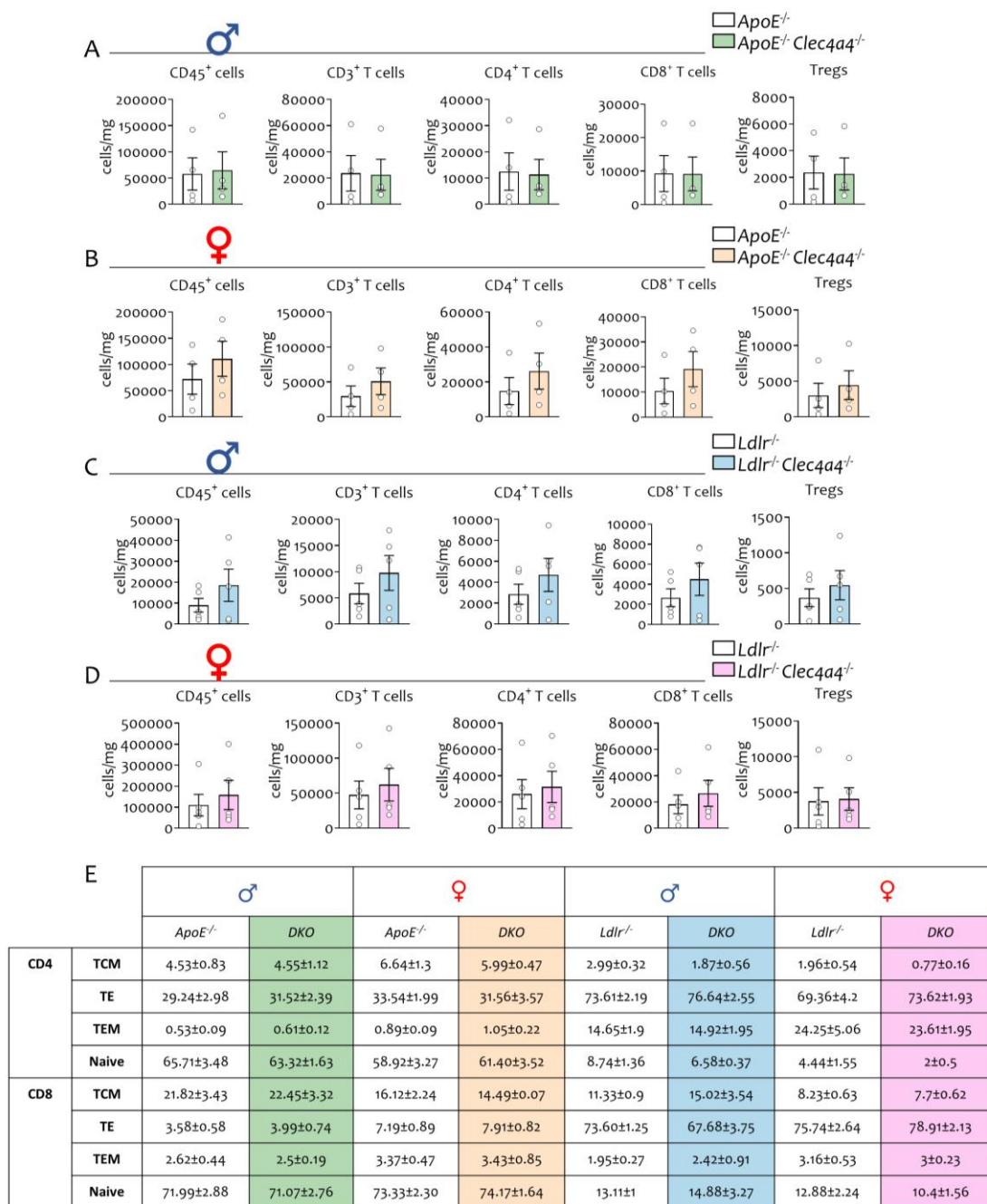


Fig. 14 Flow cytometry immunophenotype of cardiac lymph nodes (cLNs) of mice on ApoE^{-/-} or Ldlr^{-/-} background. A-D) Flow cytometry analysis of CD45⁺ leukocytes and CD3⁺ T lymphocytes (as well as CD4⁺ or CD8⁺ T cells) and Tregs expressed as number of cells per mg of cLNs. E) Percentage of CD4⁺ or CD8⁺ T cell subsets (TCM, TE, TEM and T naive) of male and female mice on ApoE^{-/-} or Ldlr^{-/-} background. Results are expressed as mean±SEM. n=5 per group. Statistical analyses were performed with parametric two-sides unpaired T-test or Mann-Whitney nonparametric unpaired T-test when needed. *p<0.05.

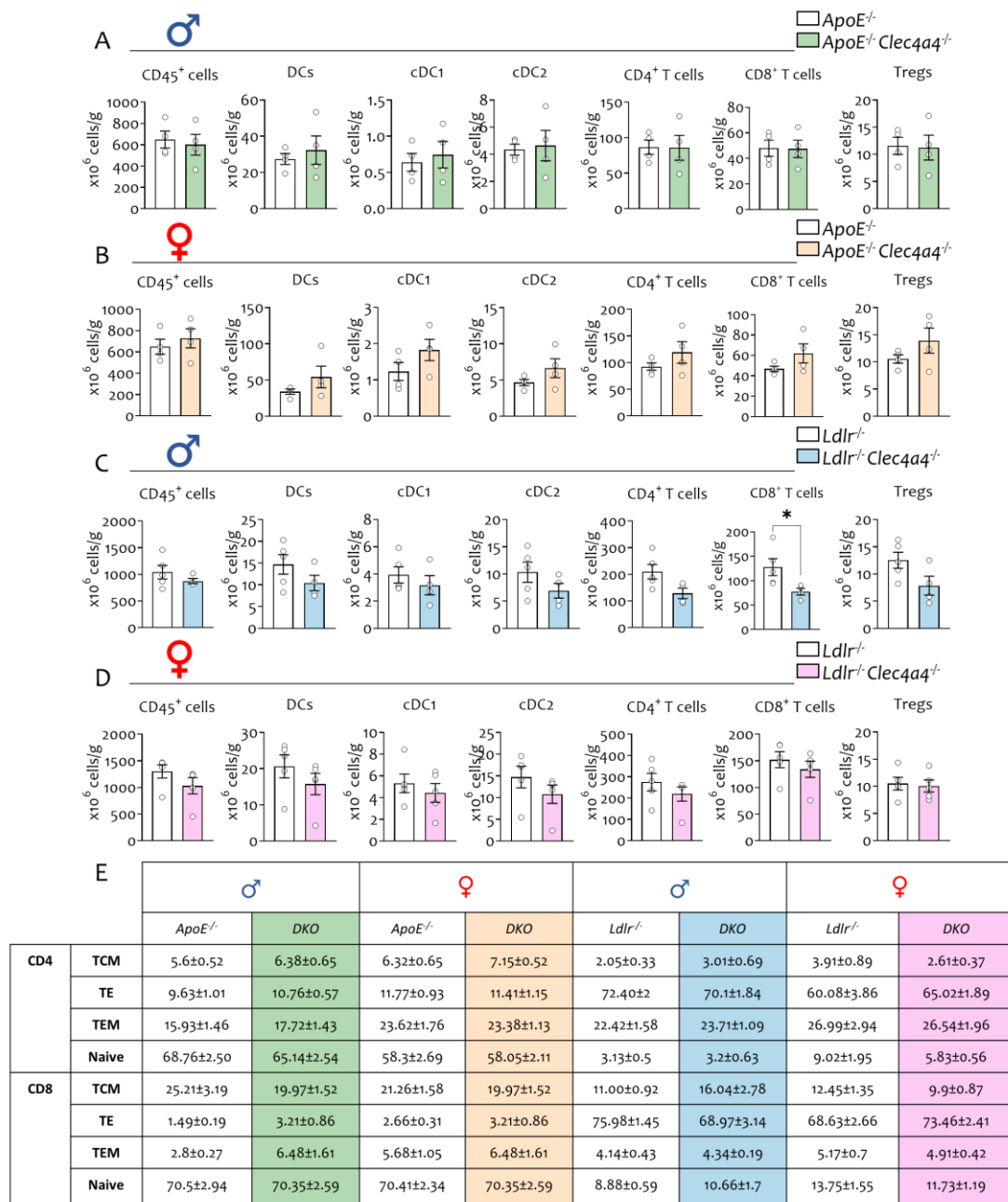


Fig. 15 Flow cytometry immunophenotype of the spleen of mice on $ApoE^{-/-}$ or $Ldlr^{-/-}$ background. A-D) Flow cytometry analysis of $CD45^{+}$ leukocytes, DCs and related subsets, T lymphocytes ($CD4^{+}$ or $CD8^{+}$ single positive cells) and Tregs expressed as number of cells per gram of spleen. E) Percentage of $CD4^{+}$ or $CD8^{+}$ T cell subsets (TCM, TE, TEM and T naive) of male and female mice on $ApoE^{-/-}$ or $Ldlr^{-/-}$ background. Results are expressed as mean±SEM. n=5 per group. Statistical analyses were performed with parametric two-sides unpaired T-test. * $p < 0.05$.

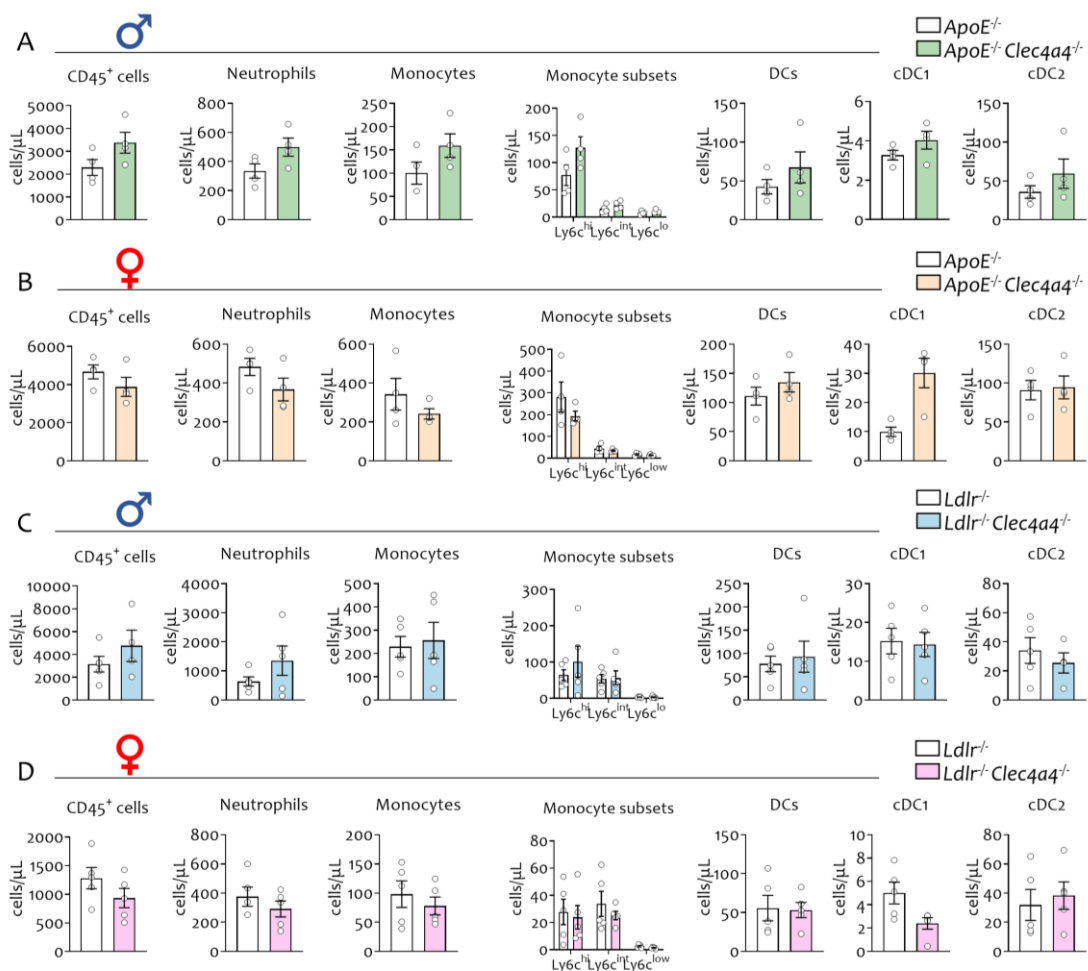


Fig. 16 Flow cytometry immunophenotype of the blood of mice on $ApoE^{-/-}$ or $Ldlr^{-/-}$ background: a focus on myeloid cells. A-D) Flow cytometry analysis of CD45⁺ leukocytes, divided into neutrophils, monocytes and DCs with their related subsets, expressed as number of cells per μ L of blood of male and female mice on $ApoE^{-/-}$ or $Ldlr^{-/-}$ background. Results are expressed as mean \pm SEM. n=5 per group. Statistical analyses were performed with parametric two-sides unpaired T-test. * $p < 0.05$.

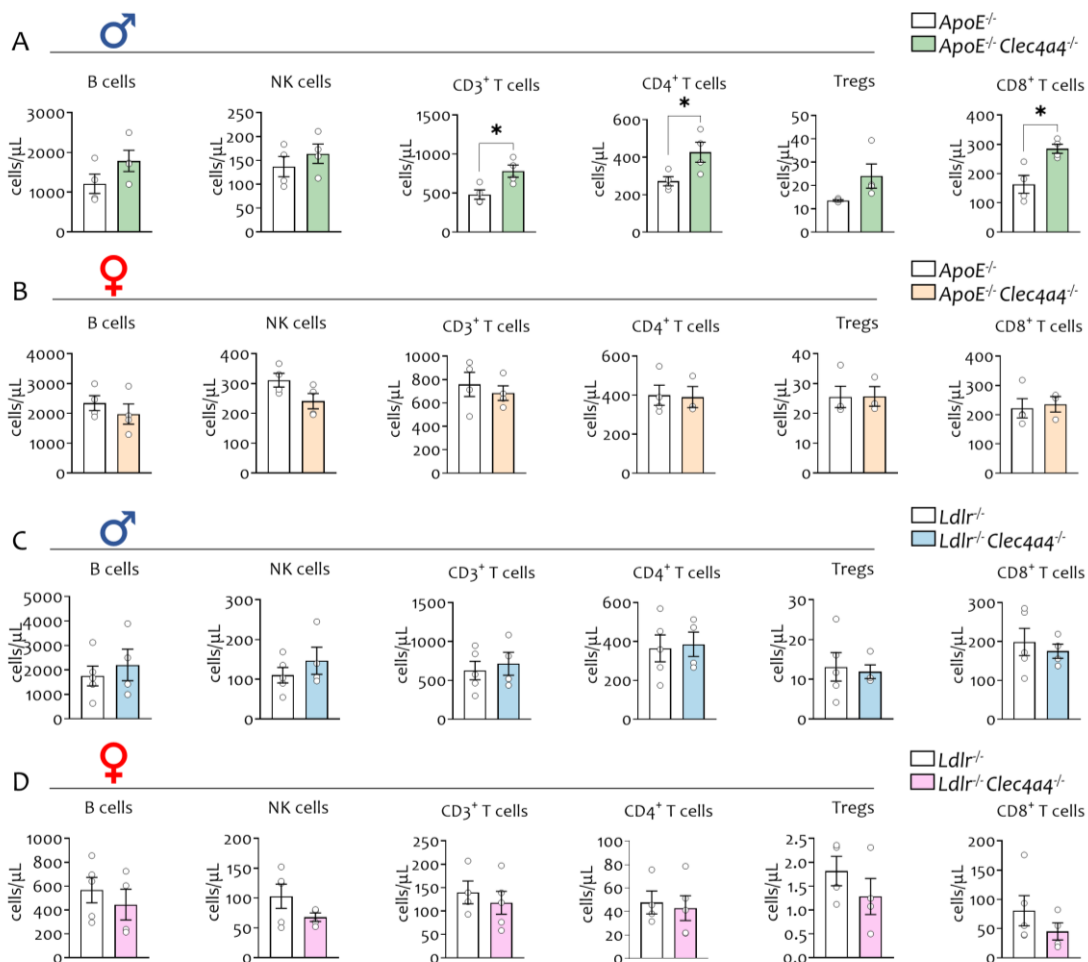


Fig. 17 Flow cytometry immunophenotype of the blood of mice on *ApoE*^{-/-} or *Ldlr*^{-/-} background: a focus on lymphoid cells. A-D) Flow cytometry analysis of B lymphocytes, NK cells, CD3⁺ lymphocytes distinguished between CD4⁺, Tregs and CD8⁺ T cells, expressed as number of cells per μL of blood of male and female mice on *ApoE*^{-/-} or *Ldlr*^{-/-} background. Results are expressed as mean±SEM. n=5 per group. Statistical analyses were performed with parametric two-sides unpaired T-test. *p<0.05.

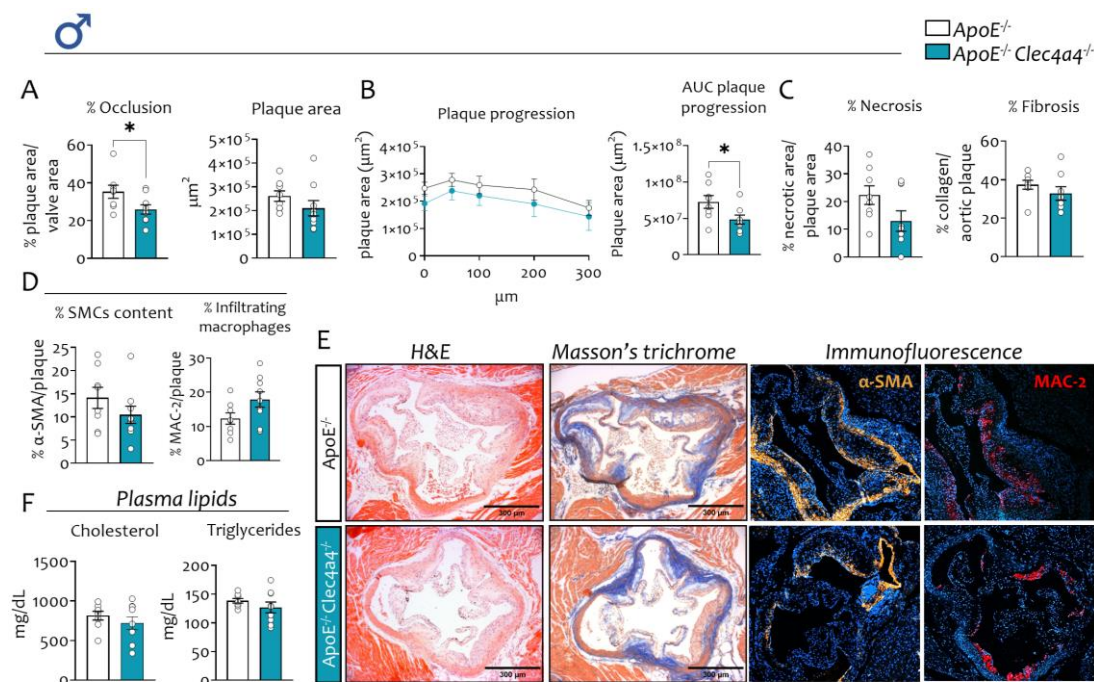


Fig. 18 Atherosclerotic plaque phenotype and plasma lipid levels of WTD-fed male DKO and ApoE^{-/-} mice. A-B) Percentage of aortic occlusion, atherosclerotic plaque area and plaque progression with related AUC along the first 300 μm from the aortic sinus of male DKO mice compared to single KO mice on ApoE^{-/-} background. C-D) Aortic plaque features analysis, such as necrosis, fibrosis, smooth muscle cell (SMC) content and infiltrating macrophages within the atheroma of male DKO mice compared to single KO. E) Representative plaque figures at 5x magnification of haematoxylin and eosin (H&E) and Masson's trichrome staining (left) and immunofluorescent staining of α -SMA and MAC-2 staining (right) at aortic sinus of male ApoE^{-/-} (above) and Clec4a4^{-/-} ApoE^{-/-} (below). F) Plasma lipid profile - cholesterol and triglyceride levels - of male DKO compared to ApoE^{-/-} mice. Scale bar of 300 μm . Results are expressed as mean \pm SEM. n = 8-9 mice per group. Statistical analyses were performed with parametric two-sides unpaired T-test. * $p < 0.05$; ** $p < 0.01$; *** $p < 0.001$.

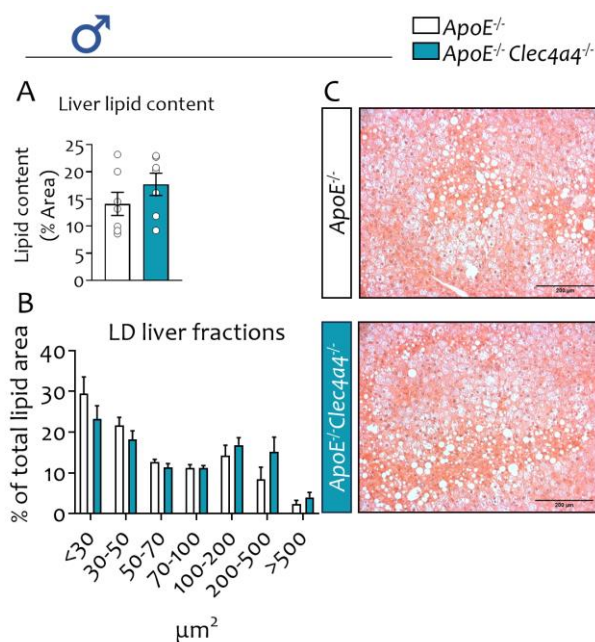


Fig.19 Hepatic lipid distribution and lipid droplet fractions of WTD-fed male DKO and ApoE^{-/-} mice. A) Percentage of hepatic steatosis – lipid content - within the liver of male DKO mice compared to ApoE^{-/-} counterpart. B) Lipid droplet distribution based on their dimensions, within the liver of male DKO compared to ApoE^{-/-} mice. C) Representative figures of 10x magnification of haematoxylin and eosin (H&E) - stained liver sections of male ApoE^{-/-} (above) and DKO (below) mice. Scale bar of 200 μm . Results are expressed as mean \pm SEM. n = 7 mice per group. Statistical analyses were performed with parametric two-sides unpaired T-test and Two-way ANOVA with Sidak’s multiple comparisons. *p<0.05.

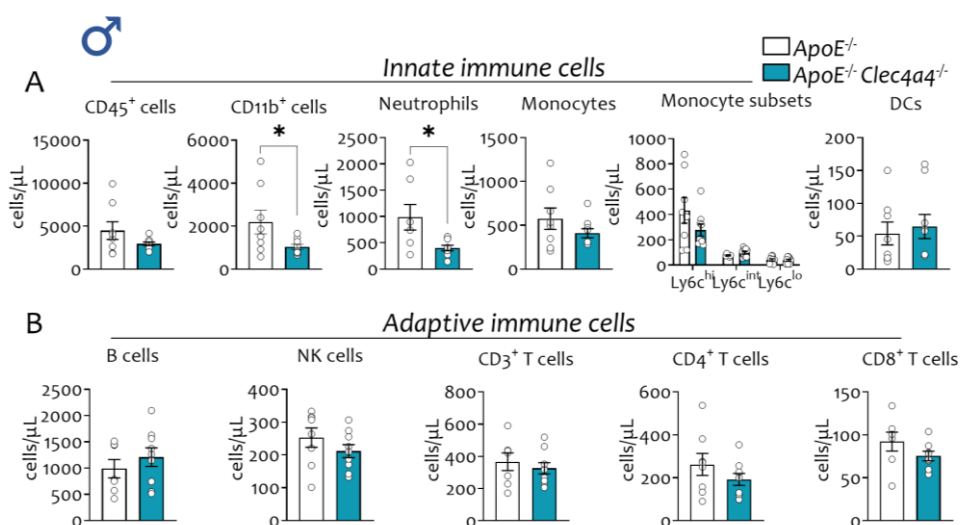


Fig. 20 Immunophenotype of circulating immune cells of WTD-fed male DKO and $ApoE^{-/-}$ mice. A) Flow cytometry analysis of the main innate immune circulating populations, namely total CD45⁺, CD11b⁺ myeloid cells, neutrophils, monocytes and their subsets and DCs, expressed as number of cells per μ L of blood in male DKO compared to single KO mice. B) Flow cytometry analysis of circulating B lymphocytes, NK cells, CD3⁺ lymphocytes distinguished between CD4⁺ and CD8⁺ T cells, expressed as number of cells per μ L of blood in male DKO compared to single KO mice. Results are expressed as mean \pm SEM. n = 8-9 mice per group. Statistical analyses were performed with parametric two-sides unpaired T-test or Mann-Whitney nonparametric unpaired T-test when needed. * $p < 0.05$.

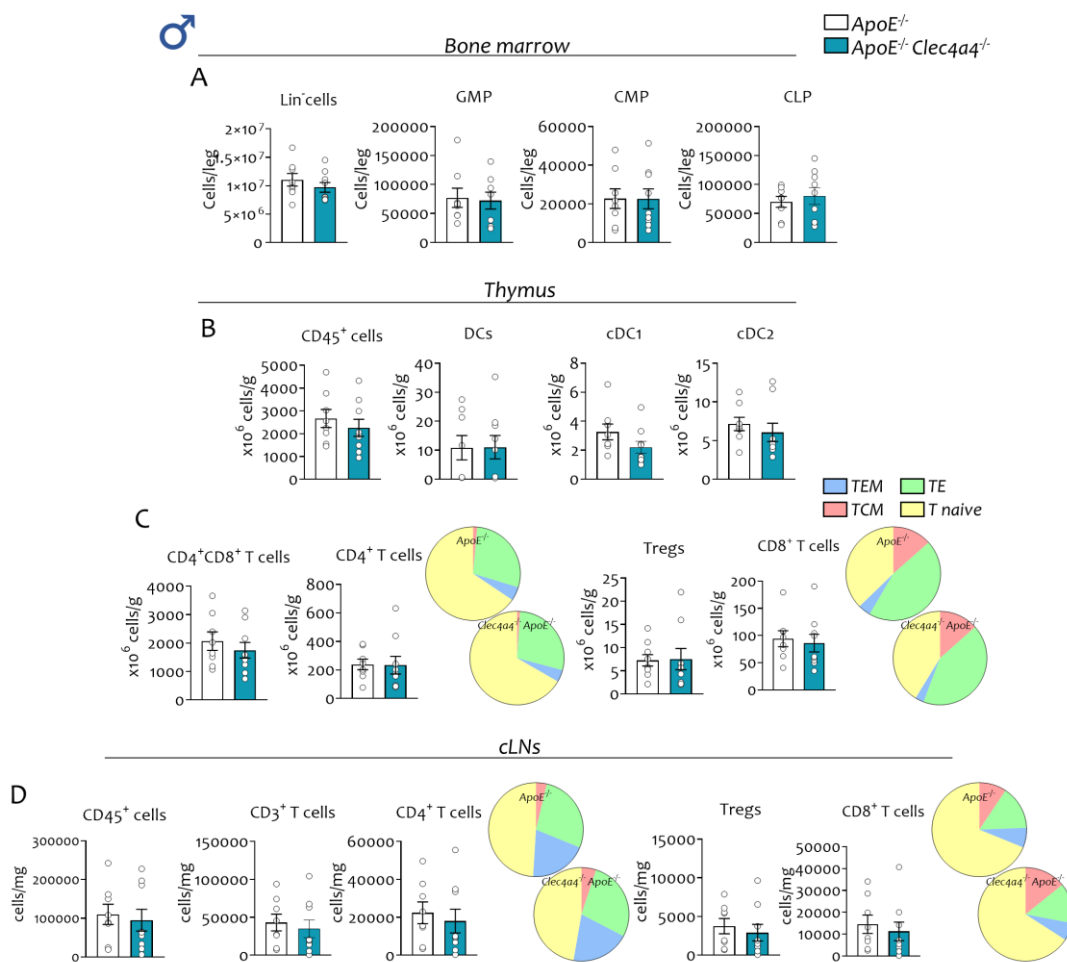


Fig. 21 Immunophenotype of bone marrow, thymus and cLNs of WTD-fed male DKO and ApoE^{-/-} mice. A) Flow cytometry analysis of bone marrow precursors, represented as lineage negative cells and divided into granulocyte-monocyte progenitors (GMPs), common myeloid progenitors (CMPs) and common lymphoid progenitors (CLPs), represented as number of cells per leg. B-C) Number of cells per gram of thymus of total CD45⁺ leukocytes, DCs with related subsets cDC1 and cDC2, double positive CD4⁺CD8⁺ cells, CD4⁺ T cells with related subsets and CD8⁺ T cells with related subsets. D) Number of cells per gram of cLNs of total CD45⁺ leukocytes, CD3⁺ lymphocytes, CD4⁺ T cells with related subsets and CD8⁺ lymphocytes with related subsets. Results are expressed as mean±SEM. n = 8-9 mice per groups. Statistical analyses were performed with parametric two-sides unpaired T-test. *p<0.05.

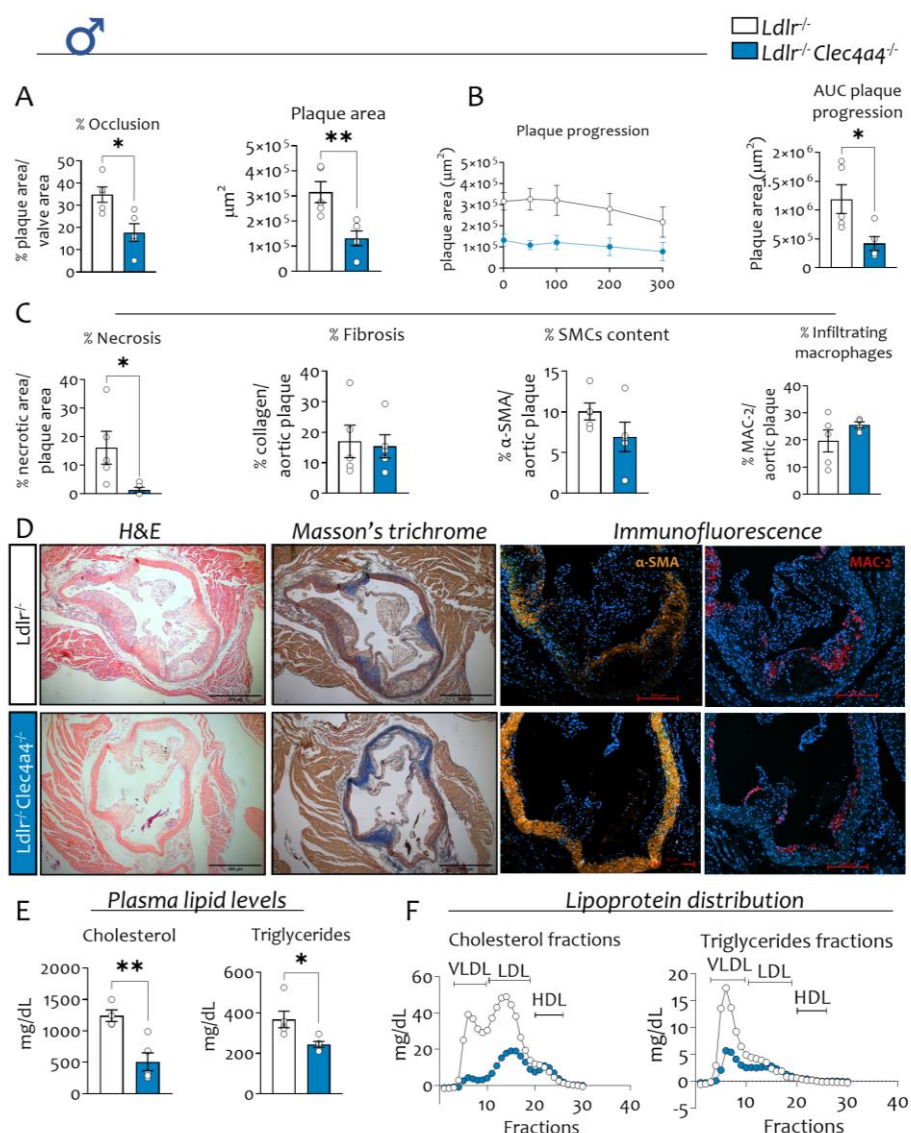


Fig. 22 Atherosclerotic plaque phenotype and plasma lipid levels of WTD-fed male DKO and *Ldlr*^{-/-} mice. A-B) Percentage of occlusion, atherosclerotic plaque area and plaque progression with related AUC along the first 300 μm from the aortic sinus of male DKO compared to *Ldlr*^{-/-} mice. C) Aortic plaque features analysis, such as necrosis, fibrosis, smooth muscle cell (SMC) content and infiltrating macrophages of male WTD-fed DKO mice compared to single KO. D) Representative plaque figures at 5x magnification of haematoxylin and eosin (H&E) and Masson's trichrome-stained sections at aortic sinus (left), and immunofluorescent staining of $\alpha\text{-SMA}$ and MAC-2 (right) of WTD-fed *Ldlr*^{-/-} (above) and *Ldlr*^{-/-} *Clec4a4*^{-/-} (below) male mice. E) Plasma lipid profile - cholesterol and triglyceride levels - of male DKO mice compared to *Ldlr*^{-/-} mice. F) Lipoprotein distribution - namely VLDL, LDL, HDL - based on cholesterol and triglyceride fractions, of male DKO mice compared to single KO mice. Scale bar of 300 μm . Results are expressed as mean \pm SEM. n = 5 mice per groups. Statistical analyses were performed with parametric two-sides unpaired T-test. * $p < 0.05$, ** $p < 0.01$.

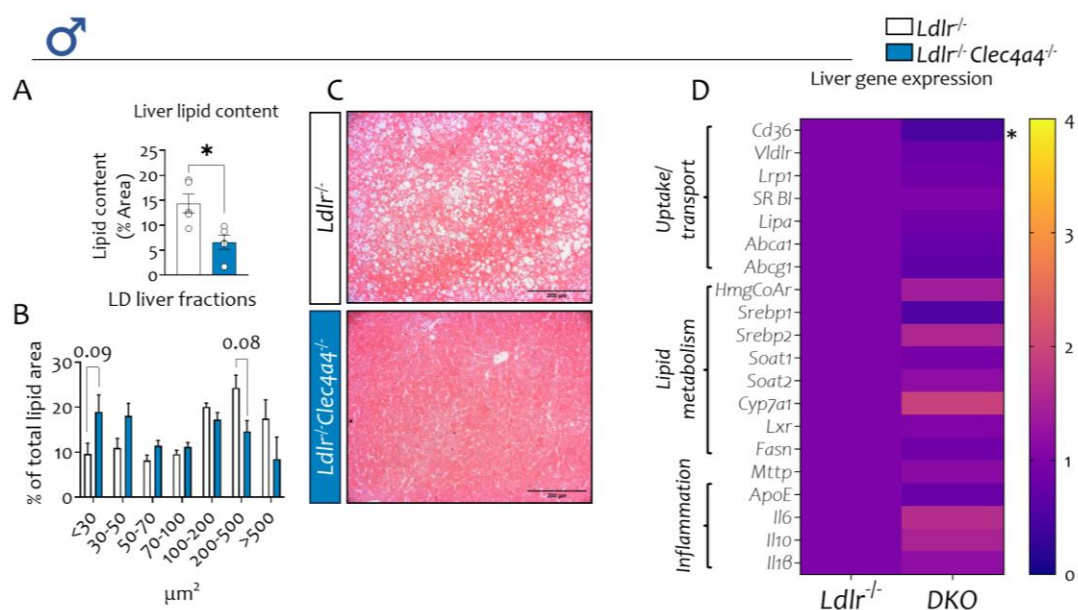


Fig. 23 Hepatic phenotype of WTD-fed male DKO and *Ldlr*^{-/-} mice. A) Percentage of hepatic steatosis – liver lipid content – of male DKO mice compared to single KO counterpart. B) Lipid droplet distribution, based on the dimensions, within the liver of male DKO and *Ldlr*^{-/-} mice. C) Representative figures at 10x magnification of haematoxylin and eosin (H&E) - stained sections of WTD-fed male *Ldlr*^{-/-} (above) and *Ldlr*^{-/-} *Clec4a4*^{-/-} (below) respectively with 200 µm of scale bar. D) Liver gene expression analysis of metabolic genes involved in lipid uptake, transport and metabolism and genes involved in the immune response. Results are expressed as mean±SEM. n = 5 mice per groups. Statistical analyses were performed with parametric two-sides unpaired T-test and Two-way ANOVA with Sidak’s multiple comparisons. **p*<0.05.

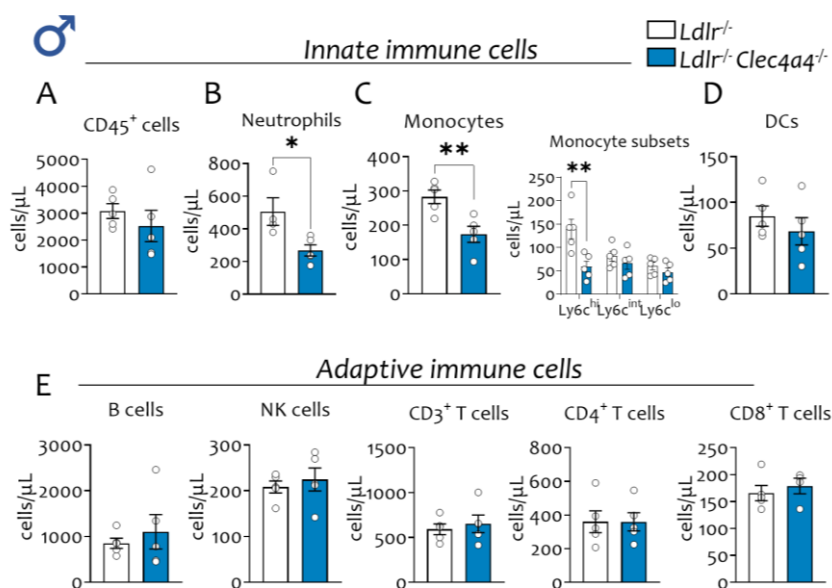


Fig. 24 Immunophenotype of circulating immune cells WTD-fed male DKO and *Ldlr*^{-/-} mice. A-D) Flow cytometry analysis of CD45⁺ leukocytes, focused on myeloid cells, such as neutrophils, monocytes and related subsets and DCs expressed as number of cells per μL of blood of WTD-fed male DKO and single KO mice. E) Number of circulating lymphoid immune cells, such as B lymphocytes, NK cells, CD3⁺ T lymphocytes and CD4⁺ or CD8⁺ subsets, expressed as number of cells per μL of blood. Results are expressed as mean \pm SEM. n = 5 mice per groups. Statistical analyses were performed with parametric two-sides unpaired T-test. * $p < 0.05$, ** $p < 0.01$.

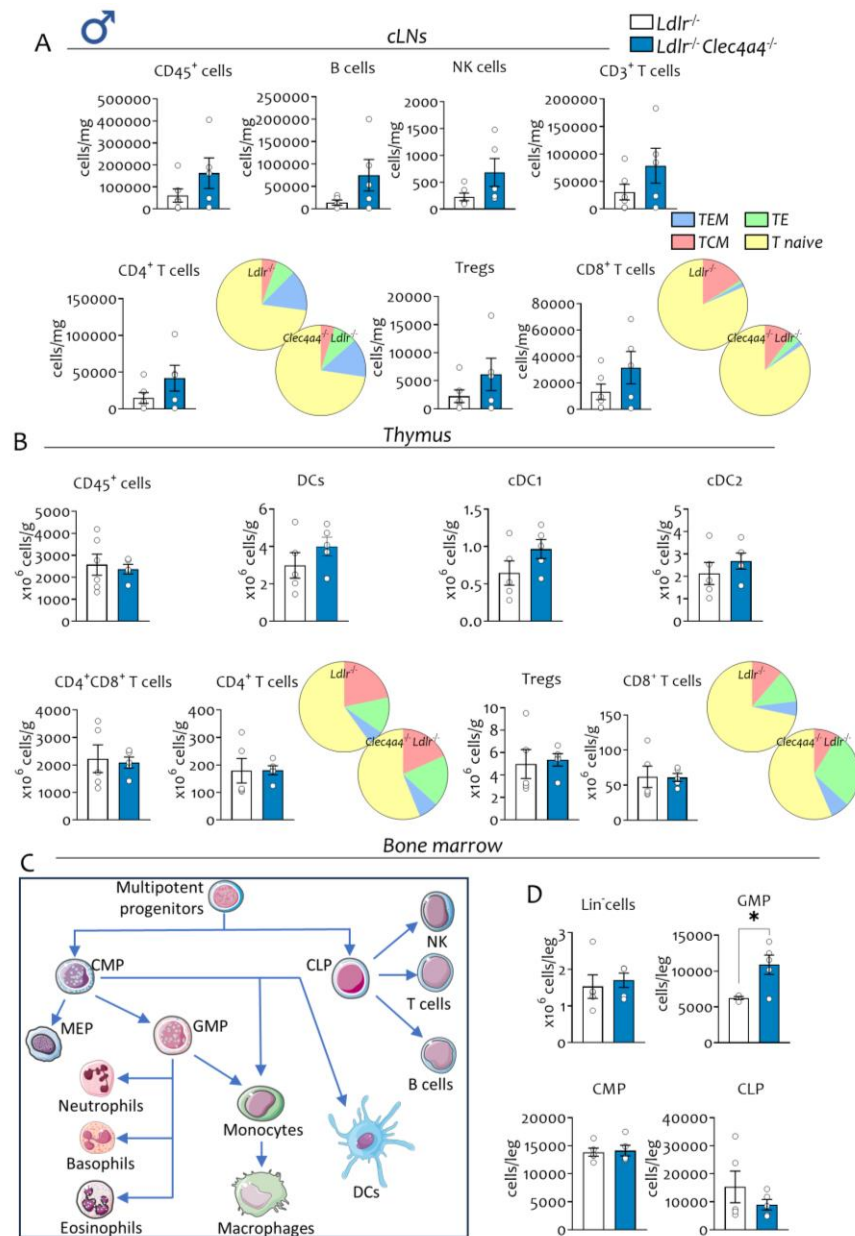


Fig. 25 Immunophenotype of cLNs, thymus and bone marrow. A) Number of cells per gram of cLNs of total CD45⁺ leukocytes, B lymphocytes, NK cells, CD3⁺, CD4⁺ and CD8⁺ T lymphocytes with related subsets (TEM, TE, TCM, T naive). B) Number of cells per gram of thymus of total CD45⁺ leukocytes, DCs, cDC1 and cDC2, CD4⁺CD8⁺, CD4⁺ and CD8⁺ T lymphocytes with related subsets. C) Representation of BM progenitors from the multipotent progenitors. D) Flow cytometry analysis of bone marrow precursors represented as number of cells per leg. Results are expressed as mean±SEM. n = 5 mice per groups. Statistical analyses were performed with parametric two-sides unpaired T-test. *p<0.05. Part of this image is created with Servier Medical Art. (CMP=Common myeloid progenitors; CLP=Common lymphoid progenitors; MEP=megakaryocyte/erythrocyte progenitors; GMP=Granulocytes/monocytes progenitors.)

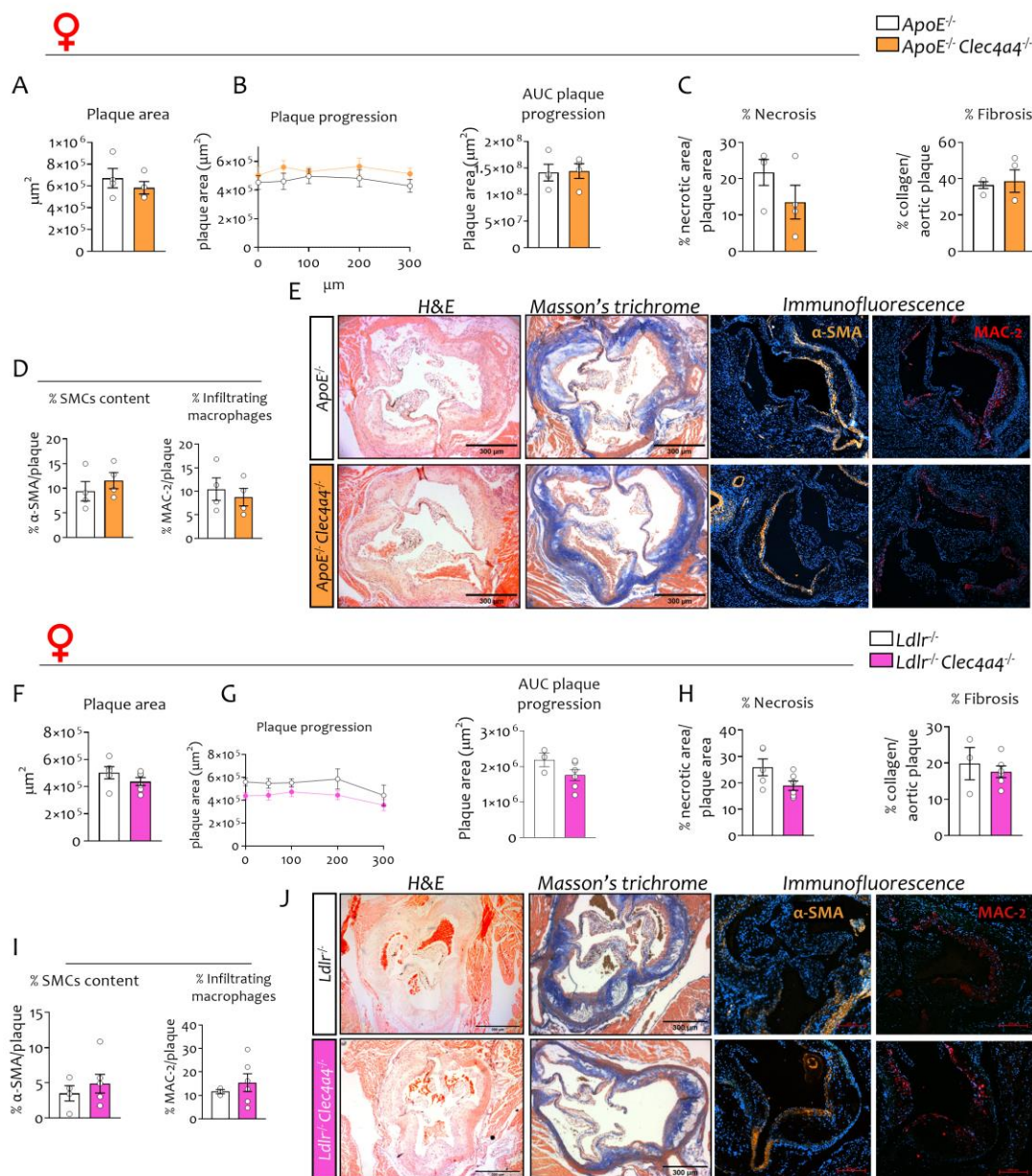


Fig. 26 Atherosclerotic plaque phenotype and plasma lipid levels of WTD-fed female DKO mice both on *ApoE*^{-/-} or *Ldlr*^{-/-} backgrounds. A-E) Aortic plaque characterization represented by aortic plaque area, progression, necrosis, fibrosis, smooth muscle cell (SMC) content and infiltrating macrophages of female DKO mice compared to *ApoE*^{-/-} mice. E) Representative plaque figures at 5x magnification of H&E and Masson's trichrome-stained sections at aortic sinus and immunofluorescent staining of α-SMA and MAC-2. F-I) Aortic plaque characterization of female DKO mice compared to *ApoE*^{-/-} mice. J) Representative plaque figures at 5x magnification of H&E and Masson's trichrome-stained sections at aortic sinus and immunofluorescent staining of α-SMA and MAC-2. Results are expressed as mean±SEM. n = 3-6 mice per groups. Statistical analyses were performed with parametric two-sides unpaired T-test. *p<0.05.

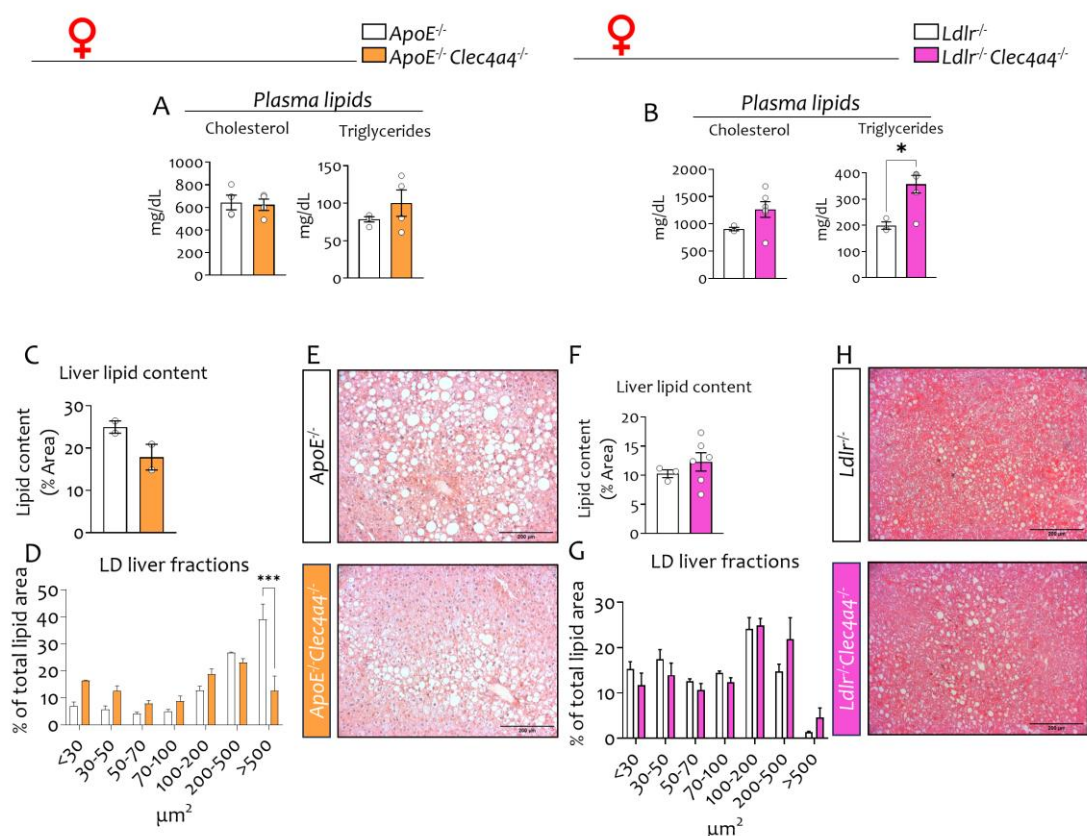


Fig. 27 Circulating lipid levels and hepatic phenotype of WTD-fed female DKO on ApoE^{-/-} Ldlr^{-/-} backgrounds. A-B) Plasma lipid levels – cholesterol and triglycerides – of WTD-fed female DKO mice compared to single KO on ApoE^{-/-} or Ldlr^{-/-} backgrounds, respectively. C-D) Percentage of hepatic steatosis – liver lipid content – and hepatic lipid droplet distribution of female DKO mice compared to single KO counterpart on ApoE^{-/-} background. E) Representative figures at 10x magnification of H&E - stained sections with 200 μm of scale bar. F-G) Percentage of hepatic steatosis – liver lipid content – and hepatic lipid droplet distribution of female DKO mice compared to single KO counterpart on Ldlr^{-/-} background. H) Representative figures at 10x magnification of H&E - stained sections with 300 μm of scale bar. Results are expressed as mean \pm SEM. n = 2 mice per ApoE^{-/-} groups; n = 3-6 mice per ApoE^{-/-} groups. Statistical analyses were performed with parametric two-sides unpaired T-test and Two-way ANOVA with Sidak's multiple comparisons. *p<0.05.

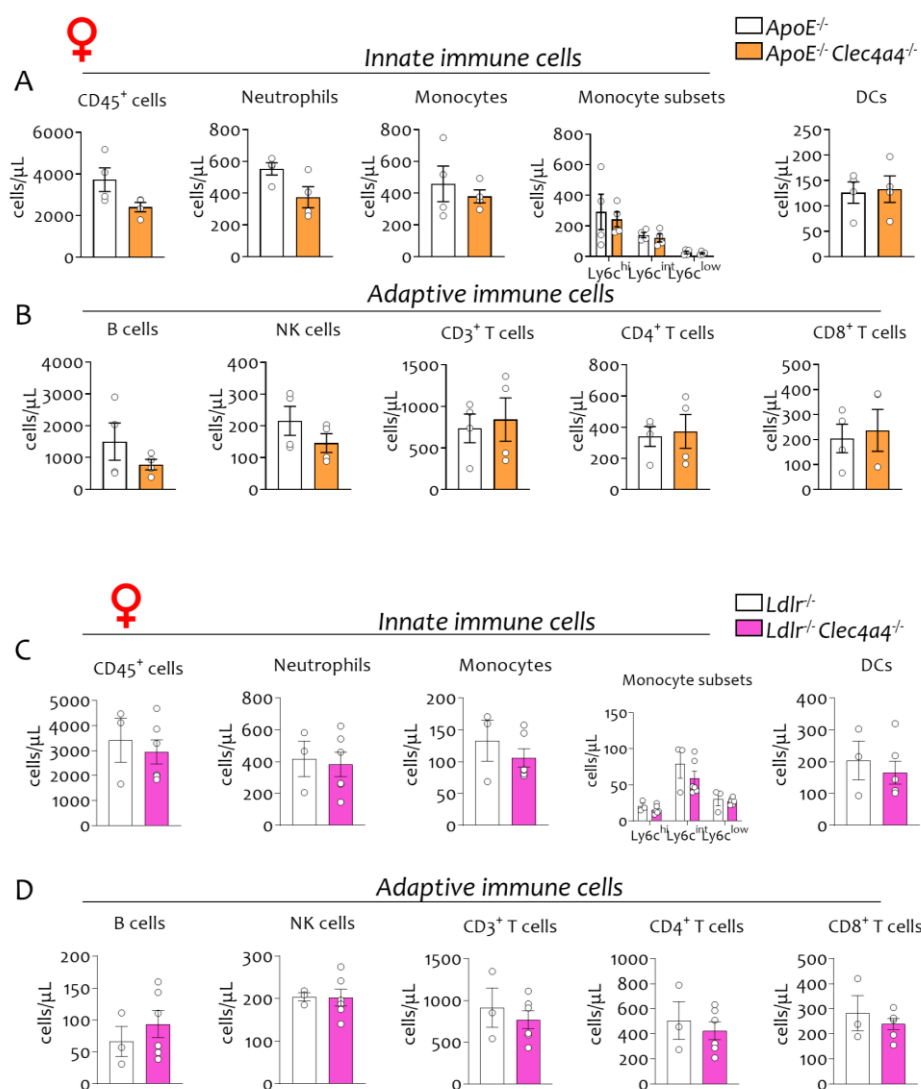


Fig. 28 Immunophenotype of circulating immune cells of WTD-fed female mice on ApoE^{-/-} or Ldlr^{-/-} background. A-D) Flow cytometry analysis of CD45⁺ leukocytes, focused on myeloid cells, such as neutrophils, monocytes and related subsets and DCs expressed, as well as lymphoid immune cells, such as B lymphocytes, NK cells, CD3⁺ T lymphocytes and their CD4⁺ or CD8⁺ subsets, as number of cells per μL of blood of female mice on ApoE^{-/-} or Ldlr^{-/-} background. Results are expressed as mean±SEM. n = 4 mice per ApoE^{-/-} groups, n = 3-6 for Ldlr^{-/-} groups. Statistical analyses were performed with parametric two-sides unpaired T-test or Mann-Whitney nonparametric unpaired T-test when needed. *p<0.05.

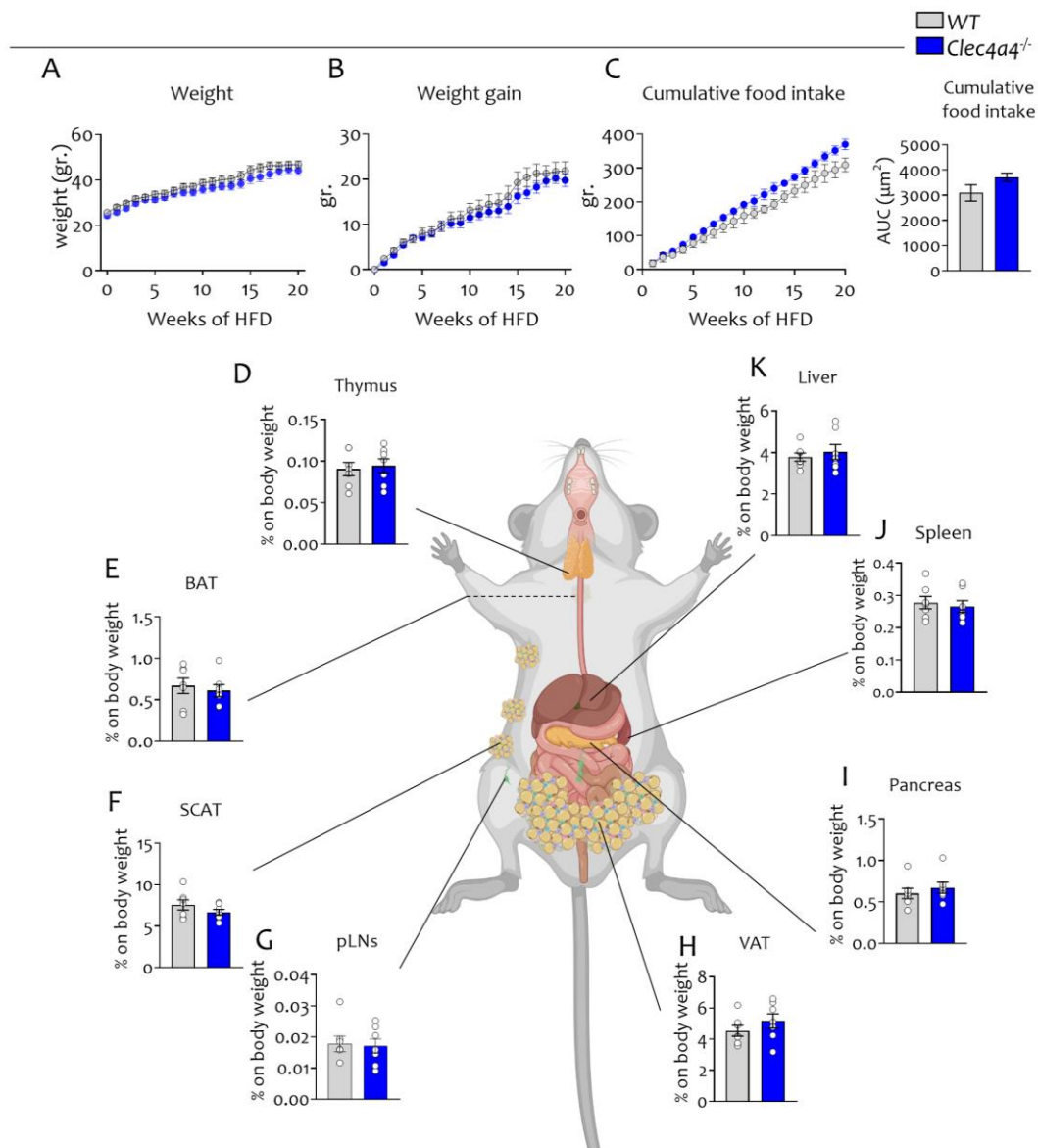


Fig. 29 Total body and organ weight of HFD-fed *Clec4a4*^{-/-} and WT mice. A-B) Total body weight and body weight gain during 20 weeks of HFD. C) Cumulative food intake during 20 weeks of HFD and the related AUC. D-K) Thymus, brown adipose tissue (BAT), subcutaneous adipose tissue (SCAT), inguinal/peripheral lymph nodes (pLNs), visceral adipose tissue (VAT), pancreas, spleen and liver weight of *Clec4a4*^{-/-} mice compared to the WT counterpart after 20 weeks of HFD, expressed as ratio on total body weight. Results are expressed as mean ± SEM. n=7 per group. Statistical analyses were performed with parametric two-sides unpaired T-test. *p<0.05. Part of this image is created with BioRender.com.

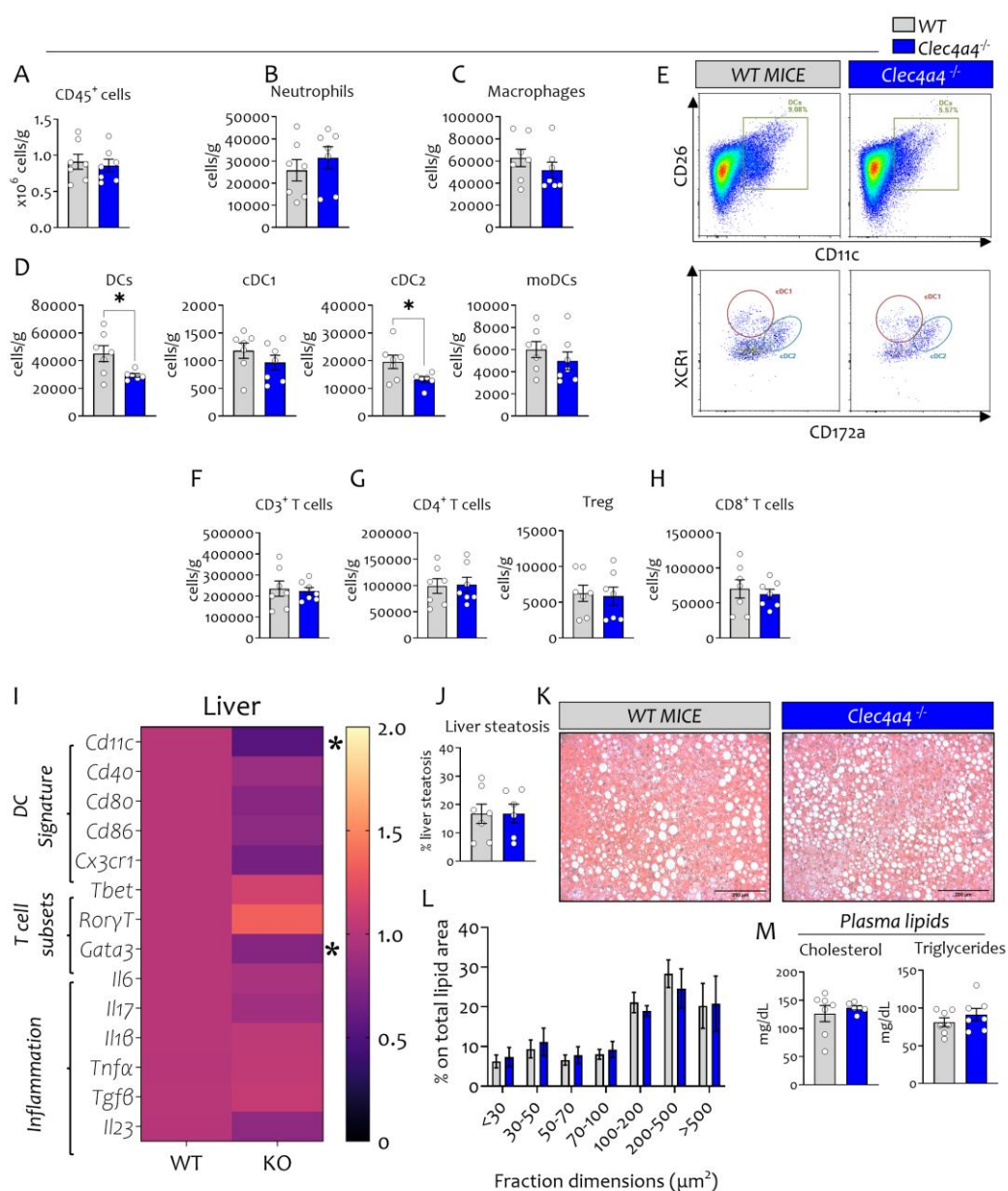


Fig. 30 Hepatic immune- and metabolic phenotype of HFD-fed KO and WT mice. A-D) Flow cytometry analysis of total CD45⁺ leukocytes, neutrophils, macrophages and DCs, with DC subsets expressed as cells per gram of liver. E) Representative flow cytometry plots of DCs and DC subsets gating strategy. F-H) Number of CD3⁺, CD4⁺ and CD8⁺ T lymphocytes per gram of liver. I) Gene expression analysis of dendritic cell markers, T lymphocytes transcription factors, and inflammation-related molecules. J-L) Histological analysis of liver steatosis and lipid droplet fraction dimensions within the liver and representative images of liver sections with 200 μm of scale bar. M) Plasma lipid levels (cholesterol and triglycerides) expressed as mg/dL. Results are expressed as mean ± SEM. n=7-4 per group. Statistical analyses were performed with unpaired t-tests or multiple unpaired t-test and Two-way ANOVA with Sidak's multiple comparisons. *p<0.05.

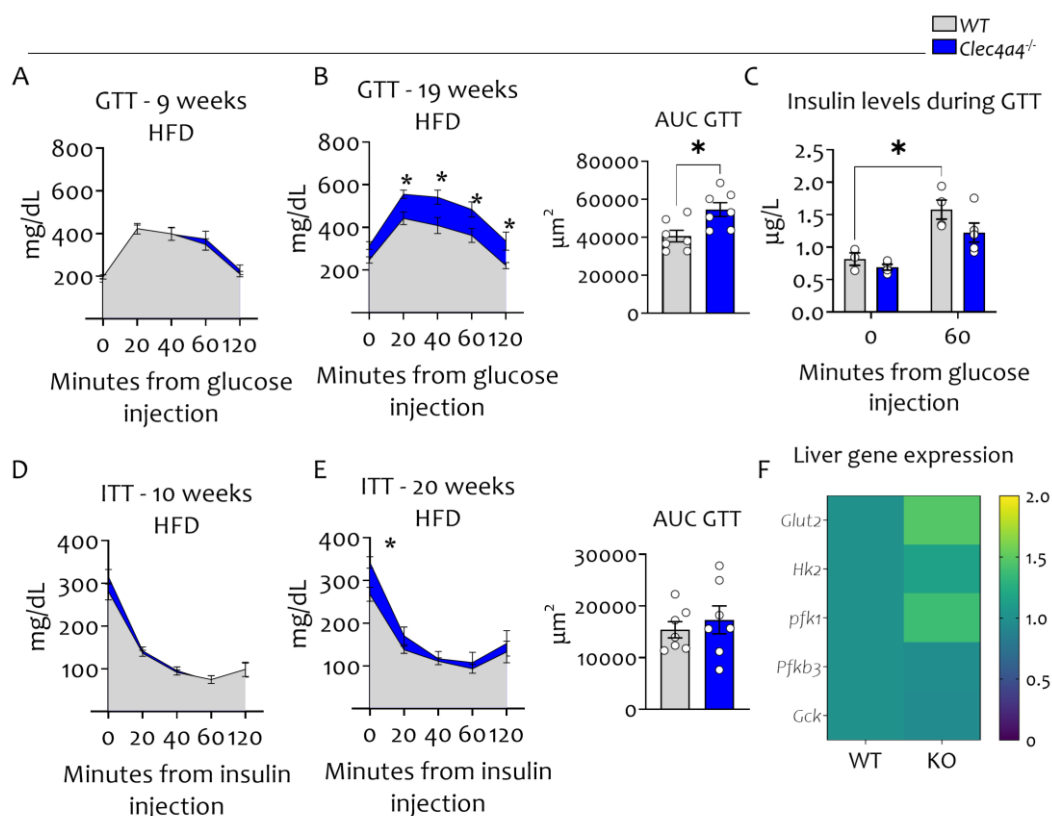


Fig. 31 Glucose metabolism analysis of HFD-fed WT and KO mice. A-B) Plasma glucose levels in WT and KO mice following intraperitoneal glucose tolerance test (0, 20, 40, 60, and 120 min) after 9 and 19 weeks of HFD respectively. C) insulin levels during glucose tolerance test (GTT) after 19 weeks of HFD. D-E) Plasma insulin levels after overnight fasting and after 60 minutes from glucose injection, expressed as mg/mL after 10 and 20 weeks of HFD respectively. F) Gene expression analysis of glucose metabolism-related genes within the liver of HFD-fed male WT and KO mice. Results are expressed as mean \pm SEM. n=7 per group. Statistical analyses were performed with parametric two-sides unpaired T-test and Two-way ANOVA with Sidak's multiple comparisons. * $p < 0.05$.

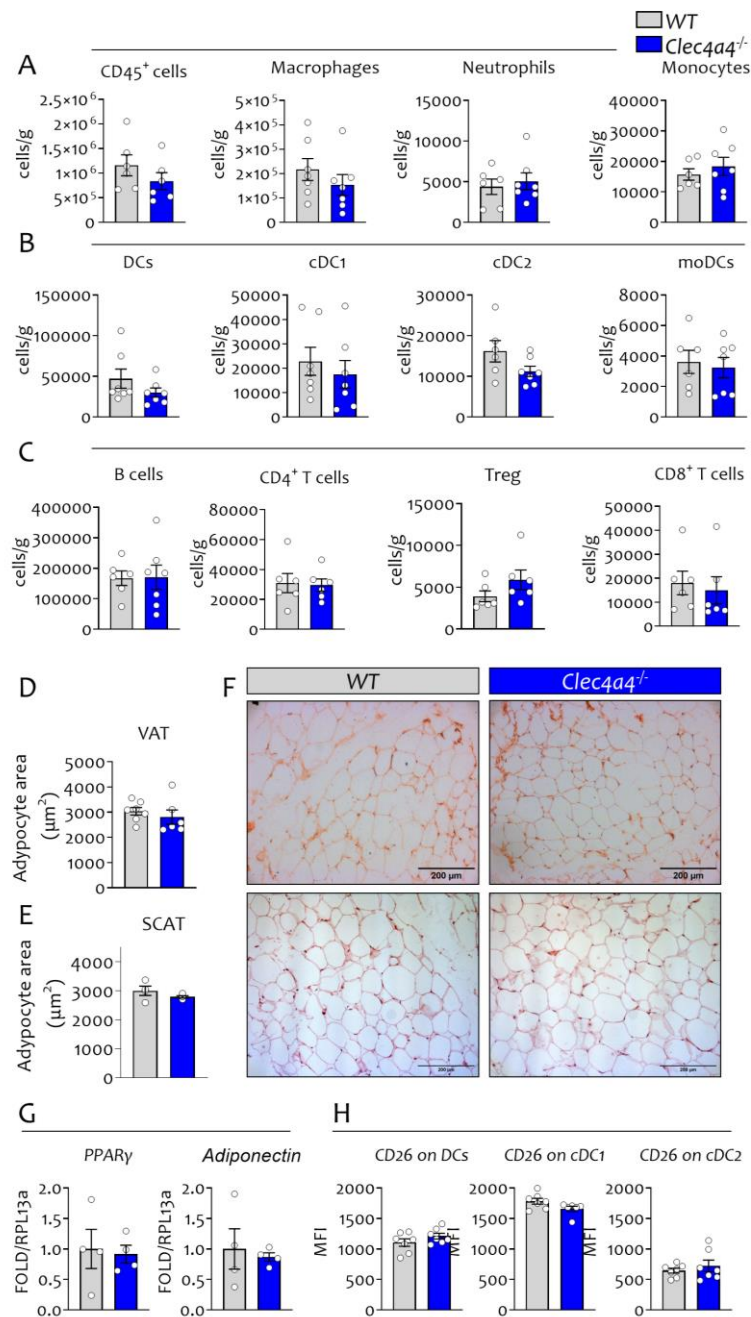


Fig. 32 Immunophenotype and histological analysis of adipose tissues. A) Flow cytometry analysis of CD45⁺ leukocytes, macrophages, neutrophils and monocytes per gram of VAT. B) Number of DCs and DC subsets (cDC1, cDC2, moDCs) per gram of VAT. C) Number of B and T (CD4⁺, Treg and CD8⁺) lymphocytes per gram of VAT. D-F) Histological analysis of adipocyte area on several sections of VAT and SCAT respectively, with representative images of 10x magnification histological sections of VAT (above) and SCAT (below) with 200 μm of scale bar of KO and WT mice. G) Gene expression analysis of *PPARγ* and *adiponectin* within the VAT. H) CD26 MFI on DCs, cDC1 and cDC2 within the VAT. Results are expressed as mean ± SEM. n=7 per group. Statistical analyses were performed with parametric two-sides unpaired T-test. *p<0.05.

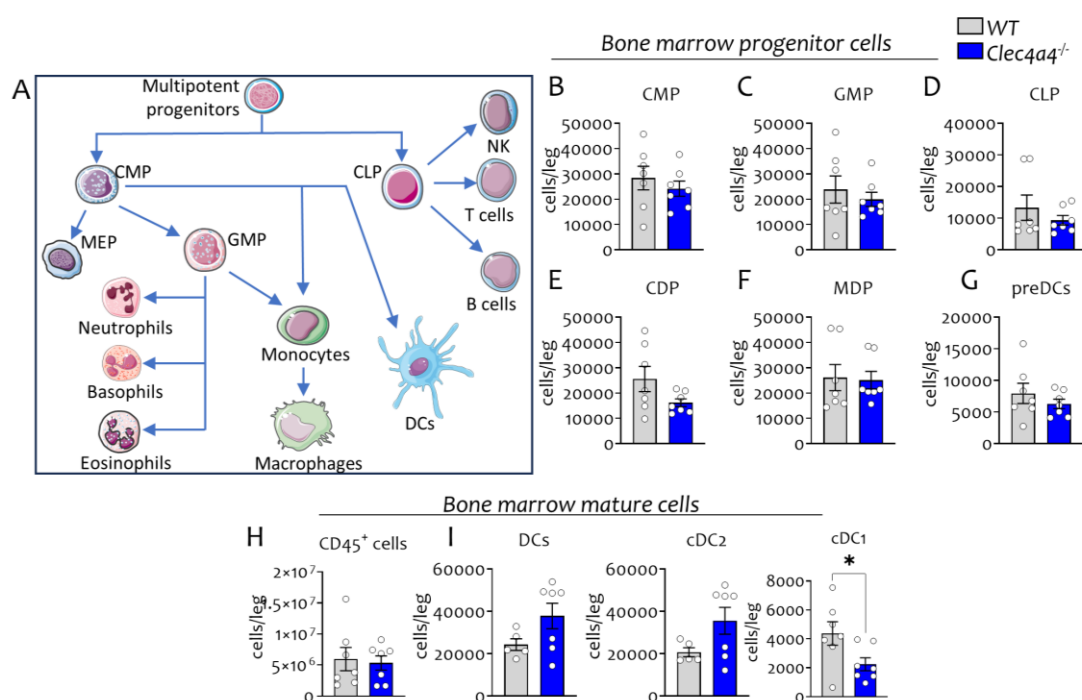


Fig. 33 Immunophenotype of bone marrow of HFD-fed KO and WT mice. A) Representative image of the bone marrow progenitors. B-D) Flow cytometry analysis of total myeloid and lymphoid progenitors (namely CMP, GMP and CLP) expressed as number of cells per leg. E-G) Number of dendritic cell progenitors (CDP and MDP) and preDCs per leg. H-I) Number of mature Cd45⁺ leukocytes and DCs with related subsets (cDC1 and cDC2) per leg. Results are expressed as mean ± SEM. n=7 per group. Statistical analyses were performed with parametric two-sides unpaired T-test.*p<0,05. Part of this image is created with Servier Medical Art.

(CMP) common myeloid progenitor; (CLP) common lymphoid progenitors, (GMP) granulocyte monocyte progenitor; (MEP) Megakaryocyte–erythroid progenitor; (DCs) dendritic cells; (CDP) common dendritic cell progenitor; (MDP) monocyte dendritic cell progenitor.

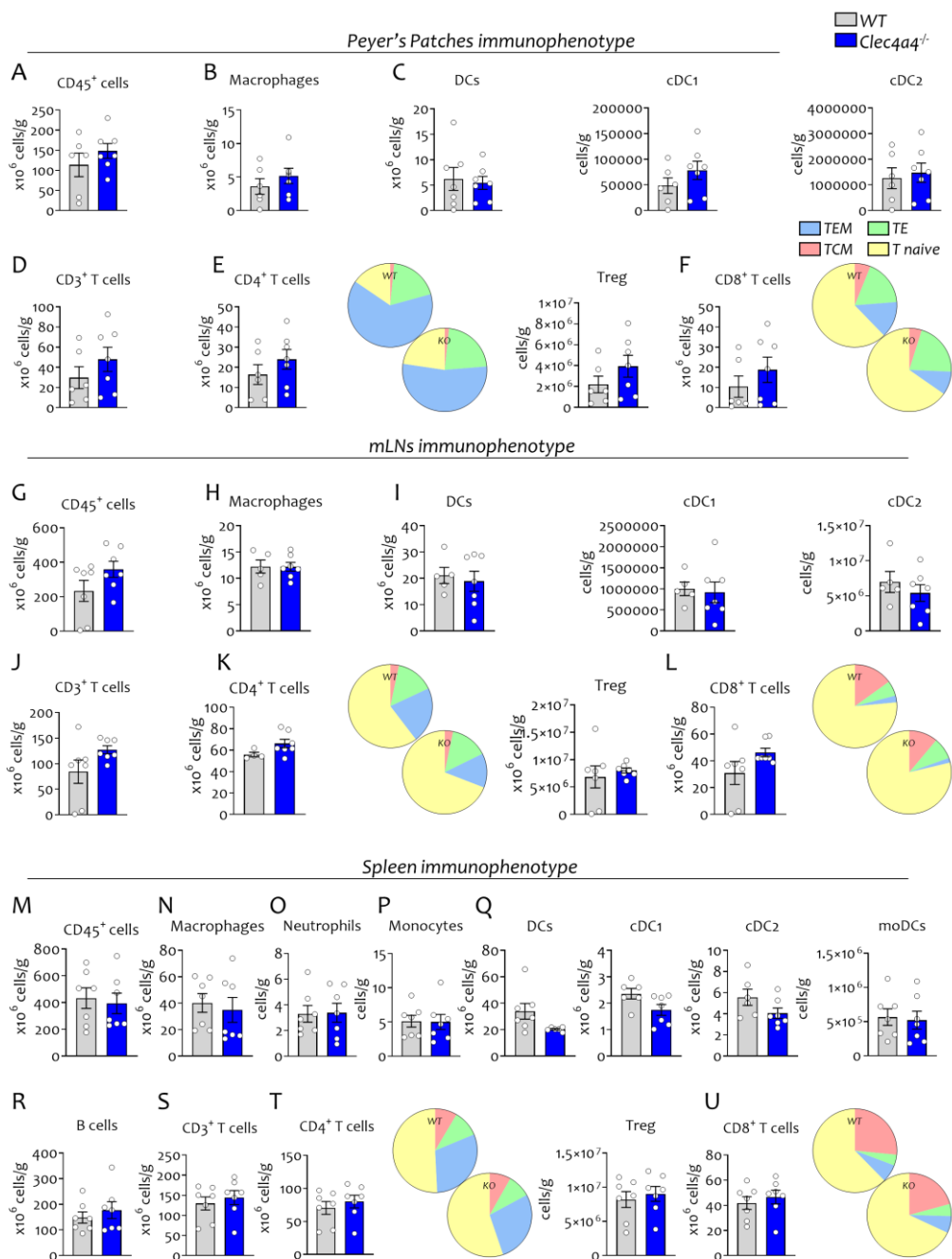


Fig. 34 Flow cytometry analysis of immune populations within Peyer's Patches, mLN and spleen. A-F) Number of total CD45⁺ leukocytes, macrophages, DCs and T lymphocytes with related subsets expressed as number of cells per gram of Peyer's Patches (Pp). G-L) Number of total CD45⁺ leukocytes, macrophages, DCs and T lymphocytes with related subsets expressed as number of cells per gram of mLN. M-U) Number of total CD45⁺ leukocytes, macrophages, neutrophils, monocytes, DCs, B and T lymphocytes with related subsets expressed as number of cells per gram of spleen. Results are expressed as mean ± SEM. n=7 per group. Statistical analyses were performed with parametric two-sides unpaired T-test or Mann-Whitney nonparametric unpaired T-test when needed. *p<0.05.

REFERENCES

1. Rao GH. Cardiometabolic Diseases: A Global Perspective. *J Cardiol Cardiovasc Ther* (2018) **12**: doi: 10.19080/jocct.2018.12.555834
2. Makover ME, Shapiro MD, Toth PP. There is urgent need to treat atherosclerotic cardiovascular disease risk earlier, more intensively, and with greater precision: A review of current practice and recommendations for improved effectiveness. *Am J Prev Cardiol* (2022) **12**: doi: 10.1016/J.AJPC.2022.100371
3. Roberts LD, Gerszten RE. Toward new biomarkers of cardiometabolic diseases. *Cell Metab* (2013) **18**:43–50. doi: 10.1016/j.cmet.2013.05.009
4. Schmidt V, Hogan AE, Fallon PG, Schwartz C. Obesity-Mediated Immune Modulation: One Step Forward, (Th)₂ Steps Back. *Front Immunol* (2022) **13**:3166. doi: 10.3389/FIMMU.2022.932893/BIBTEX
5. Esser N, Paquot N, Scheen AJ. Inflammatory markers and cardiometabolic diseases. <http://dx.doi.org/10.1179/2295333715Y0000000004> (2015) **70**:193–199. doi: 10.1179/2295333715Y.0000000004
6. Wondmkun YT. Obesity, insulin resistance, and type 2 diabetes: Associations and therapeutic implications. *Diabetes, Metab Syndr Obes* (2020) **13**:3611–3616. doi: 10.2147/DMSO.S275898
7. Jo S, Fang S. Therapeutic Strategies for Diabetes: Immune Modulation in Pancreatic β Cells. *Front Endocrinol (Lausanne)* (2021) **12**: doi: 10.3389/FENDO.2021.716692
8. Vasiljević J, Torkko JM, Knoch KP, Solimena M. The making of insulin in health and disease. *Diabetologia* (2020) **63**:1981–1989. doi: 10.1007/S00125-020-05192-7/FIGURES/2
9. Lechner K, Mckenzie AL, Kränkel N, Von Schacky C, Worm N, Nixdorff U, Lechner B, Scherr J, Weingärtner O, Krauss RM. High-Risk Atherosclerosis and Metabolic Phenotype: The Roles of Ectopic Adiposity, Atherogenic Dyslipidemia, and Inflammation. *Metab Syndr Relat Disord* (2020) **18**:176–185. doi: 10.1089/met.2019.0115
10. Neeland IJ, Ross R, Després JP, Matsuzawa Y, Yamashita S, Shai I, Seidell J, Magni P, Santos RD, Arsenault B, et al. Visceral and ectopic fat, atherosclerosis, and cardiometabolic disease: a position statement. *Lancet Diabetes Endocrinol* (2019) **7**:715–725. doi: 10.1016/S2213-8587(19)30084-1
11. Geisler CE, Renquist BJ. Hepatic lipid accumulation: cause and consequence of dysregulated glucoregulatory hormones. *J Endocrinol* (2017) **234**:R1–R21. doi: 10.1530/JOE-16-0513
12. Sun L, Zhang W, Zhao Y, Wang F, Liu S, Liu L, Zhao L, Lu W, Li M, Xu Y. Dendritic Cells and T Cells, Partners in Atherogenesis and the Translating Road Ahead. *Front Immunol* (2020) **11**: doi: 10.3389/fimmu.2020.01456
13. Soehnlein O, Libby P. Targeting inflammation in atherosclerosis — from experimental insights to the clinic. *Nat Rev Drug Discov* (2021) **20**:589–610. doi: 10.1038/s41573-021-00198-1
14. Ley K. Role of the adaptive immune system in atherosclerosis. *Biochem Soc Trans* (2020) **48**:2273–2281. doi: 10.1042/BST20200602
15. Soppert J, Lehrke M, Marx N, Jankowski J, Noels H. Lipoproteins and lipids in cardiovascular disease: from mechanistic insights to therapeutic targeting. *Adv Drug Deliv Rev* (2020) **159**:4–33. doi: 10.1016/J.ADDR.2020.07.019
16. Behbodikhah J, Ahmed S, Elyasi A, Kasselmann LJ, De Leon J, Glass AD, Reiss AB. Apolipoprotein b and cardiovascular disease: Biomarker and potential therapeutic target. *Metabolites* (2021) **11**: doi: 10.3390/metabo11100690
17. Wang HH, Garruti G, Liu M, Portincasa P, Wang DQH. Cholesterol and Lipoprotein

- Metabolism and Atherosclerosis: Recent Advances in Reverse Cholesterol Transport. *Ann Hepatol* (2017) **16**:S27–S42. doi: 10.5604/01.3001.0010.5495
18. Weitman ES, Aschen SZ, Farias-Eisner G, Albano N, Cuzzzone DA, Ghanta S, Zampell JC, Thorek D, Mehrara BJ. Obesity Impairs Lymphatic Fluid Transport and Dendritic Cell Migration to Lymph Nodes. *PLoS One* (2013) **8**: doi: 10.1371/journal.pone.0070703
 19. Martí A, Marcos A, Martínez JA. Obesity and immune function relationships. *Obes Rev* (2001) **2**:131–140. doi: 10.1046/J.1467-789X.2001.00025.X
 20. De Heredia FP, Gómez-Martínez S, Marcos A. Obesity, inflammation and the immune system. *Proc Nutr Soc* (2012) **71**:332–338. doi: 10.1017/S0029665112000092
 21. Soedono S, Cho KW. Adipose tissue dendritic cells: Critical regulators of obesity-induced inflammation and insulin resistance. *Int J Mol Sci* (2021) **22**: doi: 10.3390/ijms22168666
 22. Glass CK, Olefsky JM. Inflammation and lipid signaling in the etiology of insulin resistance. *Cell Metab* (2012) **15**:635–645. doi: 10.1016/J.CMET.2012.04.001
 23. Gancheva S, Jelenik T, Álvarez-Hernández E, Roden M. Interorgan metabolic crosstalk in human insulin resistance. *Physiol Rev* (2018) **98**:1371–1415. doi: 10.1152/PHYSREV.00015.2017/ASSET/IMAGES/LARGE/Z9J0021828570005.JPEG
 24. Sundara Rajan S, Longhi MP. Dendritic cells and adipose tissue. *Immunology* (2016) **149**:353–361. doi: 10.1111/imm.12653
 25. Bekkering S, Saner C, Riksen NP, Netea MG, Sabin MA, Saffery R, Stienstra R, Burgner DP. Trained Immunity: Linking Obesity and Cardiovascular Disease across the Life-Course? *Trends Endocrinol Metab* (2020) **31**:378–389. doi: 10.1016/j.tem.2020.01.008
 26. Tilg H, Moschen AR. Adipocytokines: mediators linking adipose tissue, inflammation and immunity. *Nat Rev Immunol* (2006) **6**:772–783. doi: 10.1038/NRI1937
 27. Alloatti A, Kotsias F, Pauwels AM, Carpier JM, Jouve M, Timmerman E, Pace L, Vargas P, Maurin M, Gehrmann U, et al. Toll-like Receptor 4 Engagement on Dendritic Cells Restrains Phago-Lysosome Fusion and Promotes Cross-Presentation of Antigens. *Immunity* (2015) **43**:1087–1100. doi: 10.1016/J.IMMUNI.2015.11.006
 28. Macdougall CE, Wood EG, Loschko J. Visceral Adipose Tissue Immune Homeostasis Is Regulated by the Crosstalk between Adipocytes and Dendritic Cell Subsets. (2018) doi: 10.1016/j.cmet.2018.02.007
 29. Macdougall CE, Longhi MP. Adipose tissue dendritic cells in steady-state. *Immunology* (2019) **156**:228–234. doi: 10.1111/imm.13034
 30. Stefanovic-Racic M, Yang X, Turner MS, Mantell BS, Stolz DB, Sumpter TL, Sipula IJ, Dedousis N, Scott DK, Morel PA, et al. Dendritic Cells Promote Macrophage Infiltration and Comprise a Substantial Proportion of Obesity-Associated Increases in CD11c + Cells in Adipose Tissue and Liver. *DIABETES* (2012) **61**: doi: 10.2337/db11-1523
 31. Patsouris D, Li PP, Thapar D, Chapman J, Olefsky JM, Neels JG. Ablation of CD11c-positive cells normalizes insulin sensitivity in obese insulin resistant animals. *Cell Metab* (2008) **8**:301–309. doi: 10.1016/J.CMET.2008.08.015
 32. Wu H, Perrard XD, Wang Q, Perrard JL, Polsani VR, Jones PH, Smith CW, Ballantyne CM. CD11c Expression in Adipose Tissue and Blood and Its Role in Diet-Induced Obesity. *Arterioscler Thromb Vasc Biol* (2010) **30**:186–192. doi: 10.1161/ATVBAHA.109.198044
 33. Liu R, Nikolajczyk BS. Tissue Immune Cells Fuel Obesity-Associated Inflammation

- in Adipose Tissue and Beyond. *Front Immunol* (2019) **10**:1587. doi: 10.3389/FIMMU.2019.01587
34. Zheng M, Tian Z. Liver-Mediated Adaptive Immune Tolerance. *Front Immunol* (2019) **10**:480451. doi: 10.3389/FIMMU.2019.02525/BIBTEX
 35. Khin PP, Lee JH, Jun HS. Pancreatic Beta-cell Dysfunction in Type 2 Diabetes. *Eur J Inflamm* (2023) **21**: doi: 10.1177/1721727X231154152/ASSET/IMAGES/LARGE/10.1177_1721727X231154152-FIG2.JPEG
 36. Eguchi K, Nagai R. Islet inflammation in type 2 diabetes and physiology. *J Clin Invest* (2017) **127**:14–23. doi: 10.1172/JCI88877
 37. Eguchi K, Manabe I, Oishi-Tanaka Y, Ohsugi M, Kono N, Ogata F, Yagi N, Ohto U, Kimoto M, Miyake K, et al. Saturated fatty acid and TLR signaling link β cell dysfunction and islet inflammation. *Cell Metab* (2012) **15**:518–533. doi: 10.1016/J.CMET.2012.01.023
 38. Dalmas E. Role of innate immune cells in metabolism: from physiology to type 2 diabetes. *Semin Immunopathol* 2019 414 (2019) **41**:531–545. doi: 10.1007/S00281-019-00736-5
 39. Dlodla P V, Mabhida SE, Ziqubu K, Nkambule BB, Mazibuko-Mbeje SE, Hanser S, Basson AK, Pheiffer C, Kengne AP. Pancreatic β -cell dysfunction in type 2 diabetes: Implications of inflammation and oxidative stress. *World J Diabetes* (2023) **14**:130. doi: 10.4239/WJD.V14.I3.130
 40. Zirpel H, Roep BO. Islet-Resident Dendritic Cells and Macrophages in Type 1 Diabetes: In Search of Bigfoot’s Print. *Front Endocrinol (Lausanne)* (2021) **12**:290. doi: 10.3389/FENDO.2021.666795/BIBTEX
 41. Chakhtoura M, Haber R, Ghezzawi M, Rhayem C, Tcheroyan R, Mantzoros CS. Pharmacotherapy of obesity: an update on the available medications and drugs under investigation. *eClinicalMedicine* (2023) **58**:101882. doi: 10.1016/j.eclinm.2023.101882
 42. Wang S, Song P, Zou MH. AMP-activated protein kinase, stress responses and cardiovascular diseases. *Clin Sci (Lond)* (2012) **122**:555. doi: 10.1042/CS20110625
 43. Kim EK, Lee SH, Jhun JY, Byun JK, Jeong JH, Lee SY, Kim JK, Choi JY, Cho M La. Metformin Prevents Fatty Liver and Improves Balance of White/Brown Adipose in an Obesity Mouse Model by Inducing FGF21. *Mediators Inflamm* (2016) **2016**: doi: 10.1155/2016/5813030
 44. Zhuge F, Ni Y, Nagashimada M, Nagata N, Xu L, Mukaida N, Kaneko S, Ota T. DPP-4 Inhibition by Linagliptin Attenuates Obesity-Related Inflammation and Insulin Resistance by Regulating M1/M2 Macrophage Polarization. *Diabetes* (2016) **65**:2966–2979. doi: 10.2337/DB16-0317
 45. Hogan AE, Gaoatswe G, Lynch L, Corrigan MA, Woods C, O’Connell J, O’Shea D. Glucagon-like peptide 1 analogue therapy directly modulates innate immune-mediated inflammation in individuals with type 2 diabetes mellitus. *Diabetologia* (2014) **57**:781–784. doi: 10.1007/s00125-013-3145-0
 46. Larsen CM, Faulenbach M, Vaag A, Vølund A, Ehres JA, Seifert B, Mandrup-Poulsen T, Donath MY. Interleukin-1–Receptor Antagonist in Type 2 Diabetes Mellitus. *N Engl J Med* (2007) **356**:1517–1526. doi: 10.1056/NEJMOA065213/SUPPL_FILE/NEJM_LARSEN_1517SA1.PDF
 47. Zhao Y, Zhang J, Zhang W, Xu Y. A myriad of roles of dendritic cells in atherosclerosis. *Clin Exp Immunol* (2021) doi: 10.1111/cei.13634
 48. Herrero-Fernandez B, Gomez-Bris R, Somovilla-Crespo B, Gonzalez-Granado JM. Immunobiology of atherosclerosis: A complex net of interactions. *Int J Mol Sci*

- (2019) **20**:5293. doi: 10.3390/ijms20215293
49. Bobryshev Y V. Dendritic cells and their role in atherogenesis. *Lab Investig* (2010) **90**:970–984. doi: 10.1038/labinvest.2010.94
 50. Bobryshev Y V., Ivanova EA, Chistiakov DA, Nikiforov NG, Orekhov AN. Macrophages and Their Role in Atherosclerosis: Pathophysiology and Transcriptome Analysis. *Biomed Res Int* (2016) **2016**: doi: 10.1155/2016/9582430
 51. Noz MP, Bekkering S, Groh L, Nielen TMJ, Lamfers EJP, Schlitzer A, Messaoudi S El, van Royen N, Huys EHJPG, Preijers FWMB, et al. Reprogramming of bone marrow myeloid progenitor cells in patients with severe coronary artery disease. *Elife* (2020) **9**:1–24. doi: 10.7554/ELIFE.60939
 52. Yvan-Charvet L, Pagler T, Gautier EL, Avagyan S, Siry RL, Han S, Welch CL, Wang N, Randolph GJ, Snoeck HW, et al. ATP-binding cassette transporters and HDL suppress hematopoietic stem cell proliferation. *Science* (2010) **328**:1689–1693. doi: 10.1126/SCIENCE.1189731
 53. Zhou Y, Huang C, Hu Y, Xu Q, Hu X. Lymphatics in Cardiovascular Disease. *Arterioscler Thromb Vasc Biol* (2020) **40**:E275–E283. doi: 10.1161/ATVBAHA.120.314735
 54. Milasan A, Ledoux J, Martel C. Lymphatic network in atherosclerosis: the underestimated path. *Futur Sci OA* (2015) **1**: doi: 10.4155/FSO.15.61
 55. Dai X, Zhang D, Wang C, Wu Z, Liang C. The pivotal role of thymus in atherosclerosis mediated by immune and inflammatory response. *Int J Med Sci* (2018) **15**:1555–1563. doi: 10.7150/ijms.27238
 56. Bellini R, Bonacina F, Norata GD. Crosstalk between dendritic cells and T lymphocytes during atherogenesis: Focus on antigen presentation and break of tolerance. *Front Cardiovasc Med* (2022) **0**:2010. doi: 10.3389/FCVM.2022.934314
 57. Roy P, Orecchioni M, Ley K. How the immune system shapes atherosclerosis: roles of innate and adaptive immunity. *Nat Rev Immunol* 2021 224 (2021) **22**:251–265. doi: 10.1038/s41577-021-00584-1
 58. Bonacina F, Martini E, Svecla M, Nour J, Cremonesi M, Beretta G, Moregola A, Pellegatta F, Zampoleri V, Catapano AL, et al. Adoptive transfer of CX3CR1 transduced-T regulatory cells improves homing to the atherosclerotic plaques and dampens atherosclerosis progression. *Cardiovasc Res* (2021) **117**:2069–2082. doi: 10.1093/CVR/CVAA264
 59. Nettersheim FS, De Vore L, Winkels H. Vaccination in Atherosclerosis. *Cells* (2020) **9**: doi: 10.3390/cells9122560
 60. Christ A, Günther P, Lauterbach MAR, Duewell P, Biswas D, Pelka K, Scholz CJ, Oosting M, Haendler K, Baßler K, et al. Western Diet Triggers NLRP3-Dependent Innate Immune Reprogramming. *Cell* (2018) **172**:162-175.e14. doi: 10.1016/j.cell.2017.12.013
 61. Heidt T, Sager HB, Courties G, Dutta P, Iwamoto Y, Zaltsman A, Von Zur Muhlen C, Bode C, Fricchione GL, Denninger J, et al. Chronic variable stress activates hematopoietic stem cells. *Nat Med* 2014 207 (2014) **20**:754–758. doi: 10.1038/nm.3589
 62. Figdor CG, Van Kooyk Y, Adema GJ. C-type lectin receptors on dendritic cells and langerhans cells. *Nat Rev Immunol* (2002) **2**:77–84. doi: 10.1038/nri723
 63. Uto T, Fukaya T, Takagi H, Arimura K, Nakamura T, Kojima N, Malissen B, Sato K. Clec4A4 is a regulatory receptor for dendritic cells that impairs inflammation and T-cell immunity. *Nat Commun* (2016) **7**:1–15. doi: 10.1038/ncomms11273
 64. Richard M, Thibault N, Veilleux P, Eve Gareau-Pagé G, Beaulieu AD. Granulocyte macrophage-colony stimulating factor reduces the affinity of SHP-2 for the ITIM

- of CLECSF6 in neutrophils: A new mechanism of action for SHP-2. *Mol Immunol* (2006) **43**:1716–1721. doi: 10.1016/j.molimm.2005.10.006
65. Sancho D, Reis e Sousa C. Signaling by Myeloid C-Type Lectin Receptors in Immunity and Homeostasis. *Annu Rev Immunol* (2012) **30**:491–529. doi: 10.1146/annurev-immunol-031210-101352
 66. Brown GD, Willment JA, Whitehead L. C-type lectins in immunity and homeostasis. *Nat Rev Immunol* (2018) **18**:374–389. doi: 10.1038/s41577-018-0004-8
 67. Kasahara S, Clark EA. Dendritic cell-associated lectin 2 (DCAL2) defines a distinct CD8 α ⁻ dendritic cell subset. *J Leukoc Biol* (2012) **91**:437–448. doi: 10.1189/jlhb.0711384
 68. García-Vallejo JJ, Bloem K, Knippels LMJ, Garssen J, van Vliet SJ, van Kooyk Y. The consequences of multiple simultaneous C-type lectin-ligand interactions: DCIR alters the endo-lysosomal routing of DC-SIGN. *Front Immunol* (2015) **6**:87. doi: 10.3389/fimmu.2015.00087
 69. Geijtenbeek TBH, Van Vliet SJ, Engering A, 't Hart BA, Van Kooyk Y. Self- and nonself- recognition by C-type lectins on dendritic cells. *Annu Rev Immunol* (2004) **22**:33–54. doi: 10.1146/annurev.immunol.22.012703.104558
 70. Lahoud MH, Proietto AI, Ahmet F, Kitsoulis S, Eidsmo L, Wu L, Sathe P, Pietersz S, Chang H-W, Walker ID, et al. The C-Type Lectin Clec12A Present on Mouse and Human Dendritic Cells Can Serve as a Target for Antigen Delivery and Enhancement of Antibody Responses. *J Immunol* (2009) **182**:7587–7594. doi: 10.4049/jimmunol.0900464
 71. C Eklo" w, D Makrygiannakis, L Ba" ckdahl, L Padyukov, A-K Ulfgren, J C Lorentzen VM. Cellular distribution of the C-type II lectin dendritic cell immunoreceptor (DCIR) and its expression in the rheumatic joint: identification of a subpopulation of DCIR+ T cells. (2008) doi: 10.1136/ard.2007.076976
 72. Park I, Goddard ME, Cole JE, Zanin N, Lyytikäinen L-P, Lehtimäki T, Andreakos E, Feldmann M, Udalova I, Drozdov I, et al. C-type lectin receptor CLEC4A2 promotes tissue adaptation of macrophages and protects against atherosclerosis. *Nat Commun* 2022 131 (2022) **13**:1–17. doi: 10.1038/s41467-021-27862-9
 73. Clément M, Basatemur G, Masters L, Baker L, Bruneval P, Iwawaki T, Kneilling M, Yamasaki S, Goodall J, Mallat Z. Necrotic Cell Sensor Clec4e Promotes a Proatherogenic Macrophage Phenotype Through Activation of the Unfolded Protein Response. *Circulation* (2016) **134**:1039–1051. doi: 10.1161/CIRCULATIONAHA.116.022668
 74. Nour J, Moregola A, Svecla M, Da Dalt L, Bellini R, Neyrolles O, Fadini GP, Rombouts Y, Albiero M, Bonacina F, et al. Mannose Receptor Deficiency Impacts Bone Marrow and Circulating Immune Cells during High Fat Diet Induced Obesity. *Metabolites* (2022) **12**:1205. doi: 10.3390/METABO12121205/S1
 75. Price JD, Hotta-Iwamura C, Zhao Y, Beauchamp NM, Tarbell KV. DCIR2 + cDC2 DCs and Zbtb32 Restore CD4 + T-Cell Tolerance and Inhibit Diabetes. (2015) doi: 10.2337/db14-1880
 76. Bates EEM, Fournier N, Garcia E, Valladeau J, Durand I, Pin J-J, Zurawski SM, Patel S, Abrams JS, Lebecque S, et al. APCs Express DCIR, a Novel C-Type Lectin Surface Receptor Containing an Immunoreceptor Tyrosine-Based Inhibitory Motif. *J Immunol* (1999) **163**:
 77. Kanazawa N, Okazaki T, Nishimura H, Tashiro K, Inaba K, Miyachi Y. DCIR acts as an inhibitory receptor depending on its immunoreceptor tyrosine-based inhibitory motif. (2002). 261–266 p. doi: 10.1046/j.0022-202x.2001.01633.x
 78. Hsu Y, Okada R, Nishimura T, Kawasaki N, Yamamoto K, Matsumoto N. DCIR3 and

- DCIR4 are co-expressed on inflammatory and patrolling monocytes. (2017) doi: 10.1016/j.bbrc.2017.10.067
79. Kaifu T, Iwakura Y. "Dendritic cell immunoreceptor (DCIR): An ITIM-harboring C-type lectin receptor.," *C-Type Lectin Receptors in Immunity*. Springer Japan (2016). p. 101–113 doi: 10.1007/978-4-431-56015-9_7
 80. Kanazawa N, Tashiro K, Miyachi Y. Signaling and immune regulatory role of the dendritic cell immunoreceptor (DCIR) family lectins: DCIR, DCAR, dectin-2 and BDCA-2. *Immunobiology* (2004) **209**:179–190. doi: 10.1016/j.imbio.2004.03.004
 81. Troegeler A, Mercier I, Cougoule C, Pietretti D, Colom A, Duval C, Vu Manh T-P, Capilla F, Poincloux R, Pingris K, et al. C-type lectin receptor DCIR modulates immunity to tuberculosis by sustaining type I interferon signaling in dendritic cells. (2017) doi: 10.1073/pnas.1613254114
 82. Klauber TCB, Laursen JM, Zucker D, Brix S, Jensen SS, Andresen TL. Delivery of TLR7 agonist to monocytes and dendritic cells by DCIR targeted liposomes induces robust production of anti-cancer cytokines. (2017) doi: 10.1016/j.actbio.2017.01.072
 83. Meyer-Wentrup F, Cambi A, Joosten B, Looman MW, de Vries IJM, Figdor CG, Adema GJ. DCIR is endocytosed into human dendritic cells and inhibits TLR8-mediated cytokine production. *J Leukoc Biol* (2009) **85**:518–525. doi: 10.1189/jlb.0608352
 84. H Geijtenbeek TB, Gringhuis SI. Dendritic cells (DCs) are located throughout the body to capture and internalize invading pathogens, and subsequently process and present antigen on MHC class I and class II molecules to CD8 + and CD4 +. *Nat Publ Gr* (2009) doi: 10.1038/nri2569
 85. Guo J, Wu X, Too CL, Yin F, Lu X, He J, Li R, Liu X, Murad S, Padyukov L, et al. A Replication Study Confirms the Association of Dendritic Cell Immunoreceptor (DCIR) Polymorphisms with ACPA-Negative RA in a Large Asian Cohort. (2012) doi: 10.1371/journal.pone.0041228
 86. Fujikado N, Saijo S, Yonezawa T, Shimamori K, Ishii A, Sugai S, Kotaki H, Sudo K, Nose M, Iwakura Y. Dcir deficiency causes development of autoimmune diseases in mice due to excess expansion of dendritic cells. *Nat Med* (2008) **14**:176–180. doi: 10.1038/nm1697
 87. Nagae M, Yamanaka K, Hanashima S, Ikeda A, Morita-Matsumoto K, Satoh T, Matsumoto N, Yamamoto K, Yamaguchi Y. Recognition of bisecting N-acetylglucosamine: Structural basis for asymmetric interaction with the mouse lectin dendritic cell inhibitory receptor 2. *J Biol Chem* (2013) **288**:33598–33610. doi: 10.1074/jbc.M113.513572
 88. Methodology SCE, Analysis SCE, Investigation AW, Resources SCE, Writing SCE. Differential Intrasplenic Migration of Dendritic Cell Subsets Tailors Adaptive Immunity HHS Public Access. (2016) **16**:2472–2485. doi: 10.1016/j.celrep.2016.07.076
 89. Bellini R, Moregola A, Nour J, Rombouts Y, Neyrolles O, Uboldi P, Bonacina F, Norata GD. Dendritic cell marker Clec4a4 deficiency limits atherosclerosis progression. *Atheroscler Plus* (2023) **51**:8–12. doi: 10.1016/J.ATHPLU.2022.12.001
 90. Nasu J, Uto T, Fukaya T, Takagi H, Fukui T, Miyanaga N, Nishikawa Y, Yamasaki S, Yamashita Y, Sato K. Pivotal role of the carbohydrate recognition domain in self-interaction of CLEC4A to elicit the ITIM-mediated inhibitory function in murine conventional dendritic cells in vitro. *Int Immunol* (2021) **32**:673–682. doi: 10.1093/INTIMM/DXAA034
 91. Zeldovich L. Genetic drift: the ghost in the genome. *Lab Anim* 2017 466 (2017)

- 46:255–257. doi: 10.1038/labani.1275
92. Holmdahl R, Malissen B. The need for littermate controls. *Eur J Immunol* (2012) **42**:45–47. doi: 10.1002/EJL.201142048
 93. Lazic SE, Essioux L. Improving basic and translational science by accounting for litter-to-litter variation in animal models. *BMC Neurosci* (2013) **14**: doi: 10.1186/1471-2202-14-37
 94. Bonaparte D, Cinelli P, Douni E, Hérault Y, Maas A, Pakarinen P, Poutanen M, Lafuente MS, Scavizzi F. FELASA guidelines for the refinement of methods for genotyping genetically-modified rodents: A report of the Federation of European Laboratory Animal Science Associations Working Group. *Lab Anim* (2013) **47**:134–145. doi: 10.1177/0023677212473918/ASSET/IMAGES/LARGE/10.1177_0023677212473918-FIG2.JPEG
 95. Da Dalt L, Ruscica M, Bonacina F, Balzarotti G, Dhyani A, Di Cairano E, Baragetti A, Arnaboldi L, De Metrio S, Pellegatta F, et al. PCSK9 deficiency reduces insulin secretion and promotes glucose intolerance: the role of the low-density lipoprotein receptor. *Eur Heart J* (2020) **40**:357–368. doi: 10.1093/EURHEARTJ/EHY357
 96. Macchi C, Moregola A, Greco MF, Svecla M, Bonacina F, Dhup S, Dadhich RK, Audano M, Sonveaux P, Mauro C, et al. Monocarboxylate transporter 1 deficiency impacts CD8+ T lymphocytes proliferation and recruitment to adipose tissue during obesity. *iScience* (2022) **25**: doi: 10.1016/J.ISCI.2022.104435
 97. Takaba H, Takayanagi H. The Mechanisms of T Cell Selection in the Thymus. (2017) doi: 10.1016/j.it.2017.07.010
 98. Liu D, Duan L, Cyster JG. Chemo- and mechanosensing by dendritic cells facilitate antigen surveillance in the spleen*. *Immunol Rev* (2022) **306**:25–42. doi: 10.1111/IMR.13055
 99. Kumar S, Jeong Y, Ashraf MU, Bae YS. Dendritic Cell-Mediated Th2 Immunity and Immune Disorders. *Int J Mol Sci* (2019) **20**: doi: 10.3390/IJMS20092159
 100. Ibrahim MM. Subcutaneous and visceral adipose tissue: structural and functional differences. *Obes Rev* (2010) **11**:11–18. doi: 10.1111/J.1467-789X.2009.00623.X
 101. Kobayashi N, Takahashi D, Takano S, Kimura S, Hase K. The Roles of Peyer's Patches and Microfold Cells in the Gut Immune System: Relevance to Autoimmune Diseases. *Front Immunol* (2019) **10**:479654. doi: 10.3389/FIMMU.2019.02345/BIBTEX
 102. Macpherson AJ, Smith K. Mesenteric lymph nodes at the center of immune anatomy. *J Exp Med* (2006) **203**:497–500. doi: 10.1084/jem.20060227
 103. Lewis SM, Williams A, Eisenbarth SC. Structure and function of the immune system in the spleen. *Sci Immunol* (2019) **4**:6085. doi: 10.1126/SCIIMMUNOL.AAU6085/ASSET/EC821A5C-80A3-4517-9D01-0F90C4848C50/ASSETS/GRAPHIC/AAU6085-F2.JPEG
 104. Murphy AJ, Febbraio MA. Immune-based therapies in cardiovascular and metabolic diseases: past, present and future. *Nat Rev Immunol* (2021) **21**:669–679. doi: 10.1038/S41577-021-00580-5
 105. Zerneck A. Dendritic cells in atherosclerosis: Evidence in mice and humans. *Arterioscler Thromb Vasc Biol* (2015) **35**:763–770. doi: 10.1161/ATVBAHA.114.303566
 106. Getz GS, Reardon CA. Do the Apoe^{-/-} and Ldlr^{-/-} mice yield the same insight on atherogenesis? *Arterioscler Thromb Vasc Biol* (2016) **36**:1734. doi: 10.1161/ATVBAHA.116.306874
 107. Soehnlein O. Multiple roles for neutrophils in atherosclerosis. *Circ Res* (2012)

- 110:875–888. doi: 10.1161/CIRCRESAHA.111.257535
108. Richard M, Veilleux P, Rouleau M, Paquin R, Beaulieu AD. The expression pattern of the ITIM-bearing lectin CLECSF6 in neutrophils suggests a key role in the control of inflammation. *J Leukoc Biol* (2002) **71**:871–80. doi: 10.1189/jlb.71.5.871
 109. Richard M, Thibault N, Veilleux P, Breton R, Beaulieu AD. The ITIM-bearing CLECSF6 (DCIR) is down-modulated in neutrophils by neutrophil activating agents. *Biochem Biophys Res Commun* (2003) **310**:767–773. doi: 10.1016/j.bbrc.2003.09.077
 110. Wang W Le, Kasamatsu J, Joshita S, Gilfillan S, Luccia B Di, Panda SK, Kim DH, Desai P, Bando JK, Huang SCC, et al. The aryl hydrocarbon receptor instructs the immunomodulatory profile of a subset of Clec4a4+ eosinophils unique to the small intestine. *Proc Natl Acad Sci U S A* (2022) **119**:e2204557119. doi: 10.1073/PNAS.2204557119/SUPPL_FILE/PNAS.2204557119.SAPP.PDF
 111. Kanda H, Tateya S, Tamori Y, Kotani K, Hiasa KI, Kitazawa R, Kitazawa S, Miyachi H, Maeda S, Egashira K, et al. MCP-1 contributes to macrophage infiltration into adipose tissue, insulin resistance, and hepatic steatosis in obesity. *J Clin Invest* (2006) **116**:1494–1505. doi: 10.1172/JCI26498
 112. Wang CY, Liao JK. A Mouse Model of Diet-Induced Obesity and Insulin Resistance. *Methods Mol Biol* (2012) **821**:421. doi: 10.1007/978-1-61779-430-8_27
 113. Bellini R, Moregola A, Nour J, Uboldi P, Fabrizia Bonacina J, Norata GD. Dendritic cell immunoreceptor 2 (DCIR2) deficiency decreases hepatic conventional dendritic cell content but not the progression of diet-induced obesity. *Immunity, Inflamm Dis* (2023) **11**:e1024. doi: 10.1002/IID3.1024
 114. Vaduganathan M, Mensah GA, Turco JV, Fuster V, Roth GA. The Global Burden of Cardiovascular Diseases and Risk: A Compass for Future Health. *J Am Coll Cardiol* (2022) **80**:2361–2371. doi: 10.1016/J.JACC.2022.11.005
 115. Blüher M. Obesity: global epidemiology and pathogenesis. *Nat Rev Endocrinol* 2019 155 (2019) **15**:288–298. doi: 10.1038/s41574-019-0176-8
 116. Campbell JE, Newgard CB. Mechanisms controlling pancreatic islet cell function in insulin secretion. *Nat Rev Mol Cell Biol* 2021 222 (2021) **22**:142–158. doi: 10.1038/s41580-020-00317-7
 117. Sanllorente A, Lassale C, Soria-florido MT, Castañer O, Fitó M, Hernáez Á. Modification of high-density lipoprotein functions by diet and other lifestyle changes: A systematic review of randomized controlled trials. *J Clin Med* (2021) **10**:1–43. doi: 10.3390/jcm10245897
 118. Gregory SN, Perati SR, Brown ZJ. Alteration in immune function in patients with fatty liver disease. *Hepatoma Res* (2022) **8**:null-null. doi: 10.20517/2394-5079.2022.34
 119. Guilliams M, Dutertre CA, Scott CL, McGovern N, Sichien D, Chakarov S, Van Gassen S, Chen J, Poidinger M, De Prijck S, et al. Unsupervised High-Dimensional Analysis Aligns Dendritic Cells across Tissues and Species. *Immunity* (2016) **45**:669–684. doi: 10.1016/j.immuni.2016.08.015

APPENDIX

APPENDIX I – Composition of Western-Type Diet (WTD) and High-Fat Diet (HFD):

The Western-Type Diet for (WTD; Envigo, Teklad Custom Diets, Cat#TD.88137) used for inducing atherosclerosis in mice with *Ldlr*^{-/-} or *ApoE*^{-/-} background.

WTD ingredients	Grams (g)
Casein	195.0 g
DL-Methionine	3.00 g
Sucrose	341.46 g
Corn Starch	150.00 g
Anhydrous Milkfat	210.00 g
Cholesterol	1.5 g
Cellulose	50.00 g
Mineral Mix, AIN-76 (170915)	35.00 g
Calcium Carbonate	4.00 g
Vitamin Mix, Teklad (40060)	10.00 g
Ethoxyquin	0.04 g

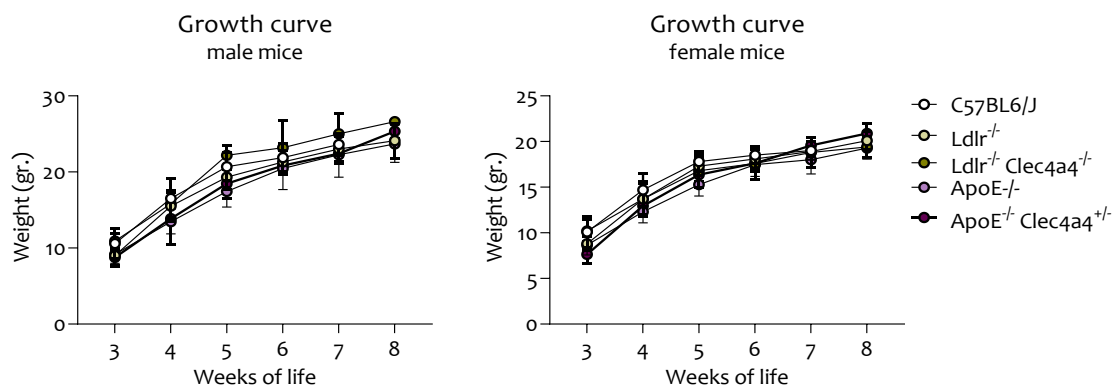
The High-Fat Diet (HFD,45% kcal% Fat, Research Diets, Inc Cat#D12451) was used for obesity-diet induced in WT and *Clec4a4*^{-/-} mice.

HFD ingredients	Grams
Casein, Lactic, 30 Mesh	200.00 g
Cysteine, L	3.00 g
Sucrose, Fine granulated	176.80 g
Lodex 10	100.00 g
Starch, Corn	72.80 g
Solka Floc, FCC200	50.00 g
Lard	177.50 g
Soybean Oil, USP	25.00 g
S10026B	50.00g
Choline Bitartrate	2.00 g
V10001C	1.00 g
Dye, Red FD&C #40, Alum. Lake 35-42%	0.05 g
Lake 35-42%	
Total	585.15 g

APPENDIX II – Mice models

	Pregnancy	N° of live births	N° pups/pregnancy
<i>Ldlr/Clec4a4</i> line	21	104	4.95
<i>ApoE/Clec4a4</i> line	15	85	5.66

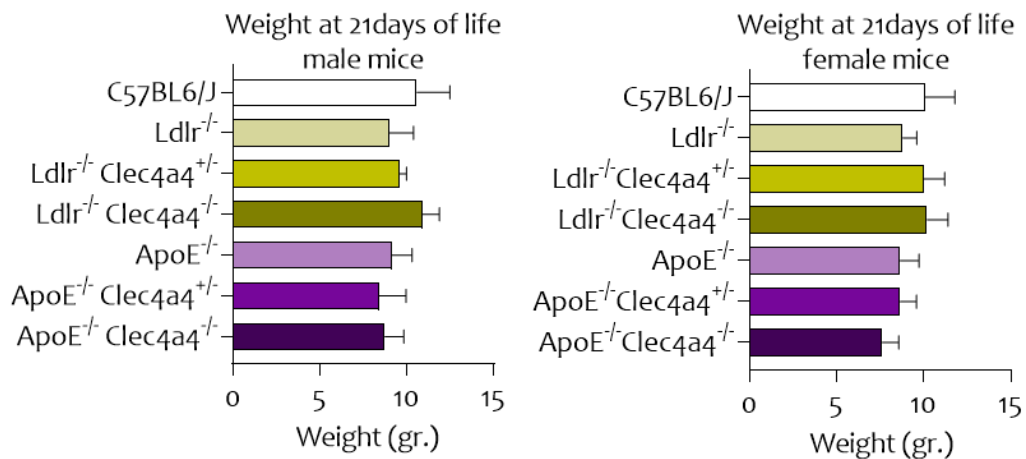
Evaluation of the novel lines produced by breeding *Clec4a4*^{-/-} mice with *Ldlr*^{-/-} or *ApoE*^{-/-} animals, determining the number of pregnancies required to obtain the number of mice necessary for our research.



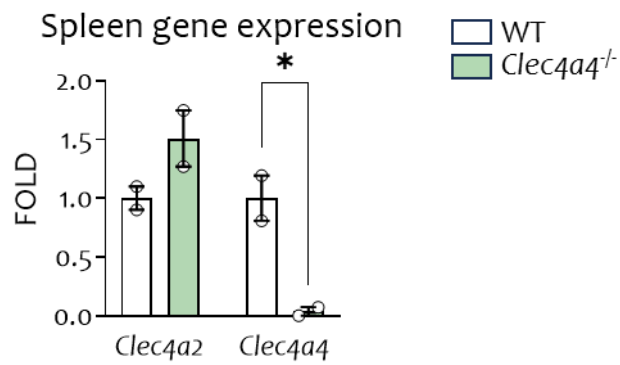
Growth curve of male and female DKO mice compared with single KO and WT mice (this last information obtained by “The Jackson Laboratory” <https://www.jax.org/>).

	% ♂ at weaning	% HO/WT	% HO/HE	% HO/HO
<i>Ldlr/Clec4a4</i> line	53.85%	27.88%	49.04%	23.08%
<i>ApoE/Clec4a4</i> line	55.29%	35.29%	37.65%	27.06%

Percentage of male pups obtained at weaning, then divided per genotype on *Ldlr*^{-/-} or *ApoE*^{-/-} background.

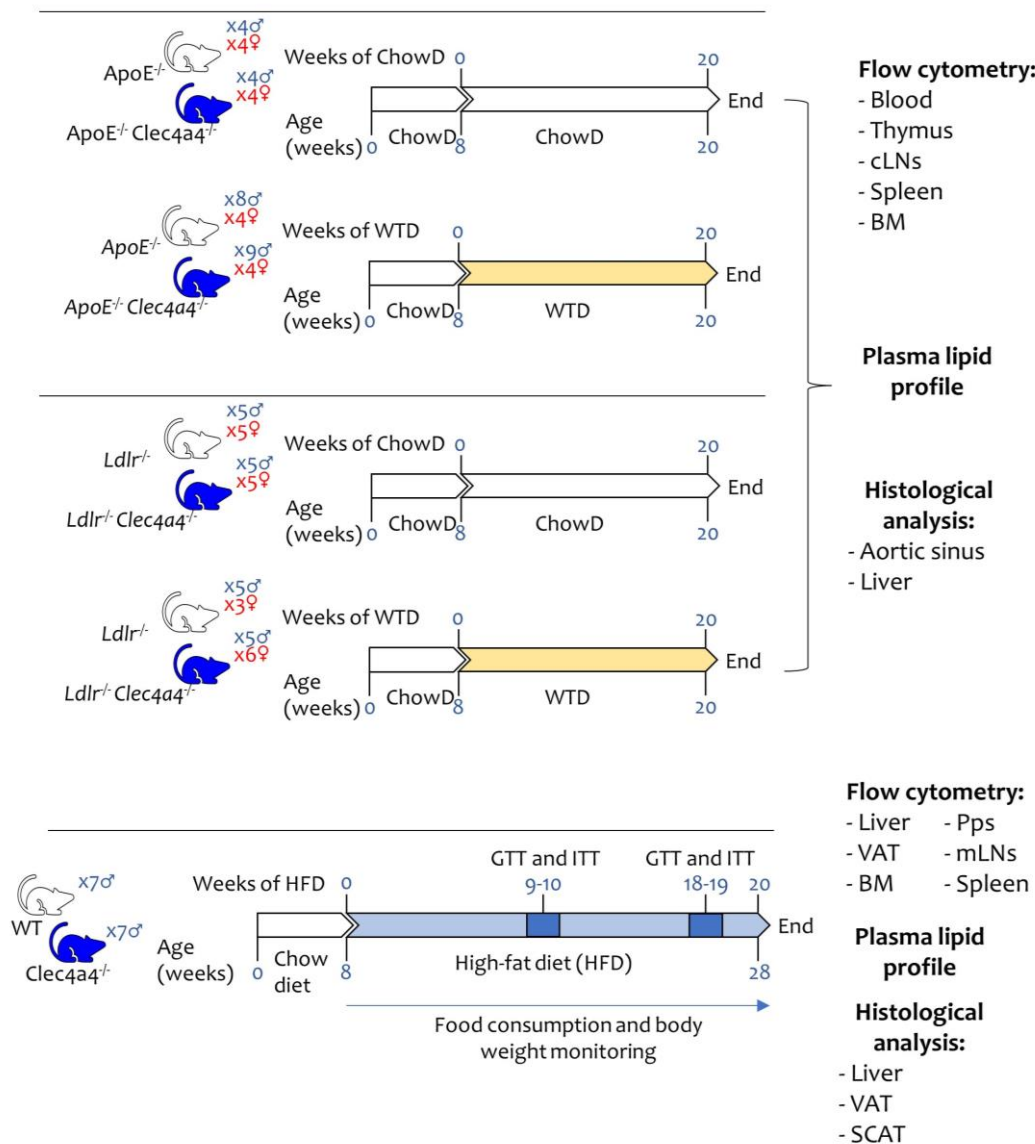


Weight after 21 days of life of male (left) and female (right) DKO mice compared to the other genotypes.



Clec4a2 and *Clec4a4* gene expression investigation on Spleen to confirm our animal model. Results are expressed as mean \pm SEM. n=2 per group. Statistical analyses were performed with unpaired t-test. * $p < 0,05$.

APPENDIX III – Experimental setup



The experimental setup for atherosclerosis and obesity mice models is shown, together with the genotype and number of mice per group. After 8 weeks of life, female and male mice were placed on Chow or WTD for 12 weeks, followed by flow cytometry analysis on several organs (blood, thymus, cLNs, Spleen, and bone marrow), plasma lipid profile, and histological analysis on aortic sinus and liver to investigate the impact of Clec4a4 deficiency both on ApoE^{-/-} or Ldlr^{-/-} background.

For the obesity studies, 8-week-old male mice were fed a HFD for 20 weeks while food consumption and body weight were tracked. Furthermore, at weeks 9 and 18, glucose tolerance tests (GTT) were performed, while insulin tolerance tests (ITT) at weeks 10 and

19. Flow cytometry study (on liver, VAT, SCAT, BM, Peyer's patches, mesenteric LNs, and Spleen) was carried out after 20 weeks of HFD, along with plasma lipid profile and histological analysis of adipocyte area on VAT and SCAT, and liver steatosis.

APPENDIX IV - List of antibodies for immunofluorescence of aortic sections

	Ab I diluted	Cat#	Company	Ab II	Cat#	Company
α -SMA	1:200	NBP2-67440	Bio-Techne	Anti-rabbit AF555 1:1000	A27039	Invitrogen
MAC-2	1:500	CL8942AP	Cedarlane	Anti-rat AF555 1:1000	A21434	Invitrogen

APPENDIX V - qPCR primer sequences

Gene	Fw primer	Rev primer
<i>Rpl-13a</i>	5'-GCCCTCAAGGTGTTGGAT-3'	5'-GAGCAGCAGGGACCACCAT-3'
<i>Clec4a4</i>	5'-CCTGAACACAAGTGCTGGTT-3'	5'-ACCTTTGTGCCAGAACGTAG-3'
<i>Clec4a2</i>	5'-TCCAGCAGCTCAATGAGACA-3'	5'-TCCGTCAGAAGAGAGCCTTG-3'
<i>Hmg-CoAr</i>	5'-TGTGGTTTGTGAAGCCGTCAT-3'	5'-TCAACCATAGCTCCGTAGTTGTC-3'
<i>Srebp1</i>	5'-CCAGAGGGTGAGCCTGACAA-3'	5'-AGCCTCTGCAATTTCCAGATCT-3'
<i>Srebp2</i>	5'-GCGGACAACACACAATATCATTG-3'	5'-TGACTAAGTCCTTCAACTCTATGATTTTG-3'
<i>Fasn</i>	5'-AGAGACGTGTCACCTCTGGACTT-3'	5'-AGAGACGTGTCACCTCTGGACTT-3'
<i>Lxr</i>	5'-CGACAGAGCTTCGTCCACAA-3'	5'-GCTCGTCCCCCAGCATTTT-3'
<i>Vldlr</i>	5'-TGGAATTACACTCGACCTTGTC-3'	5'-CTAGAGAGCATGTGCAACTTGGA-3'
<i>Cd36</i>	5'-TGGGAGTTGGCGAGAAAACC-3'	5'-CAGGACTGCACCAATAACAGC-3'
<i>Lrp1</i>	5'-CCTTGACCCTGACAAGCCTA-3'	5'-TGTAGAGCGTGGCATACT-3'
<i>SR BI</i>	5'-TTCACGGGCGTCCAGAA-3'	5'-GATCTTGCTGAGTCCGTTCCA-3'
<i>Lipa</i>	5'-TAGGTGTAGGCACCAGGTTG-3'	5'-CTGGAGTTGCATCGGGAGT-3'
<i>Abca1</i>	5'-GGTTTGGAGATGGTTATACAATAGTTGT-3'	5'-TTCCCGGAAACGCAAGTC-3'
<i>Abcg1</i>	5'-TTCATCGTCCTGGGCATCTT-3'	5'-CGGATTTTGTATCTGAGGACGAA-3'
<i>Soat1</i>	5'-AAACCGGCTGTCAAATCTGG-3'	5'-TTCTGGGCTTCATCTTGCTCA-3'
<i>Soat2</i>	5'-AAGATGGGCTGTGGCTTTAG-3'	5'-GGTAGAAGAACCCAGGACG-3'
<i>Cyp7a1</i>	5'-TACCTGCAAATGATGGGA-3'	5'-TGTGTCAAATGCCTTCGC-3'
<i>Mttp</i>	5'-AATTAAGGCTCTGGATACATGCAA-3'	5'-TGACACCCAGCACCTGGTTT-3'
<i>ApoE</i>	5'-TGGCTACCAACCCCATCATC-3'	5'-GCAGGACAGGAGAAGGATACTCA-3'
<i>Il6</i>	5'-CTGCAAGAGACTTCCATCCAGTT-3'	5'-AGGGAAGGCCGTGGTTGT-3'
<i>Il10</i>	5'-CAGCCGGGAAGACAATAACTG-3'	CCGAGCTCTAGGAGCATGT-3'
<i>Il18</i>	5'-GGTGTGTGACGTTCCATTAGA-3'	CAGCACGAGGCTTTTTTGTG-3'
<i>Cd11c</i>	5'-ACACTGAGTGATGCCACTGT-3'	5'-AGGTCACCTAGTTGGTCTT-3'
<i>Cd40</i>	5'-CCTGCGATGGTGTCTTTGC-3'	5'-AGATGGACCGCTGTCAACAAG-3'
<i>Cd80</i>	5'-AGGAAGCCTACGGGCAAGTT-3'	5'-GGCTCAGCCTTCCACTTCA-3'
<i>Cd86</i>	5'-GGGCCGACGAGCTT -3'	5'-CCCATGTCCTTGATCTGAACATT-3'
<i>Cx3cr1</i>	5'-TCAGCATCGACCGGTACCTT -3'	5'-CTGCACTGTCGGTTGTTTCAT-3'
<i>Tbet</i>	5'-TGAGAGCCCCGAGCTCTTC -3'	5'-CCCCGCTTCTCTCAA -3'
<i>RoryT</i>	5'-CAGCCAACATGTGGAAAAGCT -3'	5'-GGGAAGGCGGCTTGGA -3'
<i>Gata3</i>	5'-GAACCGGCCCTTATCAAG -3'	5'-CAGGATGTCCCTGCTCTCTT-3'
<i>Il17</i>	5'-CAAACACTGAGGCCAAGGAC-3'	5'-TCTTCATTGCGGTGGAGAGT-3'
<i>Tnfa</i>	5'-CTCCTCACCCACACCATC-3'	5'-GAAGACCCTCCAGATAG-3'
<i>Tgfb</i>	5'-TCGACATGGAGCTGGTGAAA-3'	5'-GAGCCTTAGTTTGACAGGATCTGGCCAC-3'
<i>Il23</i>	5'-CCGTTCCAAGATCCTTCGAA-3'	5'-CAAAGACCCGGGAGCTA -3'
<i>Adipoq</i>	5'-AATTCTGAAGCCATTGTCTCC-3'	5'-AGTTATTGTCTCCTGAGAGAATG -3'
<i>Pparγ</i>	5'-CCATTCTGGCCCAACT-3'	5'-TGCGAGTGGTCTTCCATCAC-3'

APPENDIX VI - Antibodies used in flow cytometry.**Blood staining**

Antibody	Clone	Cat#	Company
LIVE/DEAD™ Fixable Aqua Dead Cell Stain Kit	-	L34957	Invitrogen™
Anti-mouse CD45 BUV563	30-F11	612924	BD Biosciences
Anti-mouse CD3 Af700	17A2	561388	BD Biosciences
Anti-mouse CD8 BV650	53-6.7	563234	BD Biosciences
Anti-mouse CD4 BUV737	RM4-5	612843	BD Biosciences
Anti-mouse CD19 PE CF594	1D3	562329	BD Biosciences
Anti-mouse Ly6C EF450	HK 1.4	48-5932-82	eBioscience
Anti-mouse Gr-1 (Ly6C – Ly6G) BV605	RB6-8C5	563299	BD Biosciences
Anti-mouse CD11c BV786	HL3	563735	BD Biosciences
Anti-mouse I-A I-E (MHC II) BUV805	53-6.7	612898	BD Biosciences
Anti-mouse CD11b APC-Cy7	M1/70	557657	BD Biosciences
Anti-mouse CD172a BUV395	P84	740282	BD Biosciences

T lymphocytes staining

Antibody	Clone	Cat#	Company
LIVE/DEAD™ Fixable Aqua Dead Cell Stain Kit	-	L34957	Invitrogen™
Anti-mouse CD45 BUV563	30-F11	612924	BD Biosciences
Anti-mouse CD19 FITC	1D3	553785	BD Biosciences
Anti-mouse CD3 PerCP Cy5.5	17A2	560527	BD Biosciences
Anti-mouse CD4 BUV737	RM4-5	612843	BD Biosciences
Anti-mouse CD8 AF488	53-6.7	553030	BD Biosciences
Anti-mouse CD44 EF450	IM7	48-0441-82	Invitrogen™
Anti-mouse CD62L BV605	MEL-14	56-3252	BD Biosciences
Anti-mouse CD25 BUV395	PC61	564022	BD Biosciences
Anti-mouse FoxP3 APC (intracellular staining)	FJK-16S	17-5773-82	eBioscience

Dendritic cell staining

Antibody	Clone	Cat#	Company
LIVE/DEAD™ Fixable Aqua Dead Cell Stain Kit	-	L34957	Invitrogen™
Anti-mouse CD45 BUV563	30-F11	612924	BD Biosciences
Anti-mouse F4/80 AF647	T45-2342	565853	BD Biosciences
Anti-mouse CD64 PE/DAZZLE	X54-5/7.1	139319	Biolegend
Anti-mouse MHC II BV650	M5/114.15.2	563415	BD Biosciences
Anti-mouse Lineage PerCP Cy5.5	-	561317	BD Biosciences
Anti-mouse CD11c BV786	HL3	563735	BD Biosciences
Anti-mouse CD26 BV711	H194-112	740678	BD Biosciences
Anti-mouse CD172a BUV395	P84	740282	BD Biosciences
Anti-mouse XCR1 FITC	ZET	148209	Biolegend

Thymus staining

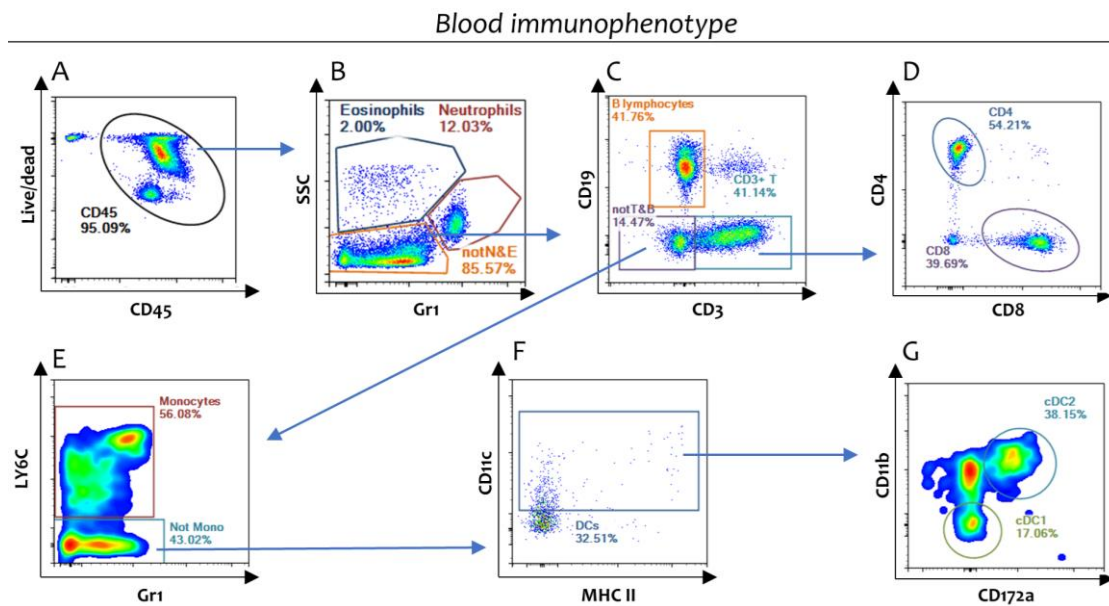
Antibody	Clone	Cat#	Company
CD45 FITC	30-F11	553079	BD Biosciences
Anti-mouse CD3 PerCP Cy5.5	17A2	560527	BD Biosciences
Anti-mouse CD44 AF700	IM7	56-0441-82	Invitrogen™
Anti-mouse CD62L BV605	MEL-14	56-3252	BD Biosciences

Anti-mouse CD4 BV786	RM4-5	563727	BD Biosciences
Anti-mouse CD8 BUV805	53-6.7	612898	BD Biosciences
Anti-mouse CD25 BUV395	PC61	564022	BD Biosciences
Anti-mouse FoxP3 APC (intracellular staining)	FJK-16S	17-5773-82	eBioscience

Bone marrow staining

Antibody	Clone	Cat#	Company
Anti-mouse Lineage PerCP Cy5.5	-	561317	BD Biosciences
Anti-mouse CD34 FITC	RAM34	553733	BD Biosciences
Anti-mouse CD127 PE	A7R34	135010	Biolegend
Anti-mouse CD117 PECy7	2B8	558163	BD Biosciences
Anti-mouse LY-6A/E BV421	D7	562729	BD Biosciences
Anti-mouse CD16/32 BV650	2.4G2	740457	BD Biosciences
Anti-mouse CD11c BV786	HL3	563735	BD Biosciences
Anti-mouse CD135 APC	A2F10	17-1351-82	Invitrogen™

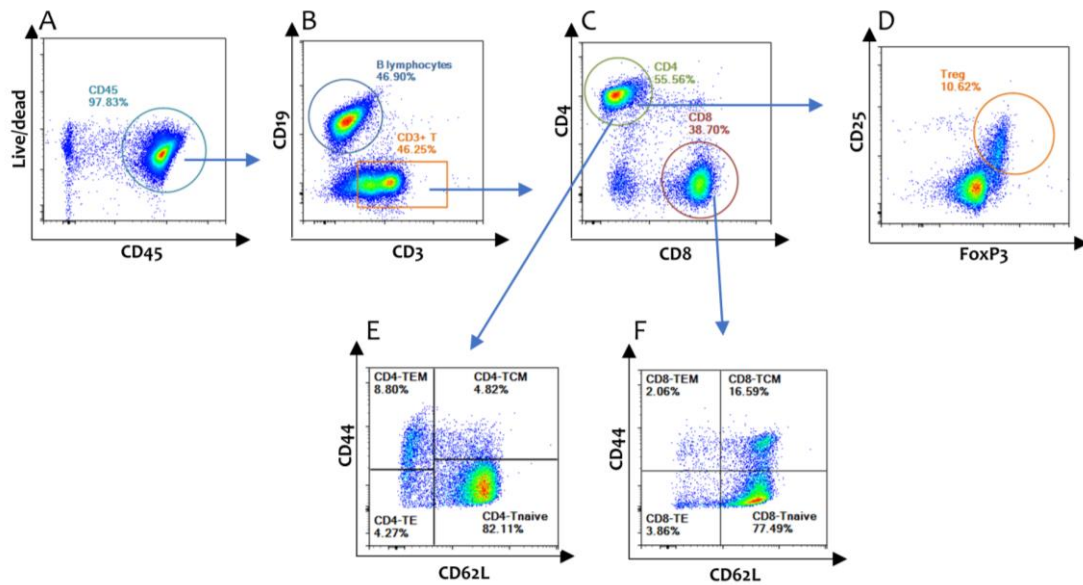
APPENDIX VII - Gating strategy of flow cytometry immunophenotype

**Gating strategy used for flow cytometry analyses of main immune populations in blood.**

Leukocytes were identified as live CD45⁺ (A) where eosinophils were excluded based on high dimensions (SSC) and gradual positivity for Gr1, while neutrophils were identified as positive for Gr1⁺ (B). From double negative cells, CD19⁺ B and CD3⁺ T lymphocytes were identified (C). T cell subsets were deepened based on CD4⁺ and CD8⁺ expression (D).

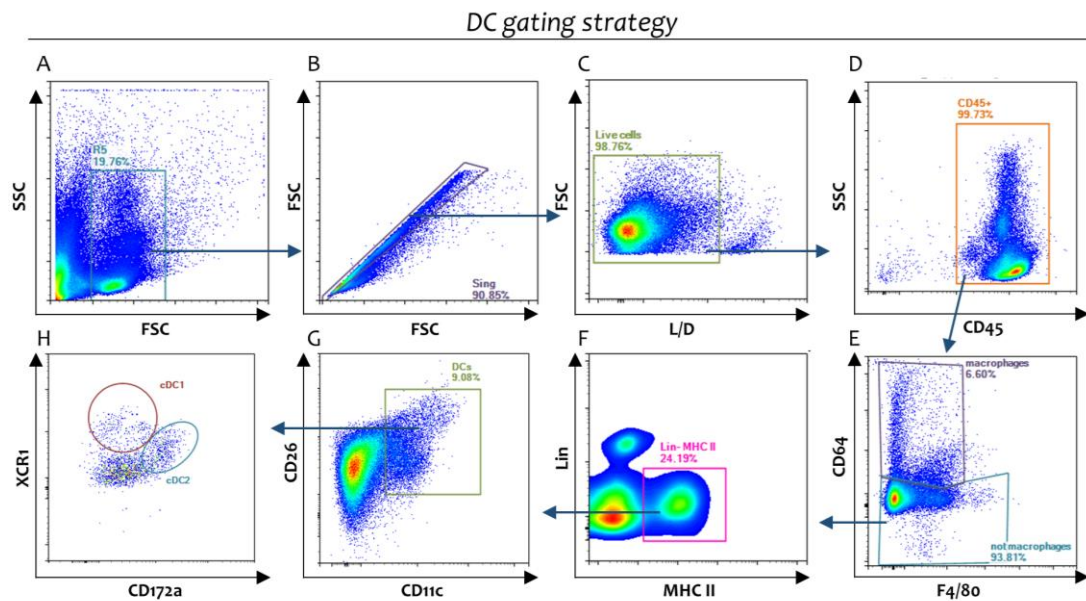
From CD19⁻CD3⁻ cells, monocytes and their subsets, were classified based on the expression of Ly6C⁺ (E). From Ly6C⁻ cells, CD11c⁺ dendritic cells were identified (F). Dendritic cells were then divided into conventional dendritic cells type 1 (cDC1: CD172⁻ CD11b⁺) and conventional dendritic cells type 2 (cDC2: CD172a⁺ CD11b⁺) (G).

T lymphocyte gating strategy



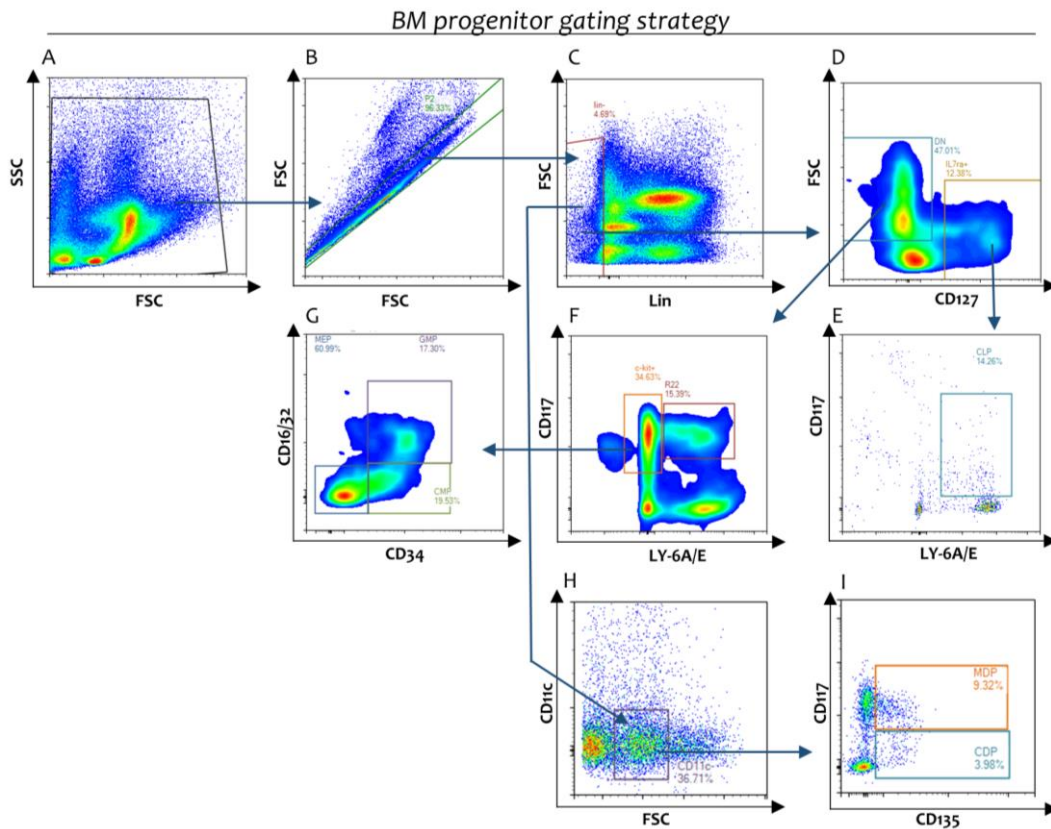
Gating strategy used for flow cytometry analyses for T lymphocyte detection in different tissues, such as LNs, VAT, Liver, Pp and Spleen.

Cells were pre-gated as singlets and next leukocytes were identified as live CD45⁺ (A). Among these, CD19⁺ B and CD3⁺T lymphocytes were identified (B), where CD4⁺ or CD8⁺ T lymphocytes were distinguished (C). From CD4⁺ T lymphocytes, Tregs were identified based on doubled positivity for CD25⁺ and FoxP3⁺ (D), while based on the expression of CD44 and CD62L, T cells subsets were divided into T naïve (CD62⁺CD44⁻), T effector (TE; CD62⁻CD44⁻), T effector memory (TEM; CD62⁻CD44⁺) and T central memory (TCM; CD62⁺CD44⁺) (E,F).



Gating strategy used for flow cytometry analyses of dendritic cell detection in different tissues, such as LNs, VAT, Liver, Pp, Spleen, and Thymus from (119) *Guilliams et al.*

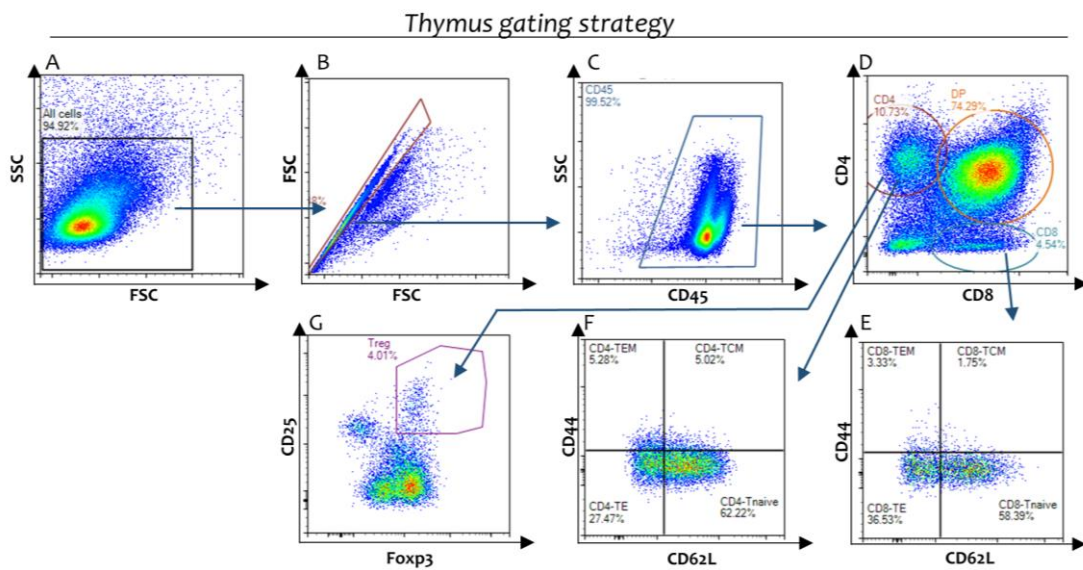
Cells were pre-gated as singlets live cells and next leukocytes were identified as live CD45⁺ (A-D) and macrophages identified as CD64⁺ (E), while from the CD64⁻, DCs were identified as MHC II⁺ lin⁻ CD11c⁺ CD26⁺ cells (F-G). DC subsets were distinguished based on the expression of XCR1 or CD172α markers (cDC1 and cDC2 respectively) (H).



Gating strategy used for flow cytometry analyses of bone marrow progenitors.

Cells were pre-gated as singlets (A-B) and next lineage negative cells were identified (C). From these, two populations were identified based on low FSC and CD127⁺, or with high FSC and negative for CD127. From the first, CLPs were identified (E) thank to the double positivity for CD117 and LY-6A/E; while from the latter the CD117⁺ and LY-6A/E⁻ population was obtained, from which GMP, CMP and MEP were identified based on CD16/32 and CD34 positivity (F-G). From Lin-CD11c⁻ cells, MDP were identified as double positive for CD135 and CD117, while CDP only CD135⁺ (H-I).

(CLP, Common lymphoid progenitor; GMP, Granulocyte/monocyte progenitor; CMP, Common myeloid progenitor; MEP, megakaryocyte/erythrocyte progenitor; MDP monocyte dendritic cell progenitor; CDP, common dendritic cell progenitor).



Gating strategy used for flow cytometry analyses for T lymphocyte detection in the thymus.

Cells were pre-gated as singlets and next leukocytes were identified as live CD45⁺ (A-C) CD4⁺, CD8⁺ and double positive CD4⁺ CD8⁺ T lymphocytes were identified (D). From CD4⁺ and CD8⁺ T lymphocytes, based on the expression of CD44 and CD62L, T cells subsets were divided into T naïve (CD62⁺CD44⁻), T effector (TE; CD62⁻CD44⁻), T effector memory (TEM; CD62⁻CD44⁺) and T central memory (TCM; CD62⁺CD44⁺) (E,F). Tregs were identified on CD4⁺ T lymphocytes based on doubled positivity for CD25⁺ and FoxP3⁺ (G).

APPENDIX VIII – Total body weight and organ weight of male and female mice on atherosclerosis backgrounds: ChowD- and WTD feeding

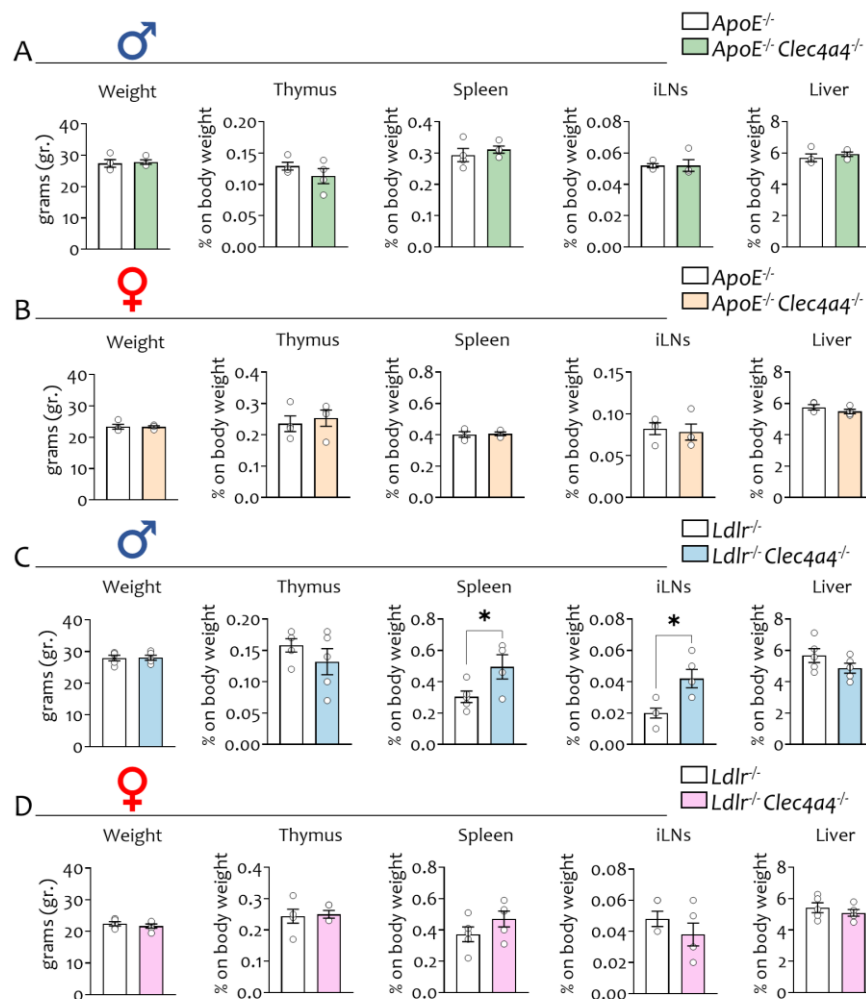


Fig.1 Total body weight and organ weight of ChowD-fed DKO mice on $ApoE^{-/-}$ or $Ldlr^{-/-}$ background. A-B) Total body weight after 12 weeks of ChowD, and Thymus, spleen, inguinal lymph nodes (iLNS) and liver weight expressed ad ratio on total body weight of male and female mice on $ApoE^{-/-}$ background. C-D) Total body weight after 12 weeks of ChowD and Thymus, spleen, iLNS and liver weight expressed ad ratio on total body weight of male and female mice on $Ldlr^{-/-}$ background. Results are expressed as mean \pm SEM. n=5 per group. Statistical analyses were performed with unpaired t-test. * $p < 0.05$.

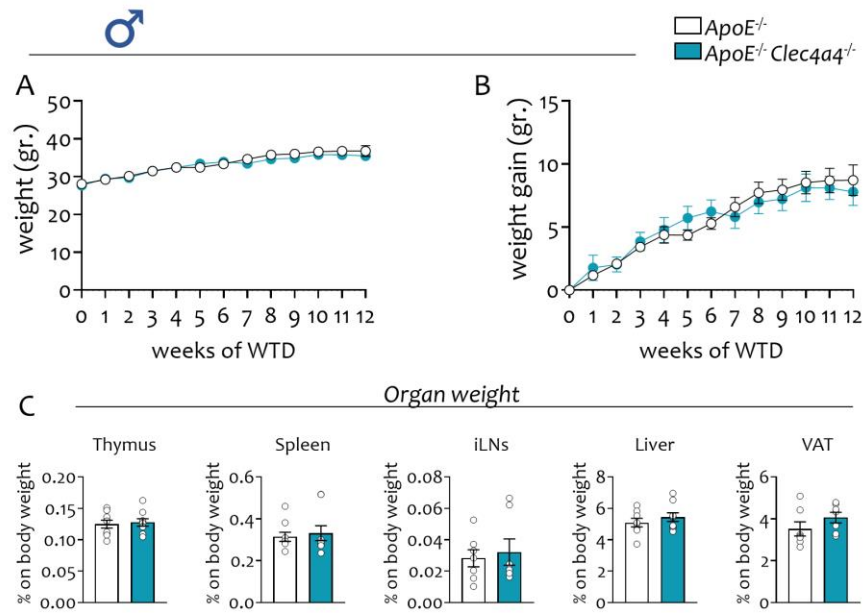


Fig.2 Total body and organ weight of WTD-fed DKO male mice on *ApoE*^{-/-} background. A-B) Weight and weight gain of male DKO mice compared to the *ApoE*^{-/-} counterpart. C) Percentage of male organ weight (thymus, spleen, iLNs, liver and VAT respectively) on total body weight. Results are expressed as mean±SEM. n=9 mice per group. Statistical analyses were performed with unpaired t-test. **p*<0.05.

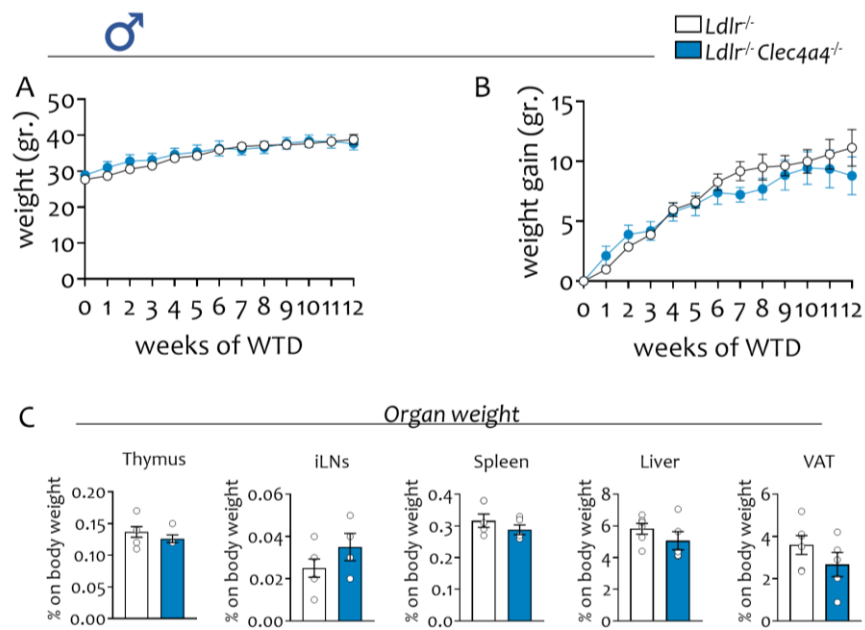


Fig.3 Total body and organ weight of WTD-fed DKO male mice on *Ldlr*^{-/-} background. A-B) Weight and weight gain of male DKO mice compared to the *Ldlr*^{-/-} counterpart. C) Percentage of male organ weight (thymus, iLNs, spleen, liver and VAT respectively) on total body weight. Results are expressed as mean \pm SEM. n=5 mice per group. Statistical analyses were performed with unpaired t-test. * p <0.05.

ACTIVITY REPORT

Rossella Bellini

Ph.D. in Pharmacological Biomolecular Sciences, Experimental and Clinical

Date and place of birth: 14/07/1993 Treviglio (BG), Italy | Nationality: Italian

Email: rossella.bellini@unimi.it

Scopus author ID: [57841661700](#)

HI (updated at 29/12/2023): 2

ORCID ID: [0000-0002-2595-7226](#)

Researcher ID: [HHN-4958-2022](#)

Publications

- **Bellini R**, Moregola A, Nour J, Uboldi P, Fabrizia Bonacina |, Norata GD. Dendritic cell immunoreceptor 2 (DCIR2) deficiency decreases hepatic conventional dendritic cell content but not the progression of diet-induced obesity. *Immunity, Inflamm Dis* (2023) 11:e1024. doi: 10.1002/IID3.1024 [IF 3.2]
- **Bellini R**, Bonacina F, Norata GD. Crosstalk between dendritic cells and T lymphocytes during atherogenesis: Focus on antigen presentation and break of tolerance. *Front Cardiovasc Med* (2022) 0:2010. doi: 10.3389/FCVM.2022.934314 [IF 3.6].
- Nour J, Moregola A, Svecla M, Da Dalt L, **Bellini R**, Neyrolles O, Fadini GP, Rombouts Y, Albiero M, Bonacina F, et al. Mannose Receptor Deficiency Impacts Bone Marrow and Circulating Immune Cells during High Fat Diet-Induced Obesity. *Metabolites* (2022) 12:1205. doi: 10.3390/METABO12121205/S1 [IF 5.58].
- **Bellini R**, Moregola A, Nour J, Rombouts Y, Neyrolles O, Uboldi P, Bonacina F, Norata GD. Dendritic cell marker Clec4a4 deficiency limits atherosclerosis progression. *Atheroscler Plus* (2023) 51:8–12. doi: 10.1016/J.ATHPLU.2022.12.001 [IF 1.6].

Congresses

Oral presentations:

[May 21st-24th, 2023] **91st EAS Congress** Mannheim, Germany. Abstract title for SaaG:” *Dendritic Cell Immunoreceptor 2 (DCIR2) deficiency impacts immune cells distribution and atherosclerosis in Ldlr^{-/-} mice;*

[Nov 27th -29th 2022] **36° SISA national congress.** Rome, Italy. Abstract title: “Role of DCIR2 (Clec4a4) in atherosclerosis experimental model Ldlr^{-/-}“;

[Nov 15th 2022] **XXIV SIF Seminar on Pharmacology** for PhD Students, Fellows, PostDoc and Specialist Trainees. Rome, Italy Abstract title: “*Lysosomal acid lipase (LAL) deficiency results in altered immune cells distribution in mice and in humans*”;

[Set 22nd – 24th 2022] **XXI CONGRESSO REGIONALE SISA-XVI CONGRESSO NAZIONALE SITeCS**, Milan, Italy. Abstract title: “*Ruolo di DCIR2 (Clec4a4) nello sviluppo dell’aterosclerosi*”

[May, 22-25th 2022] **90th EAS Congress**, Milan, Italy. Abstract title: “*Lysosomal Acid Lipase (LAL) Deficiency Alters Immune Cells Distribution in Mice And Humans*”

[Nov 28th-30th 2021] **35° SISA National Congress**, Virtual Edition. Abstract title: “*Lysosomal Acid Lipase (LAL) Inhibition Affects Dendritic Cells Maturation*”

[Nov 26th 2021] **Invited speaker** at the Congress “La prevenzione cardiovascolare nell’era post-COVID” – IV giornata della Ricerca del Centro Enrica Grossi Paoletti - Department of Pharmacological and Biomolecular Sciences

[Oct 7-9th 2021] **XX CONGRESSO REGIONALE SISA-XV CONGRESSO NAZIONALE SITeCS**, Milan, Italy. Abstract title: “*Ruolo Della Lipasi Acida Lisosomiale Nella Maturazione Delle Cellule Dendritiche*”;

[May 21st -22nd 2021] **Spring Meeting Giovani Ricercatori SIIA, SIMI, SISA 2021.** Abstract title: “*Lysosomal acid lipase impacts Dendritic cells maturation*”;

[Nov 22nd -24th 2021] **34° SISA national congress**, Virtual edition. Abstract title:” *Hypercholesterolaemia Impacts Glycans Profile On Circulating Immune Cells.*”

[Oct 15th 2020]

XIX CONGRESSO REGIONALE SISA-XIV CONGRESSO NAZIONALE SITeCS, Milan, Italy. Abstract title: *“Effetto dell’ipercolesterolemia sul profilo di N-glicosilazione delle cellule immunitarie circolanti”*.

[Oct 4th – 7th 2020]

88th EAS Congress, Virtual edition. Abstract title for SaaG: *“Glycans signature in monocytes and lymphocytes from LDLR KO mice and FH patients”*.

Grants

- **EAS Young Investigator Fellowship** to attend the 91th EAS Congress in Mannheim, May 21st-24th 2023
- **EAS Young Investigator Fellowship** to attend the 90th EAS Congress in Milan, May 22nd-25th 2022
- **Best poster** at 40^o SIF national congress, virtual edition, March 9th-13th 2021;
- **EAS Travel Grant** to attend EAS 2020 Geneva, Switzerland, May 31st-June 03rd 2020;

Member of scientific society

SISA, Società Italiana Per lo Studio dell’Aterosclerosi

EAS, European Atherosclerosis Society

SIF, Società Italiana di Farmacologia